Πετειναρέλης Αλέξανδρος

«Compression bending test mechanism for plywood-fiberglass composites.
Encoding complex 3d form into flat 2d strips through fiber orientation and layers count distribution.»

Πολυτεχνείο Κρήτης | Σχολή Αρχιτεκτόνων Μηχανικών | Πρόγραμμα Μεταπτυχιακών Σπουδών (Π.Μ.Σ.) «Χώρος, Σχεδιασμός, και Δομημένο Περιβάλλον»

Πετεινιαρέλης Αλέξανδρος
02.Οκτωβρίου 2017

Τριμελής εξεταστική επιτροπή:
Επικ. Καθηγητής Γιαννούδης Σ. (επιβλέπων)
Επικ. Καθηγητής Βαζάκας Α.
Καθηγητής Προβιδάκης Κ.

A compression bending test mechanism has been developed to measure and document the bending properties of plywood-fiberglass composite slender beams, employing Tracker, a digital video analysis and modelling tool and Grasshopper, a graphical algorithm editor for Rhino 3d.

Fiberglass is distributed along planar plywood strips, in one or more layers, in four warp-weft fiber directions of 0, 30, 45 and 60 degrees. The deflections, forces and geometry of the bending tests are analyzed and classified per case, in order to derive the bending modulus, the proportional limit and the minimum bending radius of various plywood-fiberglass layout schemes.

The results are embedded into K2Engineering, a structurally calibrated extension of Kangaroo2 grasshopper plugin, which is a 3DOF Dynamic Relaxation interactive simulation engine. K2engineering offers direct input and output of structural data that define the resulting shape and can be used to evaluate its structural performance respectively. This enables a unified, multiscalar materially informed form finding process, where the final geometry is approximated according to the local material specifications at a macro, meso and micro scale. General dimensions, i.e. width length and thickness, the number of fiberglass layers and the orientation of wood grain and glass fibers respectively, along with the resin formulation and the chosen boundary conditions can output a variable stiffness strip, that when bent, converges into a non-symmetrical shape of variable curvature without the need of a secondary support system.

«Compression bending test mechanism for plywood-fiberglass composites.
Encoding complex 3d form into flat 2d strips through fiber orientation and layers count distribution.»

Πολυτεχνείο Κρήτης | Σχολή Αρχιτεκτόνων Μηχανικών | Πρόχραμμα Μεταπτυχιακών Σπουδών (Π.Μ.Σ.) «Χώρος, Σχεδιασμός, και Δομημένο Περιβάλλον»

Acknowledgements

I would like to thank:

My supervisor *Socratis Yiannoudes* for his support.

Alexandros Vazakas and *TUC Digital Fabrication Lab* for the technical support, granting access to the lab equipment and for sharing his expertise.

Yannis Efthymiou for his suggestions and advice on structural aspects, helping me reach a critical milestone of this thesis.

Iro Skouloudi for her supportive and critical commentary

and finally,

Christos Filippidis for all our constructive conversations, convincing me to pursue this degree and above all, for being an invaluable Friend.

01

Bending-active structures

Design and simulation software
Kangaroo2 (Daniel Piker) and K2Engineering (Cecilie Brandt)

Bending-active structures

Bending-Active Structures

Form-finding strategies using elastic deformation in static and kinetic systems and the structural potentials therein

Julian Lienhard

PhD Thesis, Institut für Tragkonstruktionen und Konstruktives Entwerfen der Universität Stuttgart, 2014

The term "bending-active" is introduced by the author to describe curved beam and surface structures that base their geometry on the elastic deformation of initially straight or planar elements

[Knippers et al (2011) Construction Manual for Polymers + Membranes..]

Central argument, elastic deformation can actively be used to permanently or temporarily shape curvature in load bearing elements.

ICD/ITKE Research Pavilion 2010

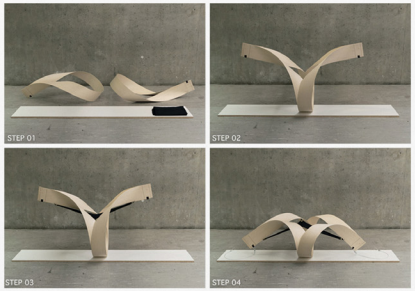

Torsion As A Design Driver In Bending-Active Tensile Structures

Evy L. M. Slabbinck, Ir. Arch. M.Sc.

Thesis Advisor: Axel Körner

Bend9 - Bending-Active design at Pier 9

Prof. Dr.-Ing. Jan Knippers

Riccardo La Magna

Simon Schleicher, Mei-yen Shipek

Active bending in this context is understood to be a form defining strategy based on systemized elastic deformation, i.e. bending. In general, bending active structures are understood to be an approach rather than a distinct structural type.

The pre-stressing of bending-active structures is generated through large nodal displacements in statically indeterminate structures. As a result, individual building elements are largely deformed and therefore exposed to a constant bending stress, i.e. pre-stress. The element stiffness is chosen so that the induced bending stress never reaches the elastic limit of the used materials. Therefore, a linear material law (Hooke's Law) is always used for the subsequent investigations. As a consequence to the large deformations of bending-active structures, the calculations generally must be performed geometrically non-linear.

Bending-active in structural terms: constrained statically indeterminate structures with residual bending stress.

In the analysis of structural systems, several aspects of nonlinearity can be differentiated:

· Nonlinear material behaviour: plastic deformation (not considered in bending-active structures).

· Nonlinear boundary conditions: change of supporting condition under deformation (may be considered in bending-active structures, where large deflections lead to additional supporting points and contact between initially separate elements).

· Geometric nonlinearity: nonlinear relationship of external forces and deflection (must be considered in all bending active structures).

Kangaroo physics for grasshopper

Kangaroo is a 3DOF (not anymore!) Dynamic Relaxation Live Physics engine for interactive simulation, form-finding, optimization and constraint solving.

For form-finding we often use fictitious material properties, such as zero-rest-length springs, which do not necessarily correspond to the real material, that the structure will be built from.
This is the case for both digital form finding tools like Kangaroo and for form-finding with actual physical models.

For instance, using chain nets to find shapes for masonry structures, or soap film for fabric - it is not that those materials accurately mimic the true building materials at all, but just that certain aspects of their behaviour can cleverly be made use of to find geometric forms well suited to the structural properties of the actual building material and the loads that will be applied to it (hanging chains and pure compressive forms, zero mean curvature and uniform fabric tension).
It really is a sort of ingenious subterfuge - in a way we are tricking nature into giving us an answer to its own challenge by asking it a different, seemingly separate, question.
Daniel Piker

K2Engineering

K2Engineering is a structurally calibrated extension of Kangaroo2, a set of customised grasshopper components with the scope of calibrating a number of kangaroo goals with regard to structural properties.

Particularly useful plugin for the analysis of form-active structures (including cablenets and gridshells) that are typically characterised by their large deformations when subjected to external loads. The underlying position-based dynamics implemented in the Kangaroo2 solver inherently deals with this non-linear behaviour. This means that both form-finding and analysis can be performed within the Grasshopper environment using K2 and K2Engineering.
Cecilie Brandt

The main purpose of this plugin is to offer a direct output of meaningful structural values that can be used to evaluate the performance. Whilst it is possible (in most cases) to input appropriate stiffness values for the existing goals and subsequently back-calculate the forces from the displacements, this approach has the advantage of avoiding duplicate functionality, simplifying the process of mapping the results back to the structure and making it more clear which properties are needed for the calibration and their correct units.

Calibrated and Interactive Modelling of Form-Active Hybrid Structures
Gregory QUINN, Anders Holden DELEURAN, Daniel PIKER, Cecilie BRANDT-OLSEN, Martin TAMKE, Mette Ramsgaard THOMSEN, Christoph GENGNAGEL
Proceedings of the IASS Annual Symposium 2016 "Spatial Structures in the 21st Century" 26-30 September, 2016, Tokyo, Japan K. Kawaguchi, M. Ohsaki, T. Takeuchi (eds.)

02

Related work - source of inspiration

Composite territories 2013
CITA Center for Information Technology and Architecture | *KADK*

Graded territories 2012
CITA Center for Information Technology and Architecture | *KADK*

ICD-ITKE Research Pavilion 2015-16
ICD - Institute for Computional Design and Construction | Stuttgart

Outlining some key aspects and findings, aiming to define and answer some of the suggested future work in their conclusions, focussing mainly on the testing methods and the simulation techniques used in each case.

CITA – Centre for Information Technology and Architecture | KADK

Computational Strategies for the Architectural Design of Bending Active Structures

Paul Nicholas, Martin Tamke

INTERNATIONAL JOURNAL OF SPACE STRUCTURES Volume 28 · Number 3 & 4 · 2013

COMPOSITE TERRITORIES

Material, element and structure

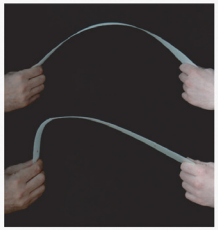

The shape of a bend strip can be determined through the variation of material stiffness: upper strip homogenous material, lower strip heterogeneous material distribution.

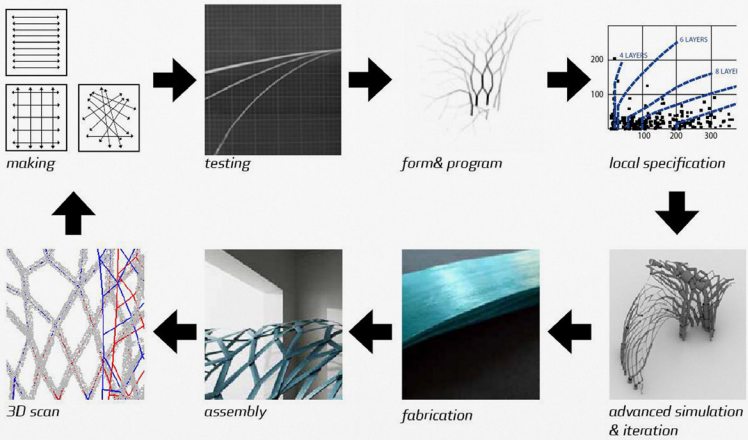

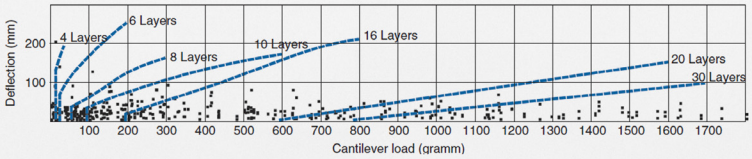

Figure 5. Look up table displaying the relationship between loading and deflection for each layering arrangement. The black dots show the initially calculated load and deflection for the elements within the Composite Territories installation.

The gridshell elements were specified so that, under self-weight, the structure would deflect to match a predefined 'target shape'

1. An algorithm iteratively assesses the particular loading condition of each single beam and the deflection that it should make to match the target shape, and finds the closest matching loading and deflection configuration from the look up table.

2. At this stage, data gathered from the empirical testing was also used to calibrate a Karamba FEA model, which includes material definitions and beam thicknesses. Optimized material distribution and beam specification is achieved through a connection to the Galapagos toolset within Rhino/Grasshopper. This tool reduces iteratively the material thickness and stiffness of elements where this does not result in any increased deviation from the target shape.

3d scan revealed deviations that stem from a lack of incorporation of bending behavior into precision in the realm of fabrication, but especially the measurement and simulation of material properties. Where cantilever testing allowed us to understand the bending effect we did not obtain material properties at the material scale, as established means of mechanical material testing can provide.

CITA – Centre for Information Technology and Architecture | KADK

Computational Strategies for the Architectural Design of Bending Active Structures

Paul Nicholas, Martin Tamke

INTERNATIONAL JOURNAL OF SPACE STRUCTURES Volume 28 · Number 3 & 4 · 2013

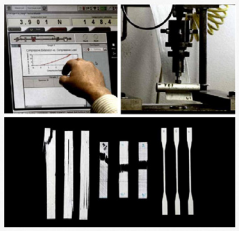

GRADED TERRITORIES (*SmartGeometry 2012 workshop*)

Material, element and structure

The workshop explored how mechanical testing, and the measures generated through testing, could inform the modelling of composite behaviour when linked to time-based simulation methods.

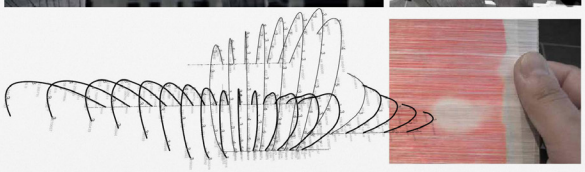

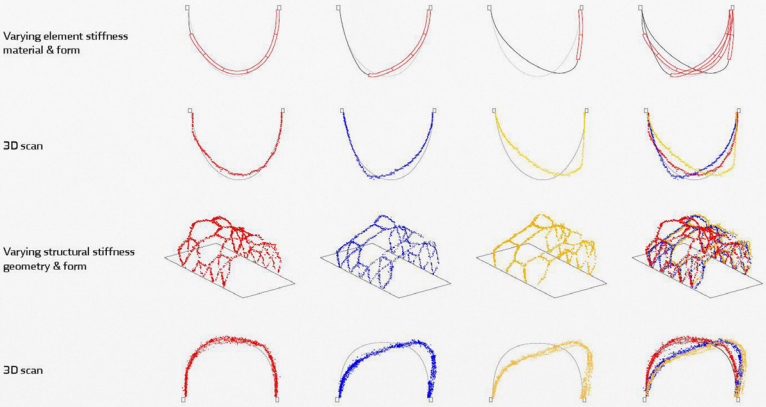

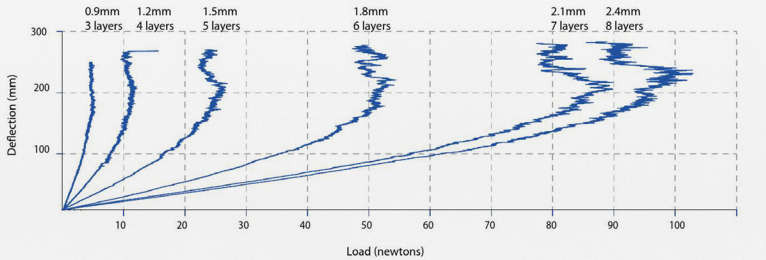

The aim for Graded Territories was to extend thinking about processes for measuring, specifying and embedding of forming information for a non-uniform stiffness composite structures.
The design was limited to two distinct structural conditions to isolate the property of bending.
1.The first was a cantilever, restrained at one end. In this condition bending was induced by the self-weight of the structure. A cantilevering strip typically combined 5 sub elements of potentially different bending stiffness.
2.The second condition was an arch, restrained at both ends, which typically combined 10 sub elements.

It became crucial to load test each combination of assemblies. As a result, each layering combination was assigned a different modulus of elasticity and sectional height. However the iterative FE form finding process was also revealed to be extremely sensitive, and lacking in the responsiveness and speed required during the architectural design process. Within the constraints of the project, it was also not possible to link the simulation process to the variation and optimization of element stiffness's.

ICD – Institute for Computational Design and Construction | Stuttgart

Textile Fabrication Techniques for Timber Shells

Elastic Bending of Custom-Laminated Veneer for Segmented Shell Construction Systems

Simon Bechert, Jan Knippers, Oliver David Krieg, Achim Menges, Tobias Schwinn, and Daniel Sonntag

S. Adriaenssens, F. Gramazio, M. Kohler, A. Menges, M. Pauly (eds.): Advances in Architectural Geometry 2016

ICD-ITKE Research Pavilion 2015-16

Material Differentiation and Form-Finding of Laminate Geometry

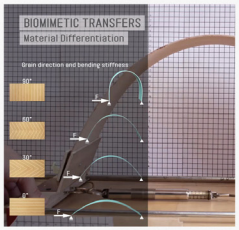

In the case of wood veneer, the fibre direction is the main medium to control each strip's bending stiffness.

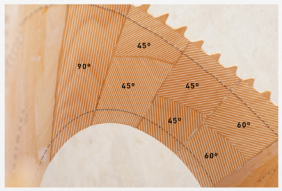

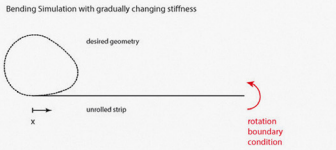

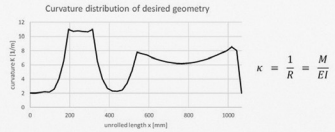

$$\kappa = \frac{1}{R} = \frac{M}{EI}$$

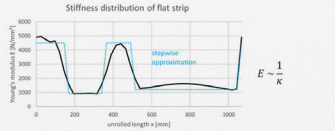

$$E \sim \frac{1}{\kappa}$$

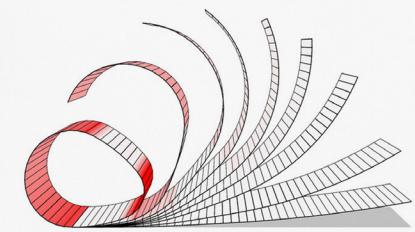

Geometric non-linear Finite Element Analysis with large displacements

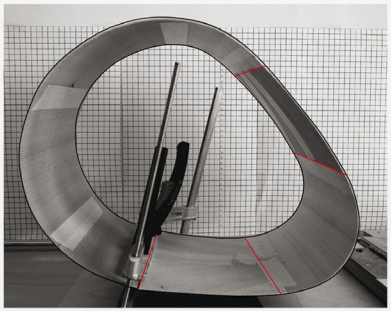

Prototype

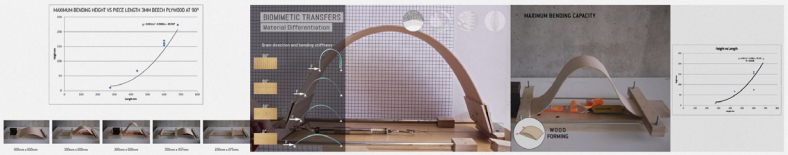

The stiffness graduation is achieved by laminating discrete veneer strips on a base material of 3 mm beech plywood to locally reinforce and thereby stiffen the resulting laminate.

A form finding algorithm is developed, which allows to compute an approximate material layout as a consequence of the curvature distribution along each strip. This tool takes into consideration minimum bending radii, veneer strip size and layer orientation to compute a material layout for the unrolled strip.

Physical tests and digital simulations were compared in order to identify the relationship between grain direction in laminated veneer and the resulting bending stiffness. These experiments also established the lower bound of curvature that the laminate would tolerate before failing. However, it is important to note that the desired shape can only be approximated. The error results from the step-like differentiated stiffness.

03

Bending mechanisms and testing methods

The work of Fukuda H. et al

A new bending test method of advanced composites

Simplified compression bending test method for advanced composites

Developent of compression bending tesy method for advanced composites

Measurement of bending properties of wood by compression bending tests

The bending mechanisms and mockups were the starting point of the first objective of this thesis. The development of an axial compression bending test mechanism, using typical fab lab equipment and computer vision, in order to specify material properties and bending behavior of plywood-fiberglass composite strips. Some key features and all the formulas to calculate stress, bending moduli etc have been based on Fukuda's et al work.

Test methods
Mockups

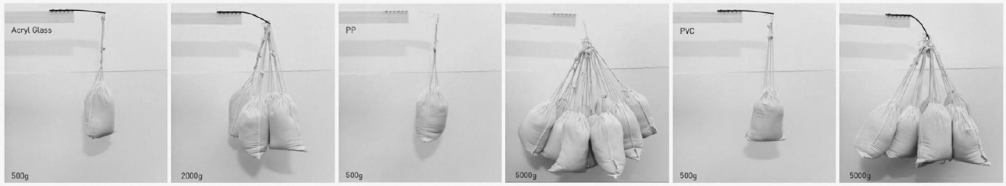

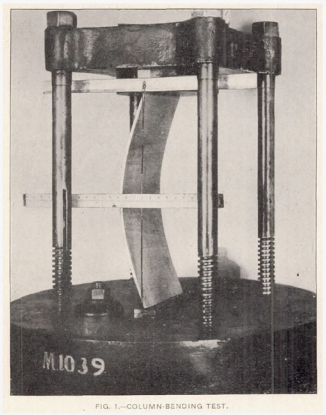

FIG. 1.—COLUMN-BENDING TEST.

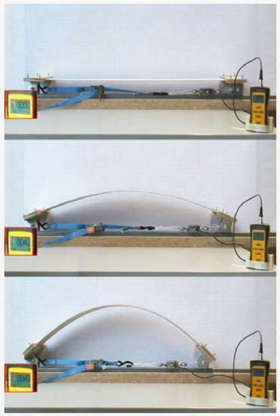

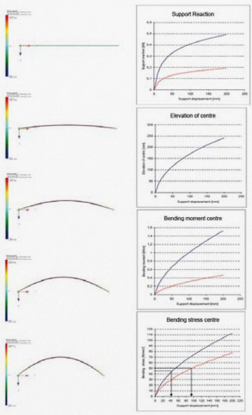

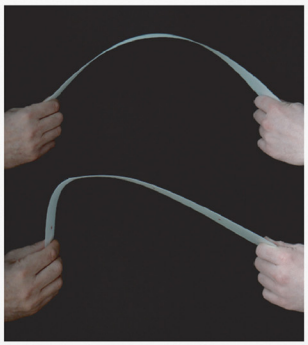

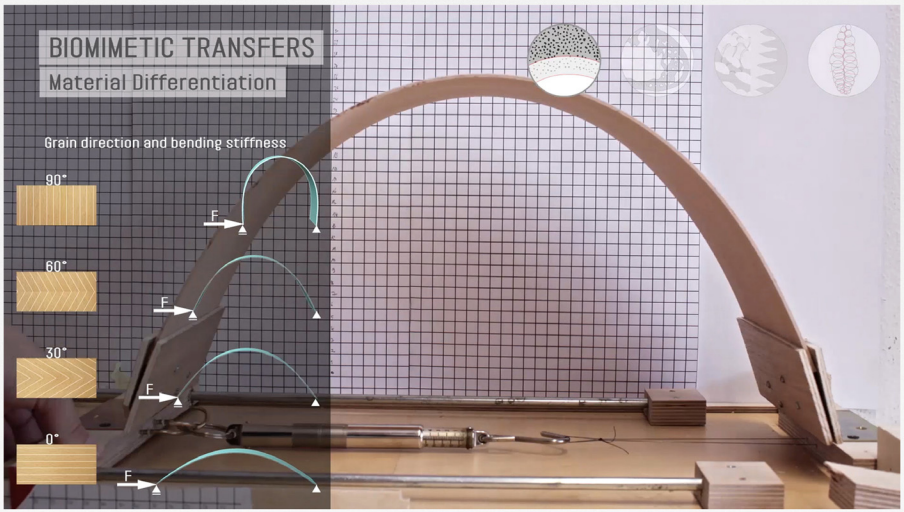

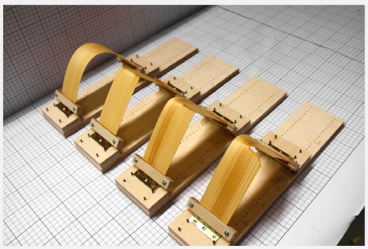

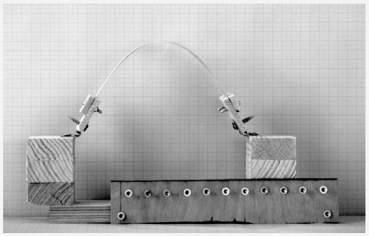

Fukuda H. A new bending test method of advanced composites. Exp Mech 1989;29:330–335

Principle of Compression Bending

Consider a bar with a rectangular cross section (width = b, thickness = t) and both ends pin-supported as shown in Fig. 3. When some compressive axial load, P, is applied to it, the bar will deform. A so-called Euler buckling will take place if the bar is perfectly straight and if there is no misalignment of the load path. But if the load is applied in a somewhat eccentric manner, the bar will deform from the beginning of loading. This paper deals with the latter case.

Denoting the deflection at midspan A as δ, the bending moment at point A becomes

$$M = P\delta \tag{3}$$

and the skin stress (bending stress) is, under the assumption of linear elasticity,

$$\sigma_b = \frac{6M}{bt^2} \tag{4}$$

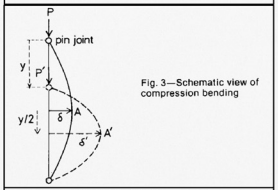

Fig. 3—Schematic view of compression bending

The bending strength is defined by

$$\sigma_{b,max} = \frac{6M_{max}}{bt^2} \tag{5}$$

where M_{max} is the bending moment at failure at point A. Thus if we measure P and δ in the experiment, the bending strength can be calculated from eq (5).

Since no loading device is attached at the location of maximum bending moment, stress concentration due to loading nose will not occur. On the other hand, the following compressive stress is generated in the specimen to satisfy the equilibrium of force in the vertical direction:

$$\sigma_{comp} = \frac{P}{bt} \tag{6}$$

If the value of eq (6) is large, the present method is not suitable for evaluating the bending strength.

H. Fukuda and M. Itabashi, Simplified compression bending testmethod for advanced composites, Composites, Part A 30, 249–256 (1999).

The bending modulus can be calculated as follows [5, 6]. According to the strength of materials,

$$EI\rho = M \tag{3}$$

holds where E is the Young's modulus, I is the moment of inertia of the section, and ρ is the radius of curvature. Denoting the radius of curvature at point A with ρ_A and using the preceding equations, Young's modulus reduces to

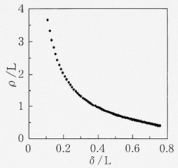

Fig. 2. Midspan deflection versus radius of curvature (elastica).

$$E = P\delta_A\rho_A/I \tag{4}$$

Therefore, if we know ρ_A in addition to P and δ_A during the test, we can calculate the Young's modulus of the specimen. There are several ways to measure or calculate ρ_A.

Fukuda H., Itabashi M. and Wada A.,"Development of compression bending test method for advanced composites – A review". Sci. Eng. Composite Mater Vol.11, pp.169–176, 2004.

ECCENTRIC COMPRESSION BENDING: ANOTHER NEW METHOD

During a series of tests of pipes, another difficulty occurred. That is, if the diameter of the pipe was large.

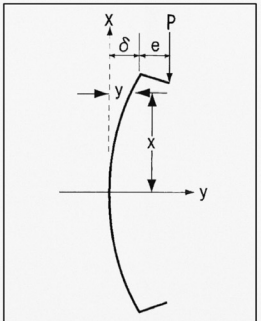

Fig. 11: Schematic view of eccentric compression bending.

the Euler buckling was not likely to occur. Then, as a successive work, we tried to induce bending by means of eccentric compression as shown in Fig.11. In this case, the bending moment of an arbitrary point x is /15/:

$$M_x = P(e + \delta - y) \tag{8}$$

and the maximum bending moment at the center of the pipe is

$$M_{max} = P(e + \delta) \tag{9}$$

instead of eq. (1) for compression bending. Strictly speaking, the value of $e\cos\alpha$ should be used instead of e in eq. (9) where α is defined in Fig. 1. However, the angle α was small in the experiment and therefore, we used eq. (9) for convenience. Then the maximum bending stress is

$$\sigma_{max} = \frac{M_{max}}{Z} \tag{10}$$

where Z is the section modulus of the pipe. If the axial compressive stress is taken into account, the maximum compressive stress is

$$\sigma_{max} = \frac{M_{max}}{Z} + \frac{P}{A} \tag{11}$$

where A is the cross sectional area of the pipe.

To realize the above idea, a set of test fixtures shown in Fig. 12 was designed and machined. Using this device, three kinds of CFRP specimens with a diameter of 15mm were tested /12/, although details of the specimen configuration are not shown here.

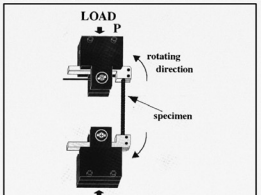

The compression bending, even the eccentric compression bending, inevitably includes compressive stress in addition to bending stress. If the ratio of the compressive stress to the bending stress is large, it is no longer called a bending test.

Hiroshi Yoshihara 09 Shinji Oka, Measurement of bending properties of wood by compression bending tests, J Wood Sci (2001) 47:262–268

Several previous studies on conventional bending test methods for wood suggest that the stress condition around the loading nose is distorted seriously, and that the bending properties are influenced by the loading condition.[1-3] We fear that the bending properties of wood cannot be evaluated properly by the conventional bending method because of the distorted stress condition.

A new bending method was recently developed by Fukuda and colleagues for advanced composites with strong orthotropy.[4-7] In their method, a compression load is applied along the long axis of the specimen with a rectangular cross section, and Young's modulus and the bending strength are measured by means of the elastica phenomenon. The materials examined in their studies were brittle, and they did not show the material's nonlinearity, which wood often shows in the large strain region.

Although we believe that Fukuda's method is promising for measuring the bending properties of wood, the bending behavior of wood during compression bending should be examined in detail. Hence we examined the applicability of the compression bending test method for evaluating the bending properties of wood by comparing it with conventional bending tests.

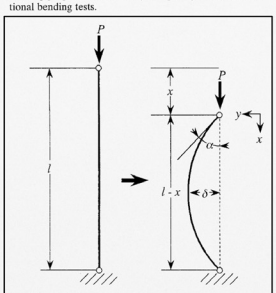

Fig. 1. Schematic diagram of compression bending

Figure 9 shows Young's modulus (E_{lc})corresponding to the length/thickness ratio (l/t). The value of E_{lc} tended to be a constant value, which was a bit larger than that obtained by the four-point bending tests E_{lb} when the length/thickness ratio was large enough. We thought that the additional deflection produced by the shearing force and the stress concentration at the loading point was smaller with the compression bending tests than with the conventional bending tests. Nevertheless, E_{lc} decreased when l/t was less than 20. We thought that this decrease was due to the following two factors. One was material nonlinearity. The smaller the l/t, the larger was the bending stress σ_{lc}. Material nonlinearity, which causes the decrease in stiffness, would be drawn instantly after the bifurcation because of the large bending stress. In addition, when l/t is quite small and the specimen is regarded as an intermediate column, material nonlinearity occurs before bifurcation. The other factor was the additional deflection caused by the shearing force. Although the influence of the shearing force during compression bending is less than with the conventional bending methods, the shearing force that produces the additional deflection cannot be eliminated entirely, and it is marked when the l/t is small. To obtain a stable Young's modulus value with the compression bending test, we believe that the length/thickness ratio should be larger than 25.

Figure 10 shows the proportional limit stress σ_{lt} corresponding to the length/thickness ratio l/t. The value of σ_{lt} was constant when the l/t was larger than 40, and it decreased with decreasing l/t. As can be seen from Eq. (17), the proportional limit stress was influenced by Young's modulus, and it showed a tendency similar to that of Young's modulus. However, the value of σ_{lt} exceeded that obtained by the four-point bending tests σ_{bp}, which was more marked in an l/t range larger than 40. We thought that this tendency was due to the absence of stress concentration at the loading points in the compression bending test.

Summarizing these results, we believe that the compression bending test should be conducted on specimens with a large length/thickness ratio (>40 in this experiment) and that the stress–strain relation should be measured by the load–loading point displacement relation for obtaining Young's modulus, proportional limit stress, and bending strength. Under these testing conditions, we would undertake the bending test without worrying about the stress concentration that necessarily occurs with conventional methods. The instability factors in the compression bending test should be reduced carefully as far as possible.

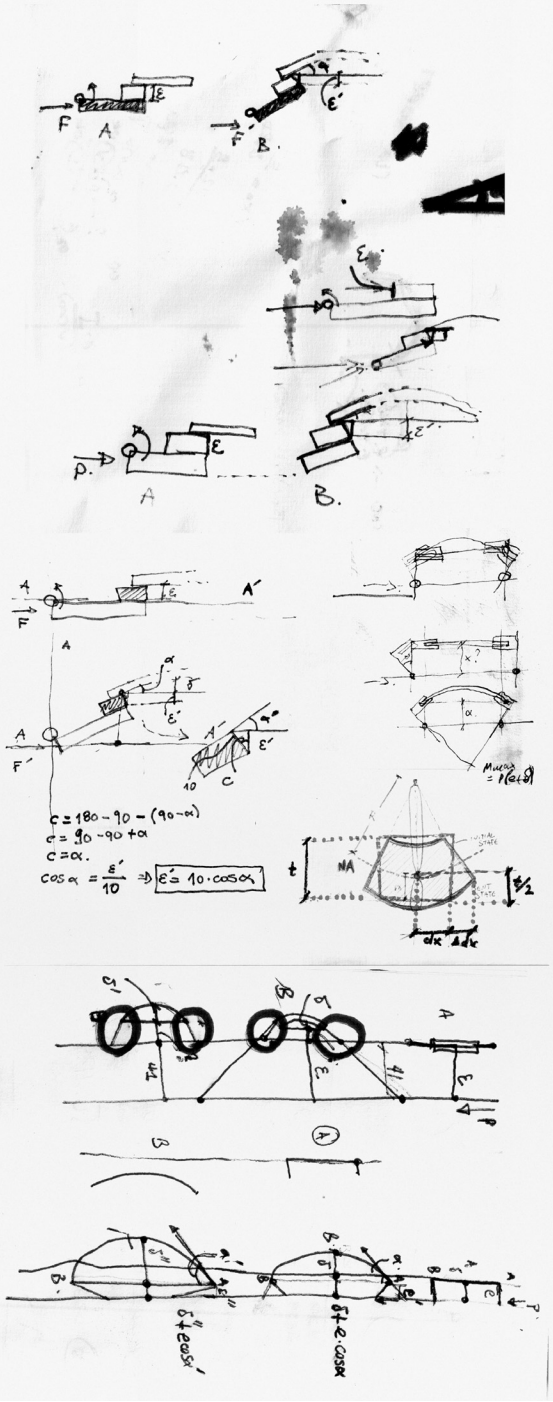

04

The compression bending test mechanism

Tracking setup

Fabrication scheme

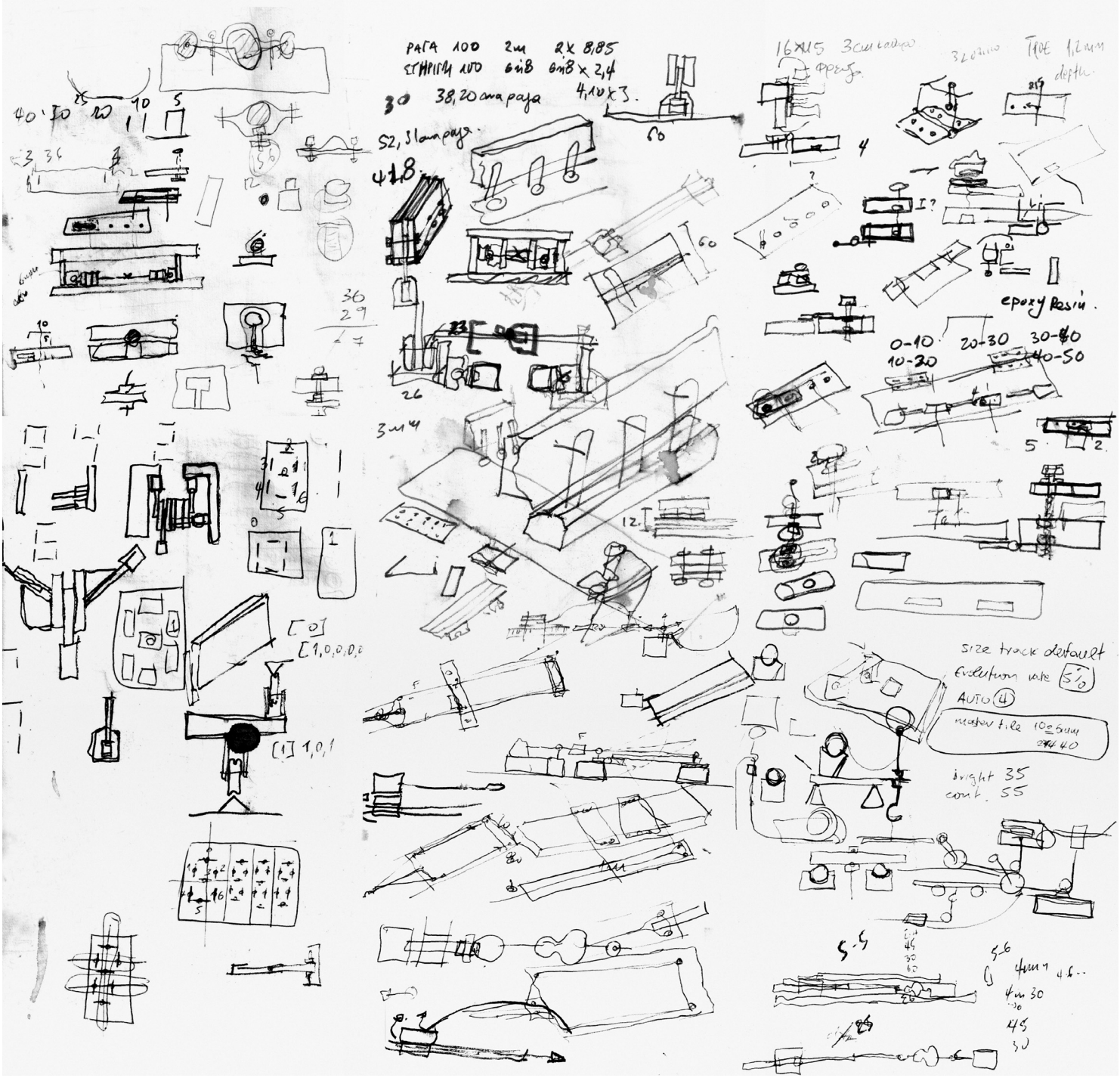
epoxy resin
0-10
10-20
20-30
30-40
40-50
size track default
Evolution rate
AUTO
master tile 105mm
bright 35
cont. 55

Test bench

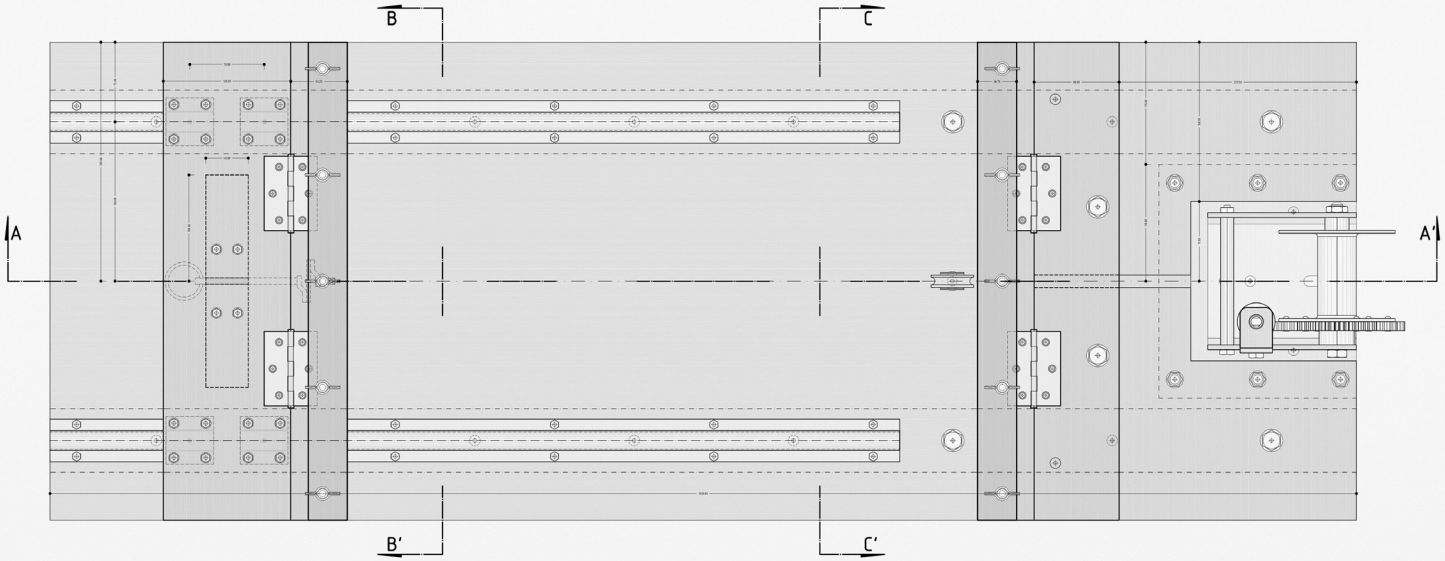

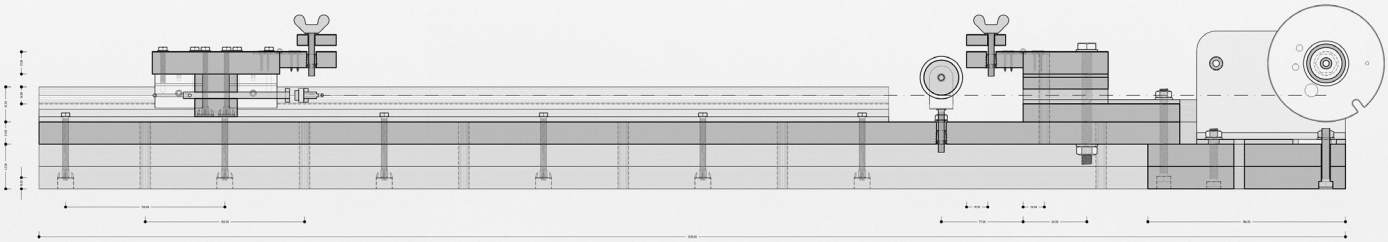

TOMH A-A'

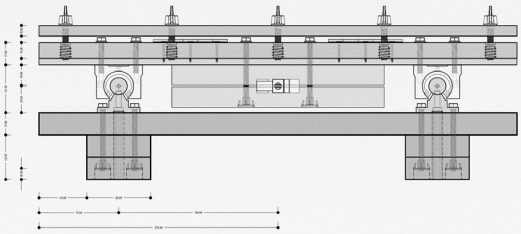

TOMH B-B'

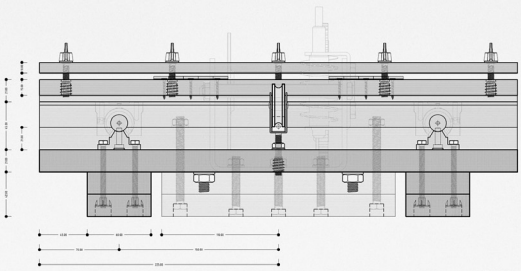

TOMH C-C'

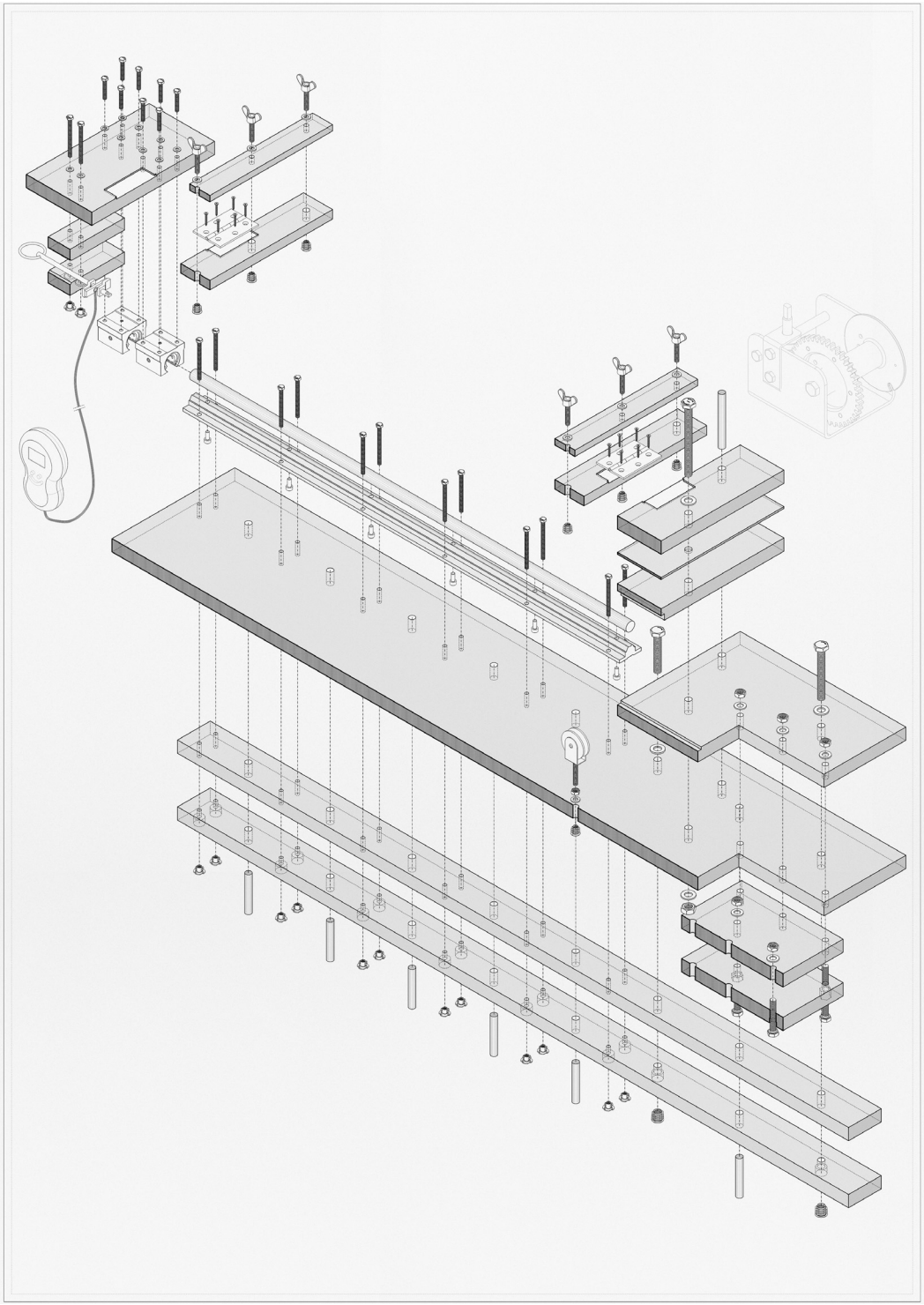

16x M5x30 bolts

28x M5x60 bolts

28x M5 t-nuts

20x M5 washers

10x M6x40 butterfly bolts

11x M6 flanged threaded inserts

11x M6 washers

3x M8x50 bolts

6x M8x80 bolts

9x M8 nuts

9x M8 washers

2x M10x60 bolts

2x M10x80 bolts

2x M10x110 bolts

2x M10 nuts

4x M10 flanged threaded inserts

8x M10 washers

4x 70x50x1.5 hinges

24x 2.5x20 phillips screws

1x 32x85 pulley

4x SBR16UU open linear bearings

2x SBR16 800 linear supported rails

1x digital scale (50kg max, 5gr/0-10kg, 10gr/10-50kg)

Tracking setup

1.Test bench
2.6x26W C6400k video light (~750 watt)
3.Tripod
4.Sony A5000 digital camera
5.Sticker markers

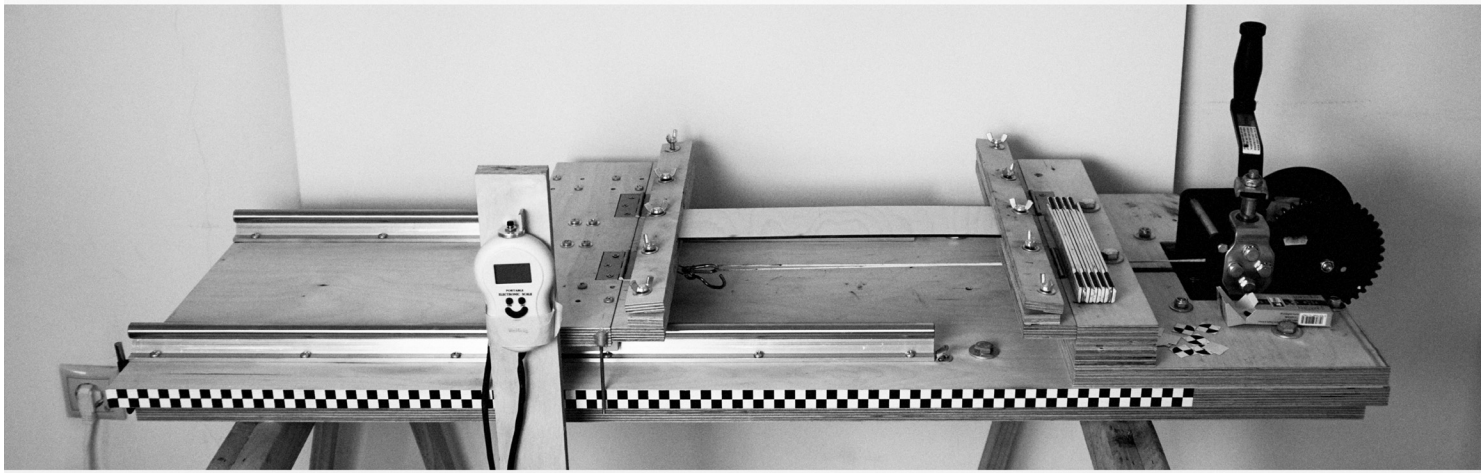

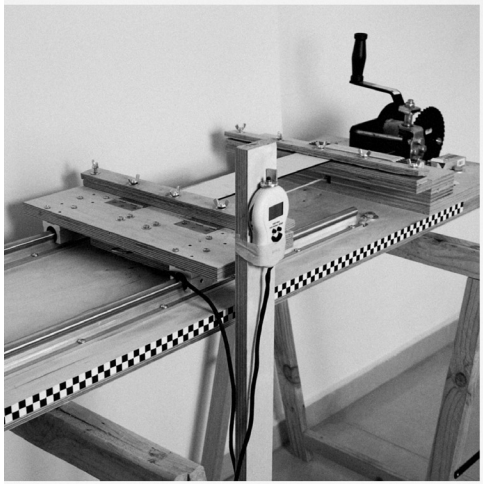

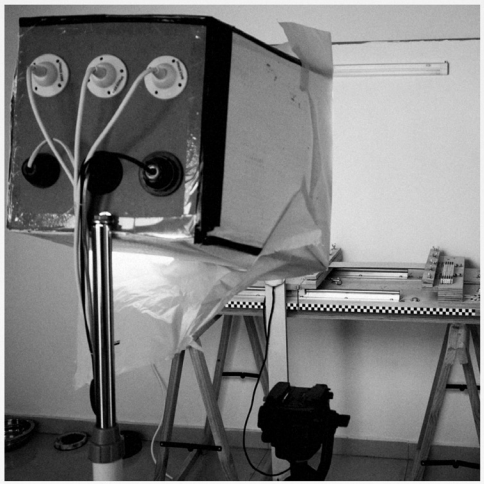

Fabrication scheme

Fiberglass at a° 0, 30, 45, 60

Plywood t:3mm w:120, l:190 (birch)

Fiberglass Layers: 1,3,4,5,6,7

Epoxy resin 30min working time

Suggested Cure time: 24h

Allowed Cure time: 24-36h

Fiberglass:

Areal weight: 195 g / m2

Weaving style: Twill 2X2

Width: 1.00 meter

Warp: Glass fiber EC13 - 136 Z28 876s, 57%, 8 ends(threads) / cm

Weft: Glass fiber EC13 - 136 Z28 876s, 43%, 6 ends / cm

Tensile strength on yarn (N): 92

Weight distribution warp 111,15 g/mq, weft 83,85 g/mq

Weight distribution warp 57% weft 43%

Laminate thickness 0,16*mm ± 15%

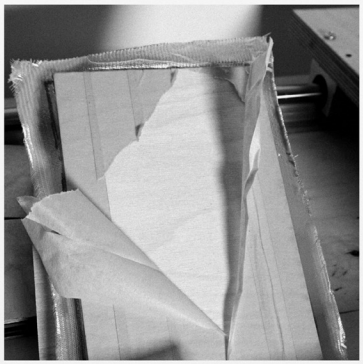

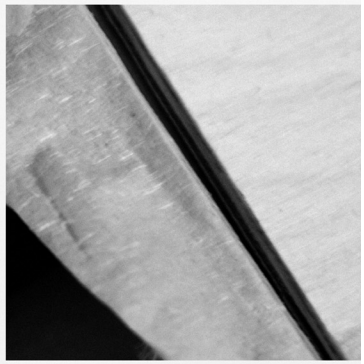

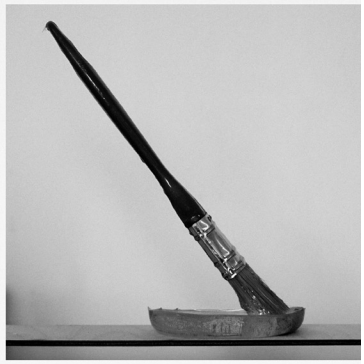

05

Tracker Video analysis and Modelling Tool setup (Douglas Brown)

(Un)Resolved Issues

Callibration-Ommited test samples

Fracture mode of all used for calculations-analysis test samples.

Tracker
Video Analysis and Modeling Tool

OSP
open source physics

Tracker is a free video analysis and modeling tool built on the Open Source Physics (OSP) Java framework. Features include object tracking with position, velocity and acceleration overlays and graphs, special effect filters, multiple reference frames, calibration points, line profiles for analysis of spectra and interference patterns, and dynamic particle models. *Douglas Brown, Cabrillo College 2008*

Video requirements/Setup

A.Resolution:1920x1080 25p
B.1 pixel ≤ 1mm of real world dimensions
1.[first frame] 2 frames before 1st gauge reading
2.[last frame] 1 frame before fracture
3.Video filter 1: Grayscale
4.Video filter 2: [Point tracking] Brightness contrast [~30,55]
5.Video filter 2: [Gauge tracking] Brightness contrast [~60,97]

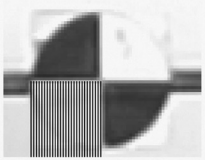

27 pixel array for 10mm

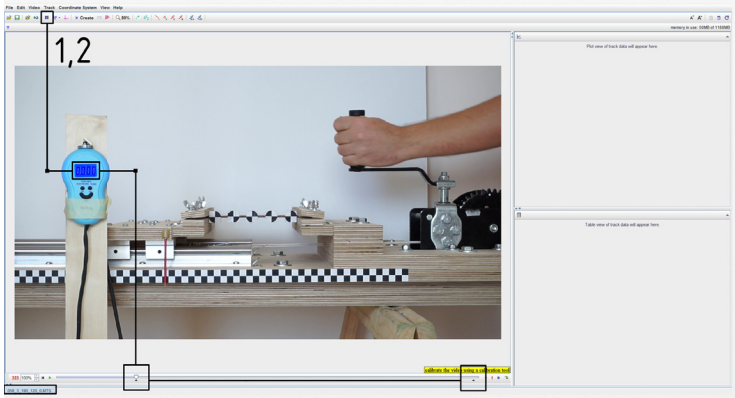

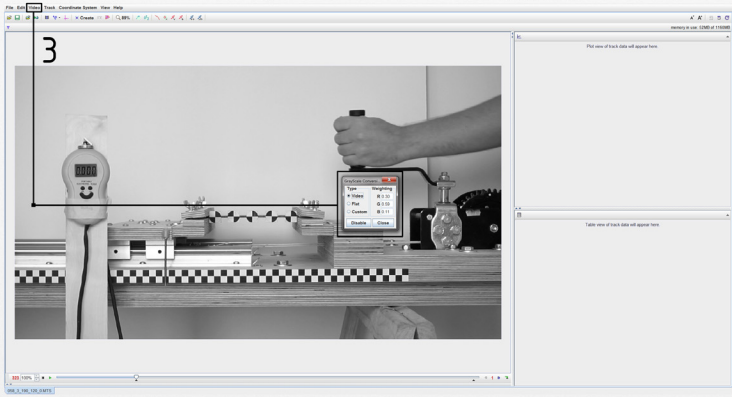

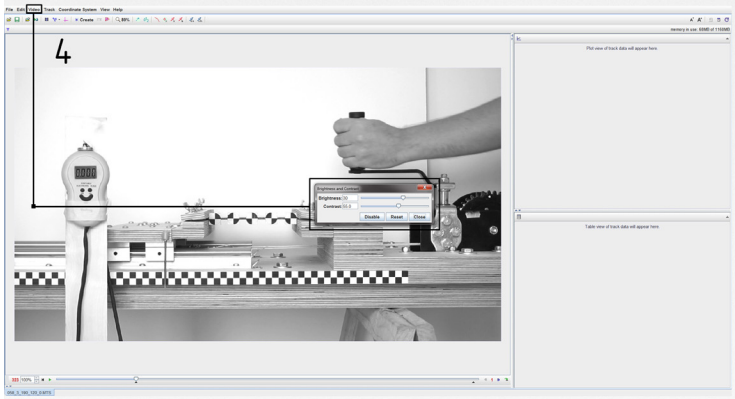

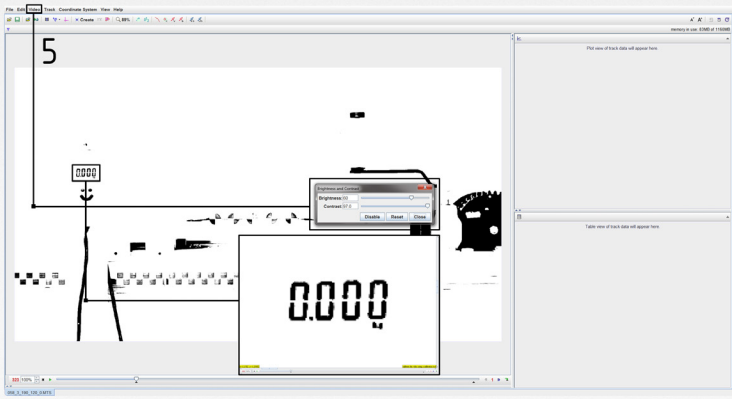

Ucs-Neutral axis points setup

[Axes] Default position at 320x240 pixel values
[Xaxis1-Xaxis2] 1st and last track points of the geometry. N.A.
[Tape A] Attached to Xaxis1-Xaxis2 points (guide for all next markers)

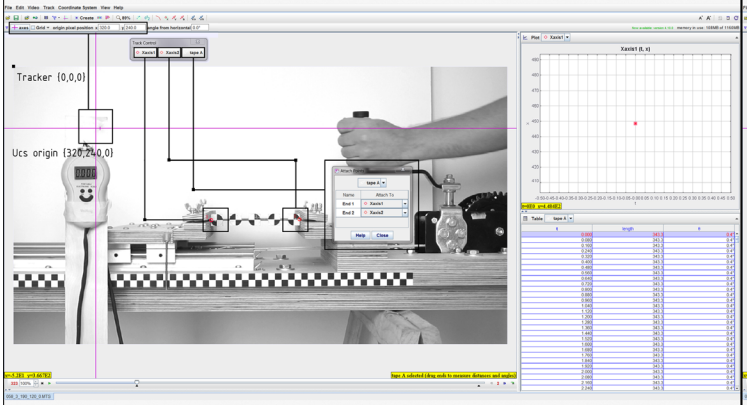

Autotracker

Creates one or more template images of a feature of interest and then searches each frame for the best match to that template. The best match is the one with the highest match score, a number that is inversely proportional to the sum of the squares of the RGB differences between the template and match pixels. Once the best match is found, it is compared with nearby match scores to determine an interpolated sub-pixel best match position.

Track points setup/Template

[Pt1-Pt5] Track points
[Sc1-Sc2] 1st scale factor reference points of constant 230mm length
[Xaxis1,Xaxis2, Pt1-Pt5, Sci1,Sc2] Pts template.trk export file

Target: User defined
Evolution Rate: 5%
Look Ahead: On
Automark: 4
Step size:2

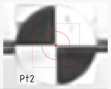

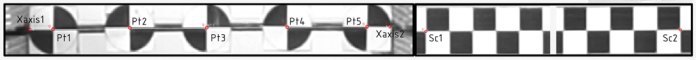

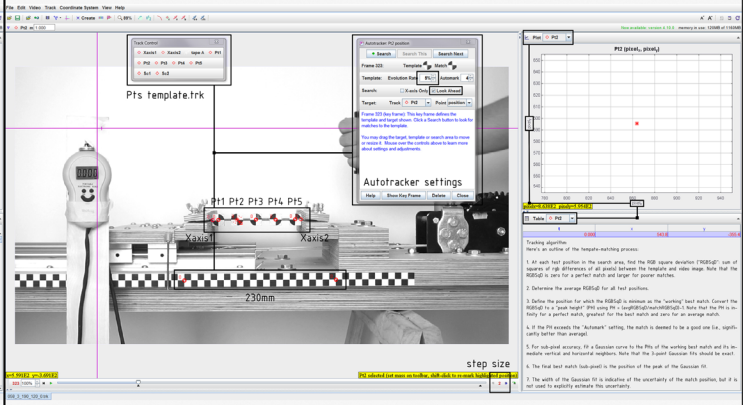

Force gauge tracking

[Rgb Region] Pixel radius: 1
Luma values: 0-255
[Rgb Region A-Z, Aa-Ac] luma.trk export file

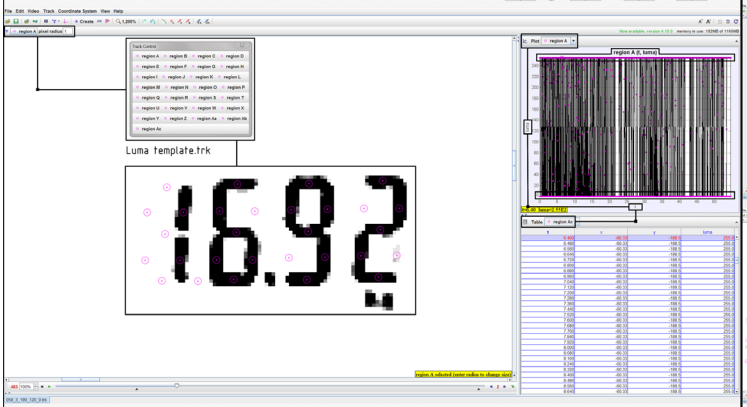

Folder/file naming convention:

#N_t_l_b_a
sample #_thickness_length_breadth_warp weft angle

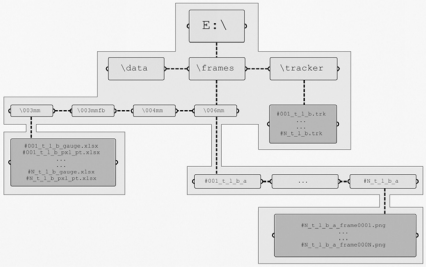

Data export

1.Tracked points [Xaxis1,Xaxis2, Pt1-Pt5, Sci1,Sc2]
067_3_190_120_45_pxl_pt.xlsx
2.Tracked luma values [Rgb Region A-Z, Aa-Ac]
067_3_190_120_45_gauge.xlsx
3.Frames [000-NNN]
067_3_190_120_45_000.png

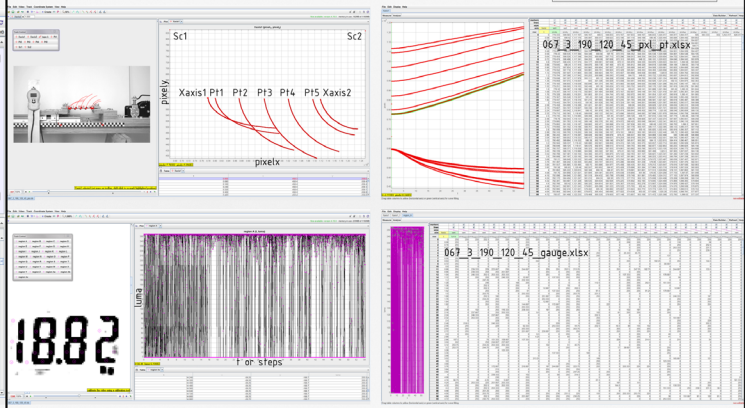

(Un)Resolved issues

[Jumpy]
Snap through buckling, Possible buckling mode 2 at first steps.
Resolution: Increase eccentricity

[Jerky]
Vibrations, Low overall bench weight, partially corrupted lead screw-gear transmission, continuous AF mode, variable exposure, excessive rotation and x axis point transformations.
Resolution: Frequent winch and linear guides oiling, lead screw bolt calibration, lock focus, lock exposure.

[Masky]
Too wide bench clamps, lens distortion, uneaven exposure
Resolution: Distant and high tripod FOV setup, centered video light position, lens zoom set at max optical 50mm (75mm fullframe equivalent)

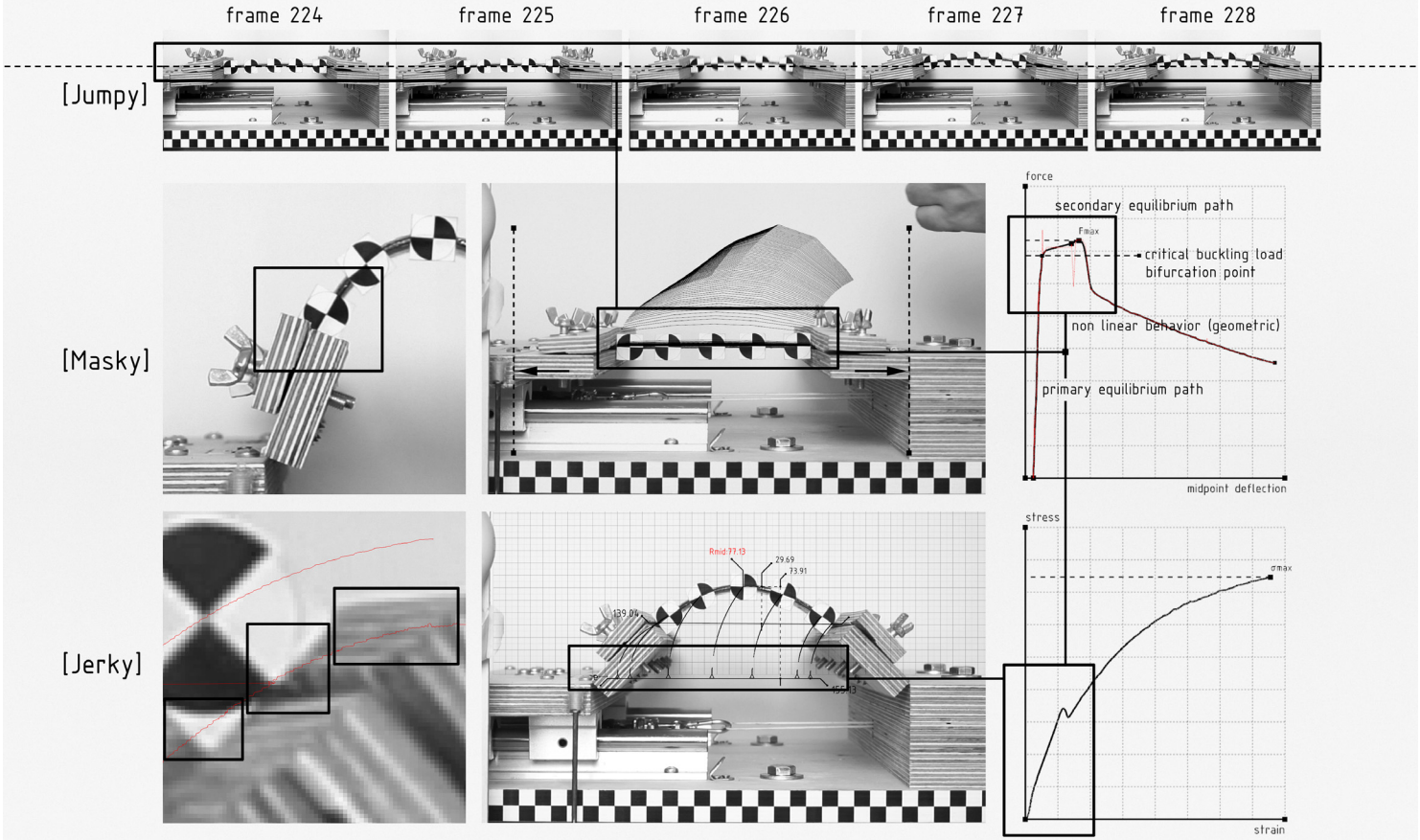

Calibration-Omitted tests

Fracture mode (test sample#, fiberglass wf angle)

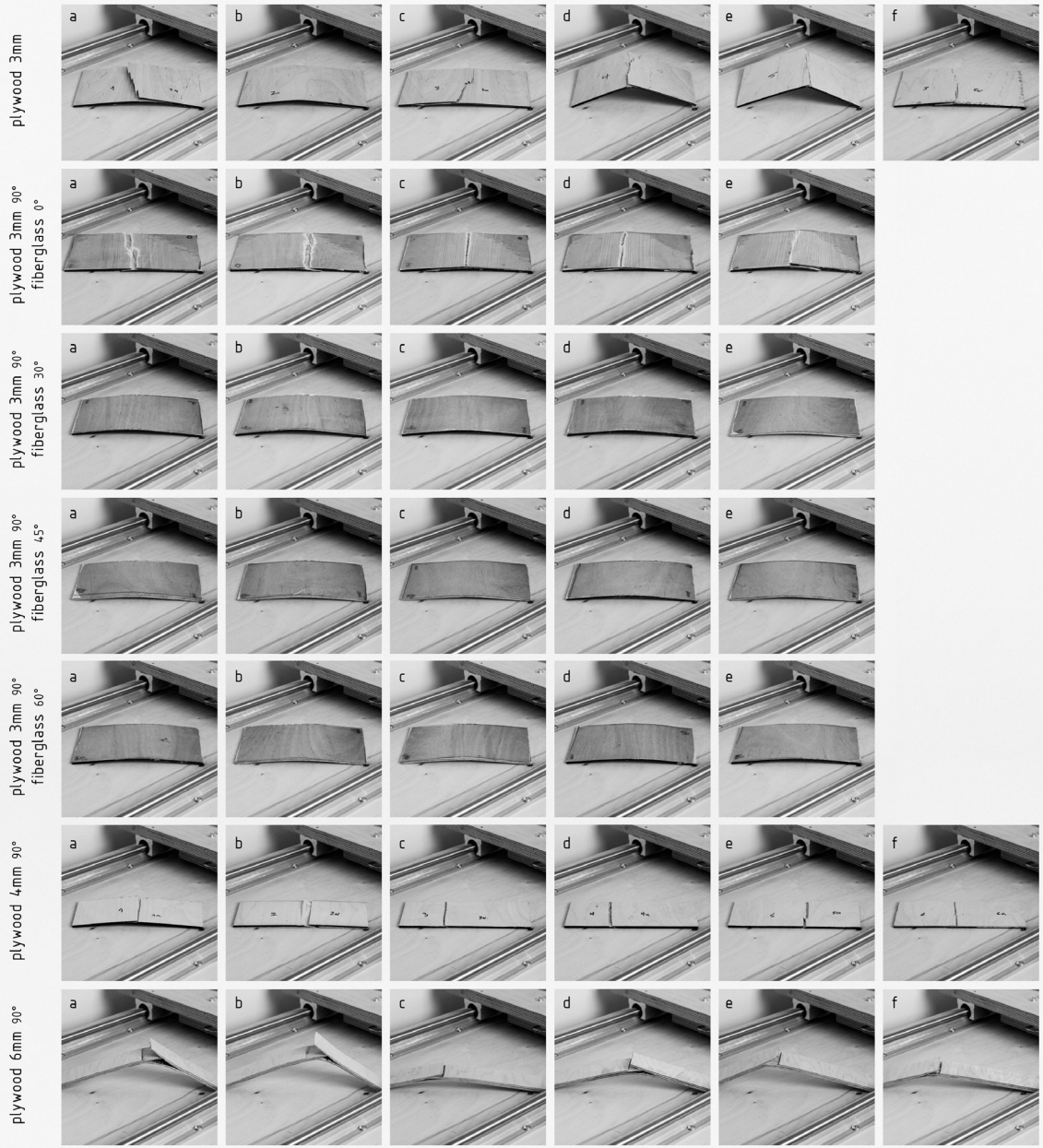

Fracture mode (layers#, fiberglass wf angle)

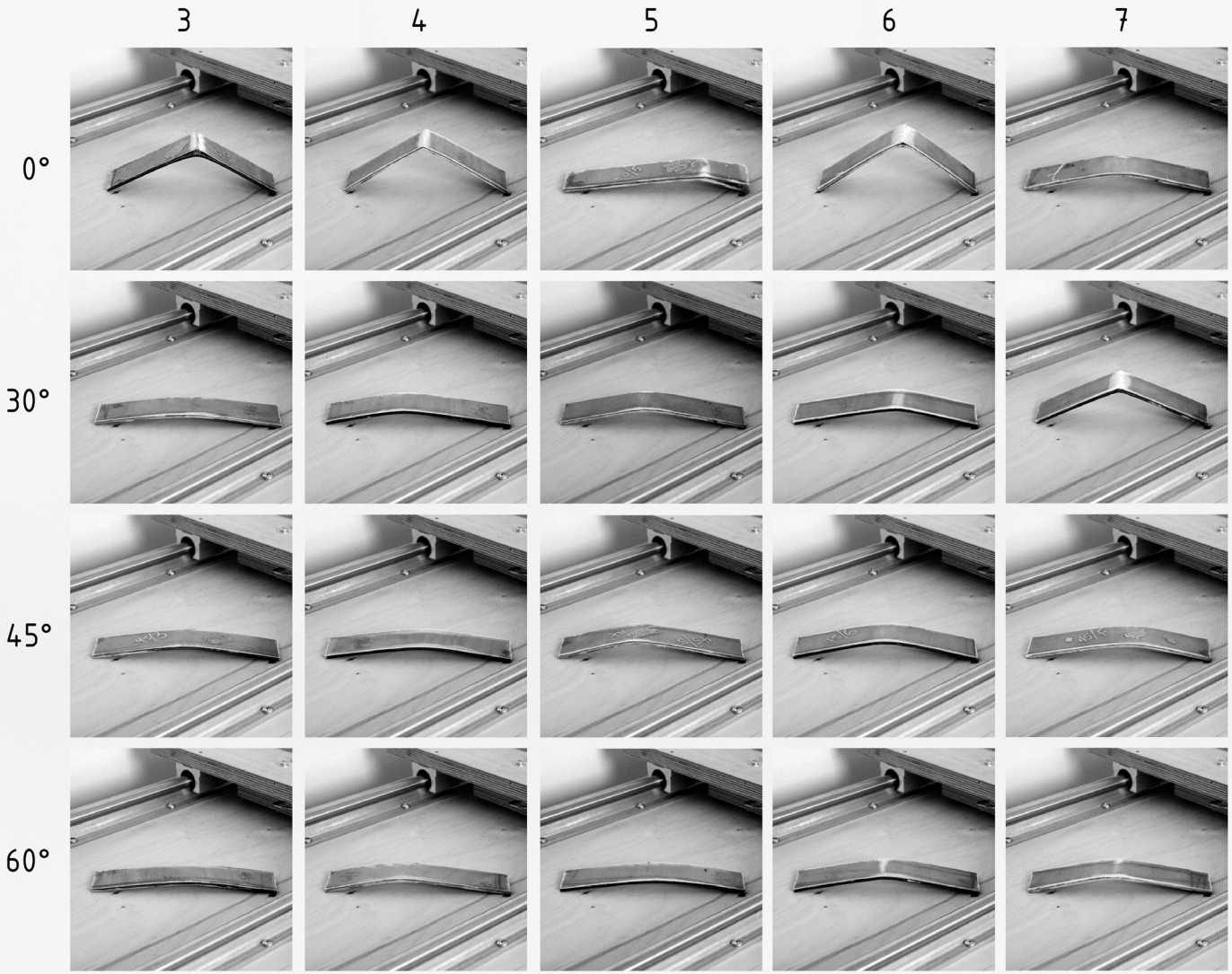

06

Grasshopper Definition

Imports all necessary files
File/folder naming convention embeds test sample dimensions, to be used in stress etc calculations

Applies transformations that align the Neutral Axis of the test sample to the world x axis and bring the analysis data to real world scale.

Tracked markers for each frame are set as 2d points.

The computer vision samples of the diy force gauge lcd screen are transformed to force (N) values. Neighbour averaging along with standard deviation and variance are applied to take care of unreadable values and to filter out unreasonable spike values respectively.

Central deflections and force gauge values make up the deflection-force curve diagrams.

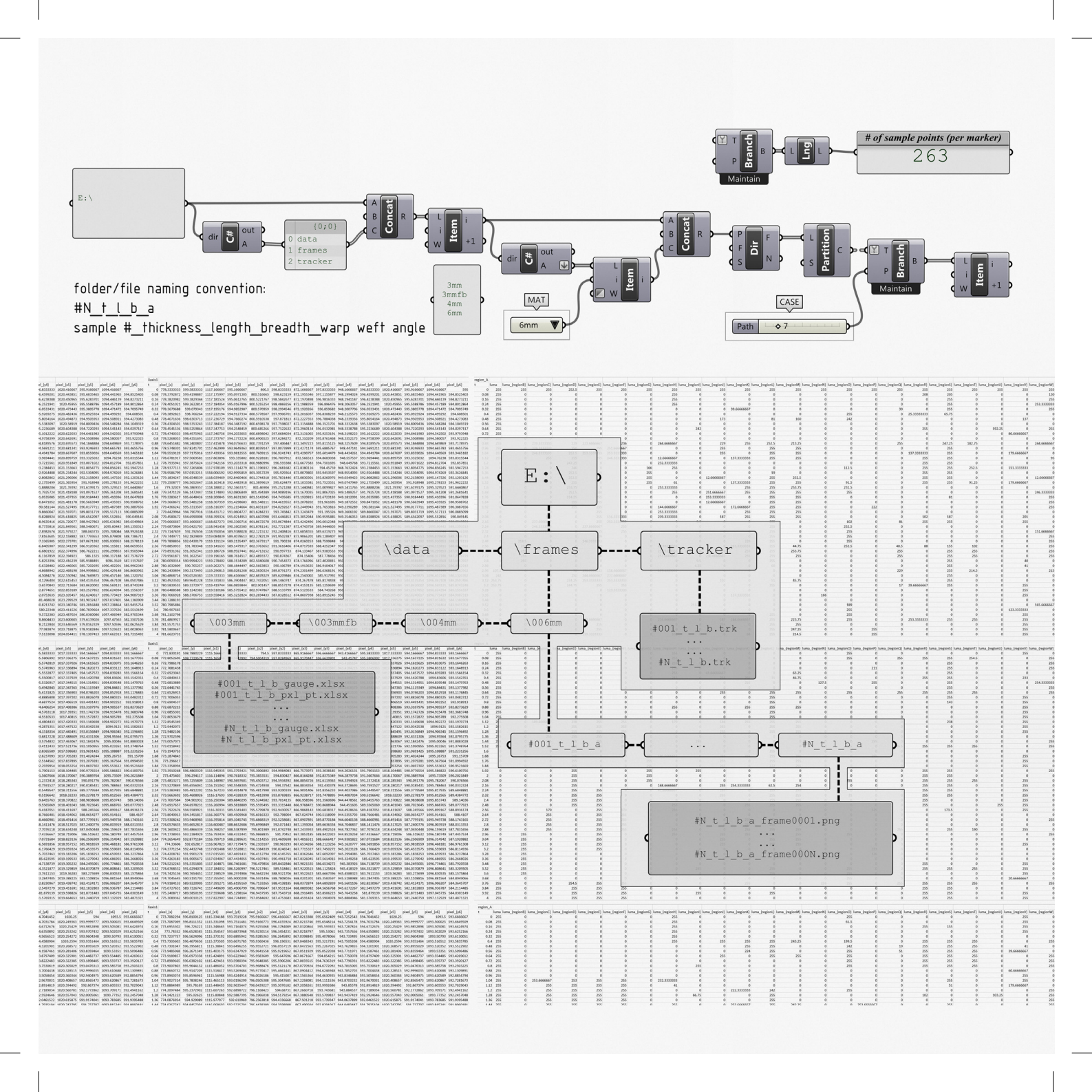
Maintain
# of sample points (per marker)
263
E:\
{0;0}
0 data
1 frames
2 tracker
dir
out
Concat
Item
Partition
Dir
Lng
Path
MAT
CASE
3mm
3mmfb
4mm
6mm
6mm
Path
7
folder/file naming convention:
#N_t_l_b_a
sample #_thickness_length_breadth_warp weft angle
\data
\frames
\tracker
\003mm
\003mmfb
\004mm
\006mm
#001_t_l_b.trk
#N_t_l_b.trk
#001_t_l_b_gauge.xlsx
#001_t_l_b_pxl_pt.xlsx
#N_t_l_b_gauge.xlsx
#N_t_l_b_pxl_pt.xlsx
#001_t_l_b_a
#N_t_l_b_a
#N_t_l_b_a_frame0001.png
#N_t_l_b_a_frame000N.png

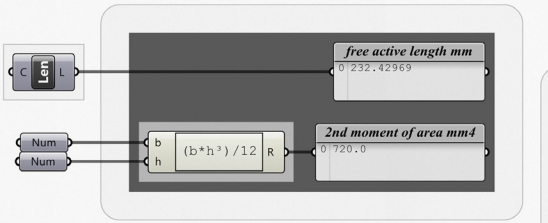

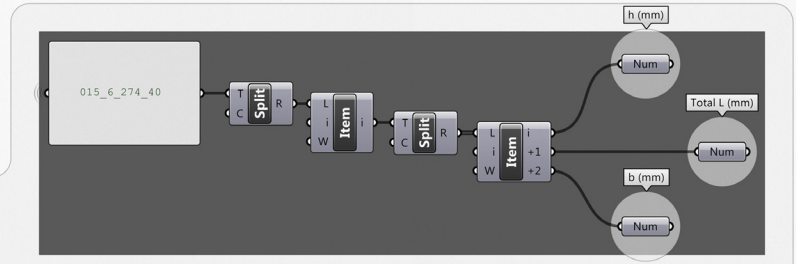

Material DIM

Images

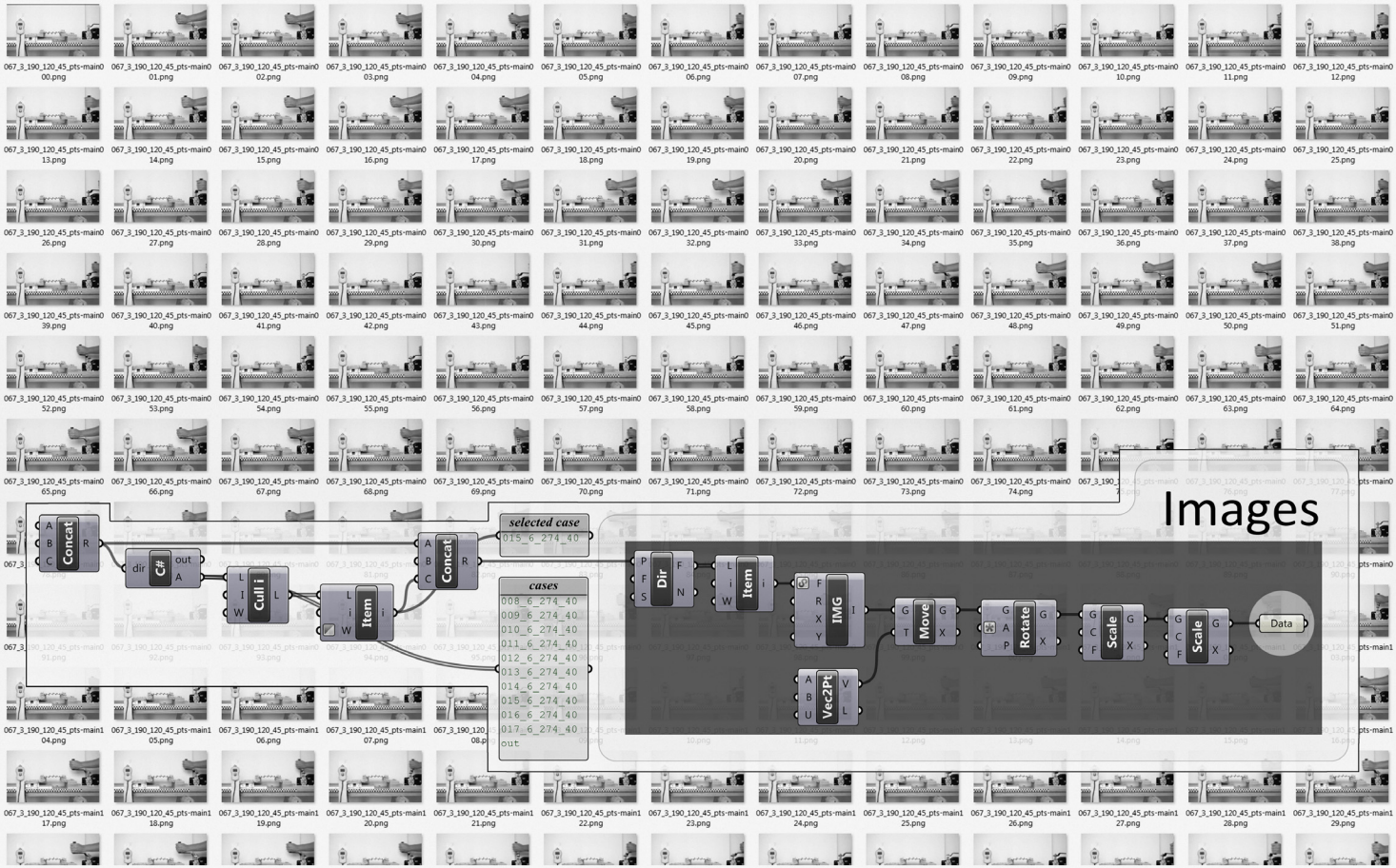

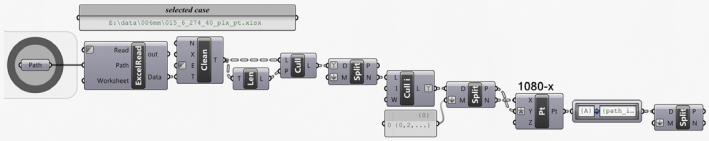
selected cave
E:\data\006mm\015_6_274_40_pix_pt.xlsx
Path
Read
Path
Worksheet
ExcelRead
out
data
Clean
Len
Cull
Split
Cull i
1080-x
Path
Split

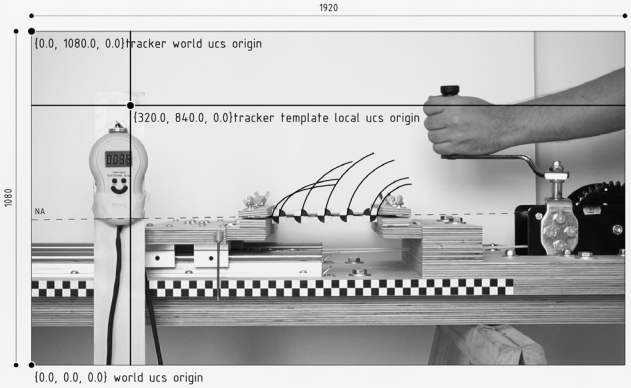
1920
1080
{0.0, 1080.0, 0.0}tracker world ucs origin
{320.0, 840.0, 0.0}tracker template local ucs origin
NA
{0.0, 0.0, 0.0} world ucs origin

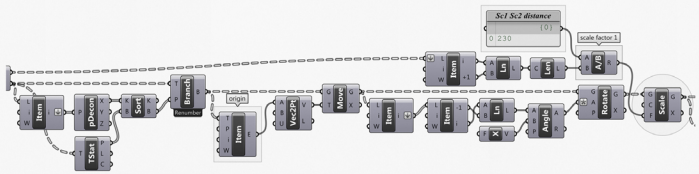
Sc1 Sc2 distance
scale factor 1
Item
Ln
Len
A/B
Rotate
Scale
pRecon
Sort
Branch
Reverse
TStart
origin
Move
Vec2Pt
Angle

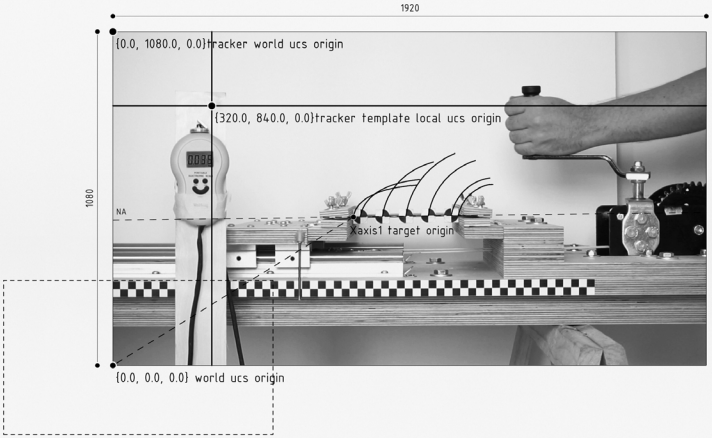
1920
1080
{0.0, 1080.0, 0.0}tracker world ucs origin
{320.0, 840.0, 0.0}tracker template local ucs origin
NA
Xaxis1 target origin
{0.0, 0.0, 0.0} world ucs origin

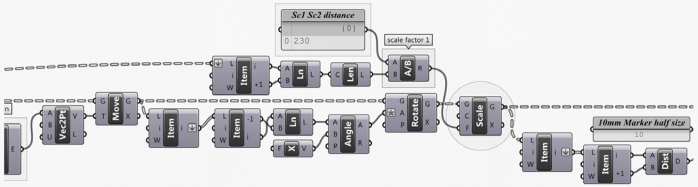
Sc1 Sc2 distance
scale factor 1
Item
Ln
Len
A/B
Rotate
Scale
Move
Vec2Pt
Angle
10mm Marker half size
Dist

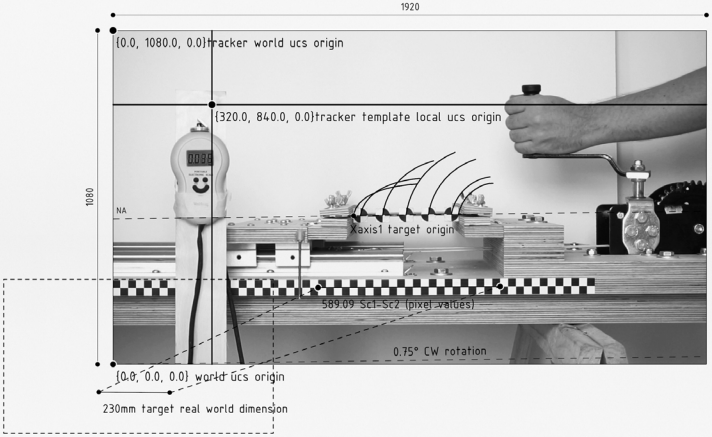
1920
1080
{0.0, 1080.0, 0.0}tracker world ucs origin
{320.0, 840.0, 0.0}tracker template local ucs origin
NA
Xaxis1 target origin
589.09 Sc1-Sc2 [pixel values]
0.75° CW rotation
{0.0, 0.0, 0.0} world ucs origin
230mm target real world dimension

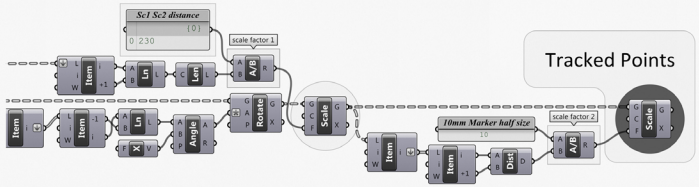
Sc1 Sc2 distance
scale factor 1
Tracked Points
Item
Ln
Len
A/B
Rotate
Scale
Angle
10mm Marker half size
scale factor 2
Dist

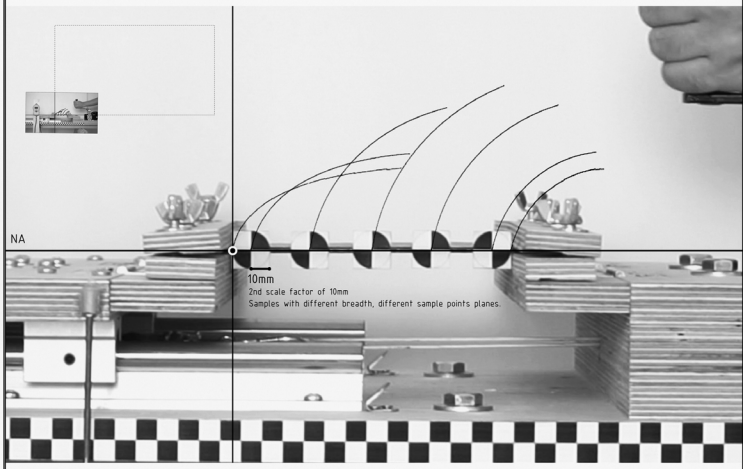
NA
10mm
2nd scale factor of 10mm
Samples with different breadth, different sample points planes.

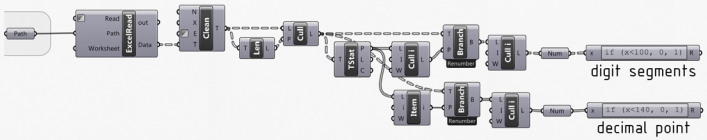
digit segments
decimal point

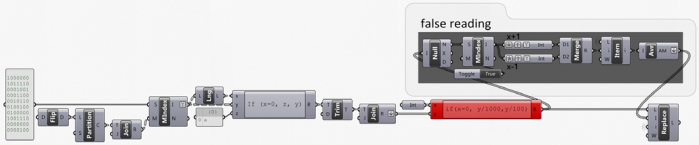
false reading

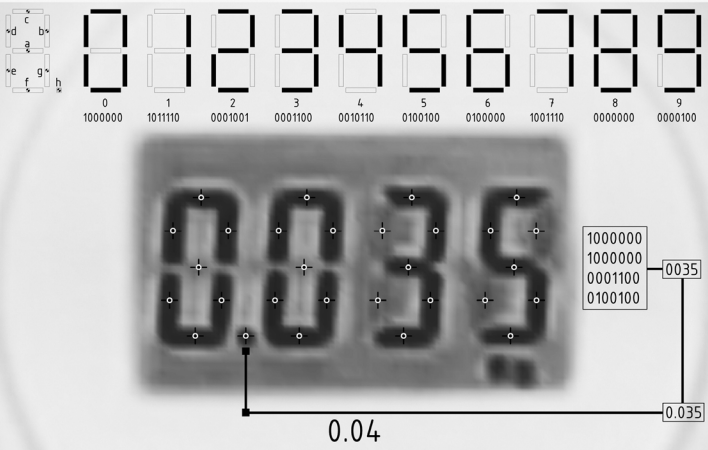
0 1 2 3 4 5 6 7 8 9
0 1 2 3 4 5 6 7 8 9
1000000
1011110
0001001
0001100
0010110
0100100
0100000
1001110
0000000
0000100
0.035
1000000
1000000
0001100
0100100
0035
0.04
0.035

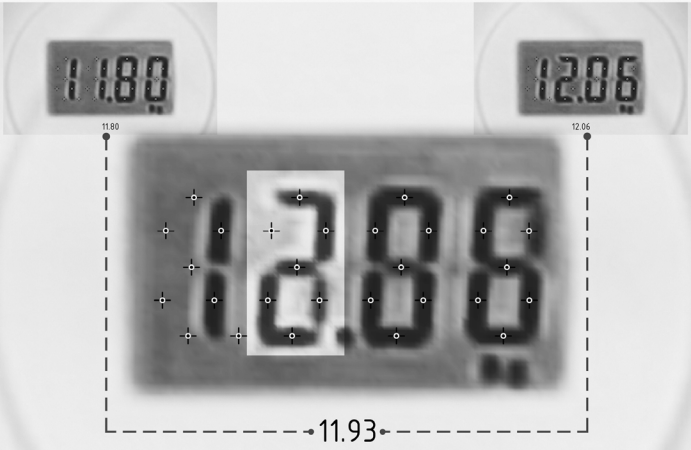
11.80
12.06
11.93

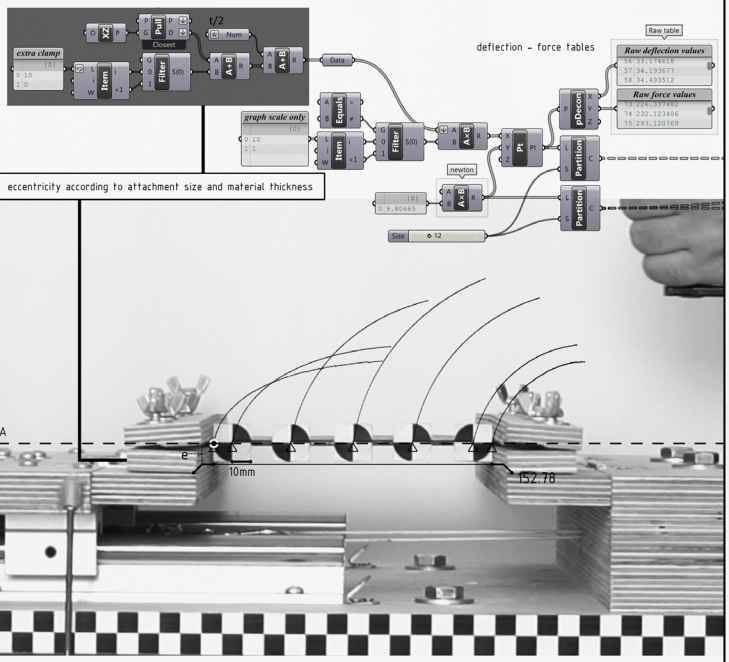
extra clamp
t/2
deflection - force tables
Raw table
Raw deflection values
Raw force values
graph scale only
eccentricity according to attachment size and material thickness
newton
NA
e
10mm
152.78

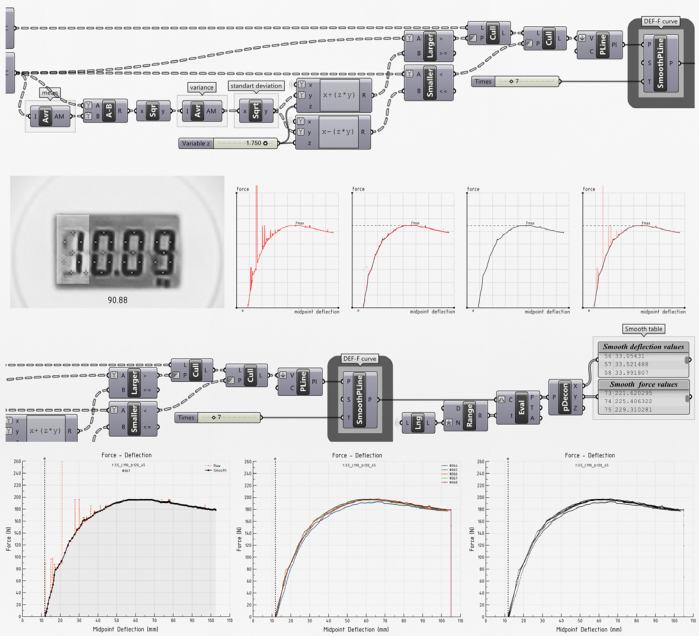
DEF-F curve
Smooth table
Smooth deflection values
Smooth force values
90.88
Force - Deflection
Midpoint Deflection (mm)
Force (N)

07

Grasshopper Definition

Geometric representation of tracked points as polylines.

Central deflections and endpoints are the inputs of the elastica curve script component (as shared by Will McElwain at grasshopper3d.com forum).

Tracked polylines and resulting elasticas are represented in various possible configurations, to understand and evaluate tracked results, for overlaps, to spot possible test mechanism shortcomings etc.

The elasticas curvature radii ρ at midpoint deflections are used for the stress etc calculations.

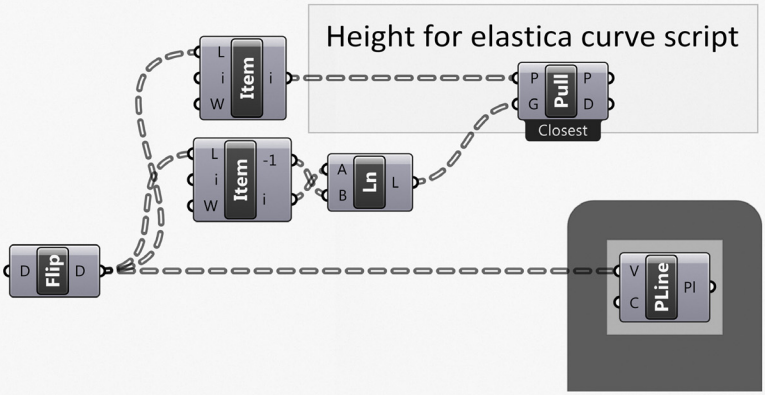
Height for elastica curve script
Item
Item
Pull
Closest
Ln
Flip
PLine

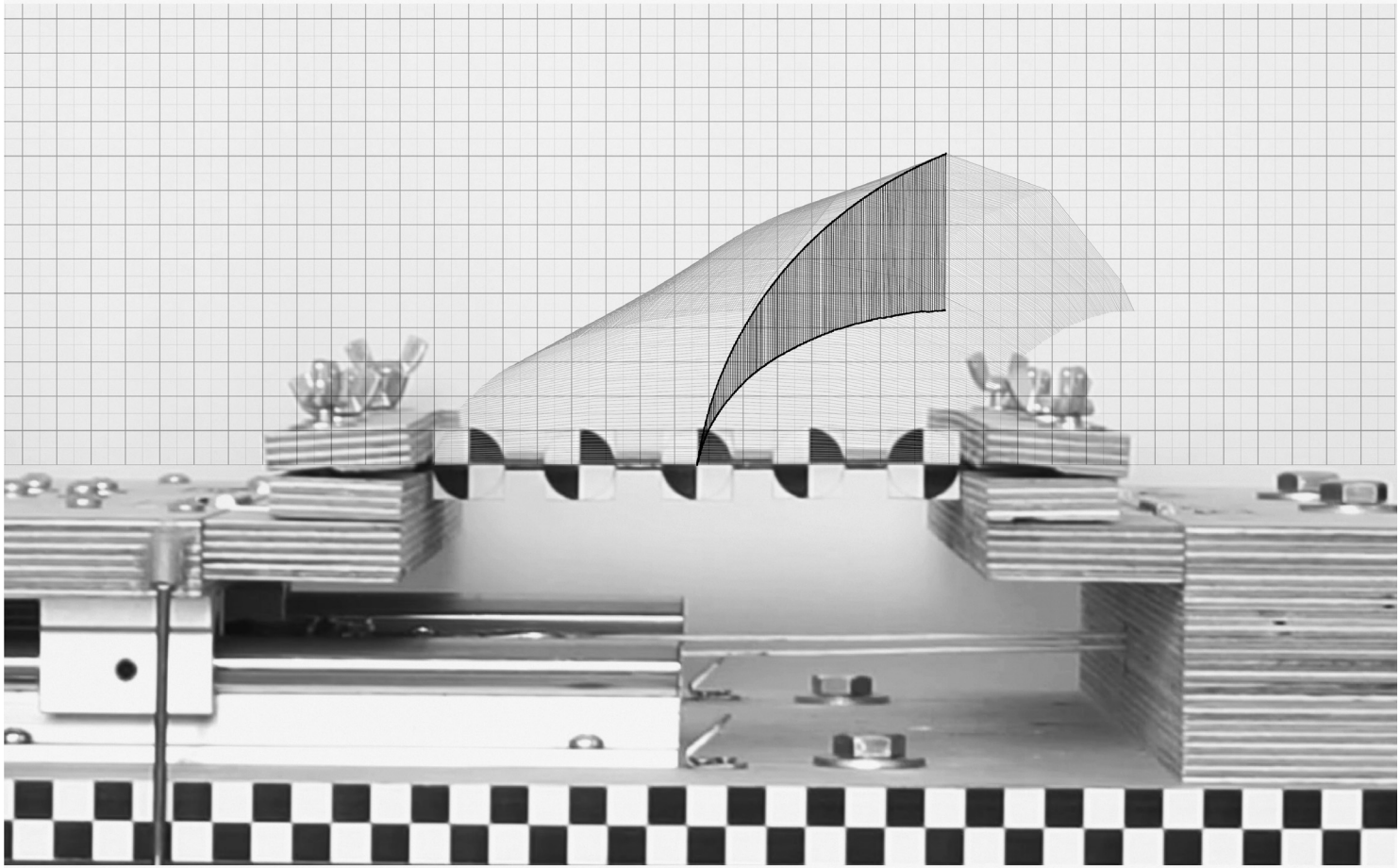

Height for elastica curve script

Deflection Polys Video

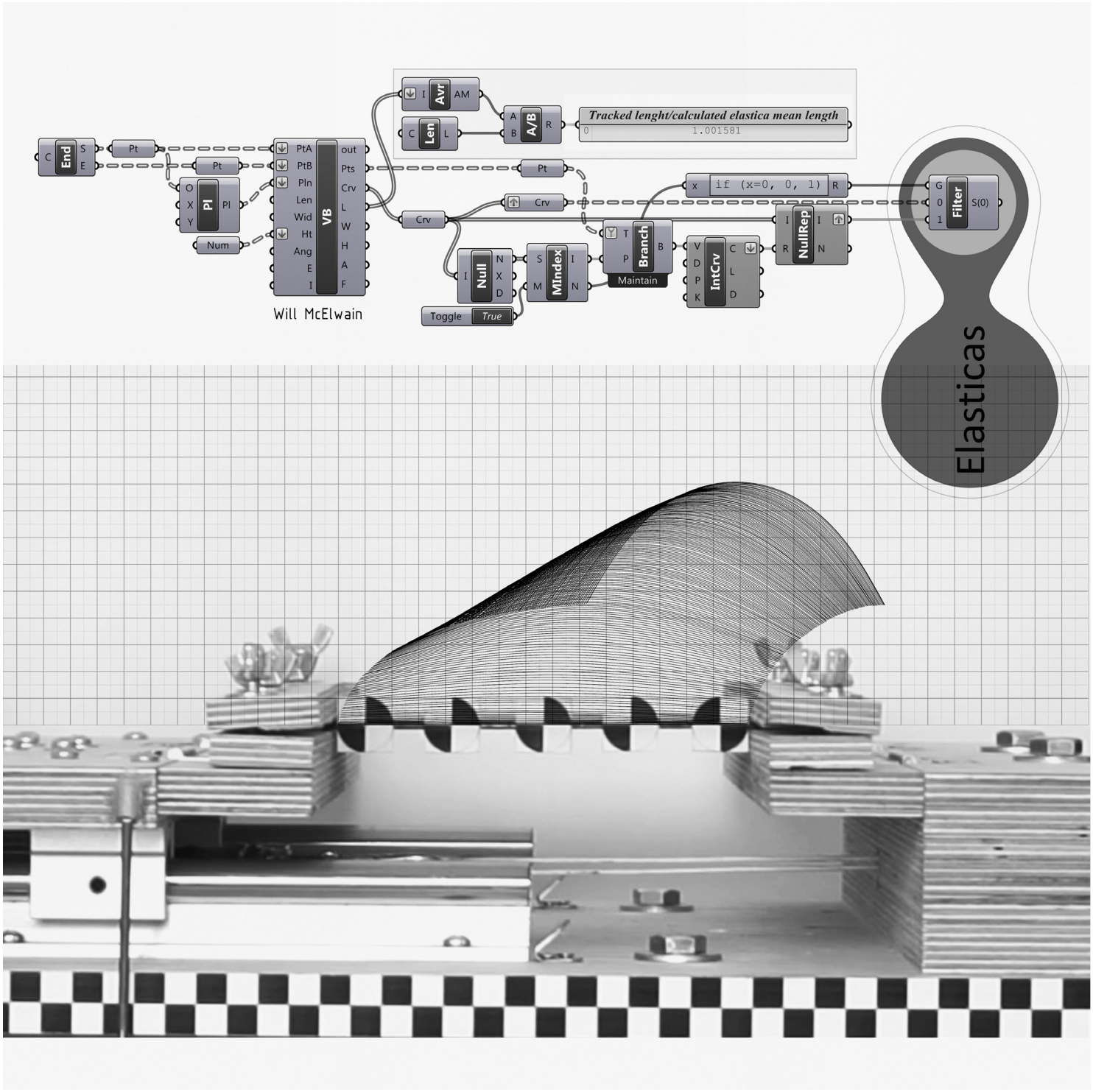
End
Pt
Pl
Num
VB
PtA
PtB
Pln
Len
Wid
Ht
Ang
out
Pts
Crv
L
W
H
A
F
Avr
AM
Len
A/B
Tracked lenght/calculated elastica mean length
1.001581
Null
MIndex
Branch
Maintain
IntCrv
NullRep
if (x=0, 0, 1)
Filter
S(0)
Toggle
True
Will McElwain
Elasticas

Deflection Polys
Centered Floored

load point x translation
{0}
0.008283
Nettelbladt

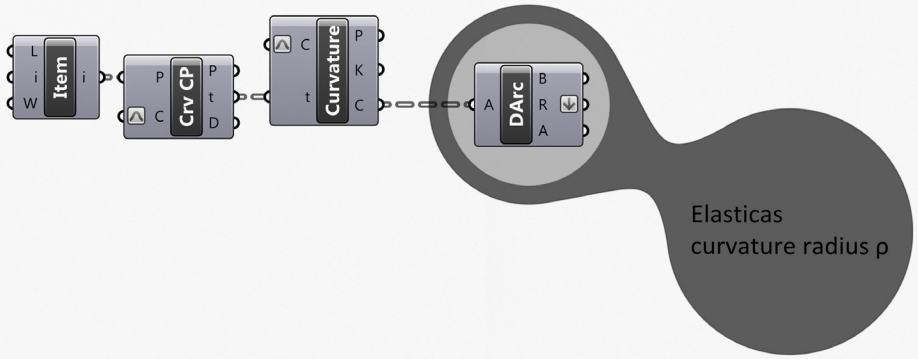
L
i
W
Item
i
P
C
Crv CP
P
t
D
C
t
Curvature
P
K
C
A
DArc
B
R
A
Elasticas
curvature radius ρ

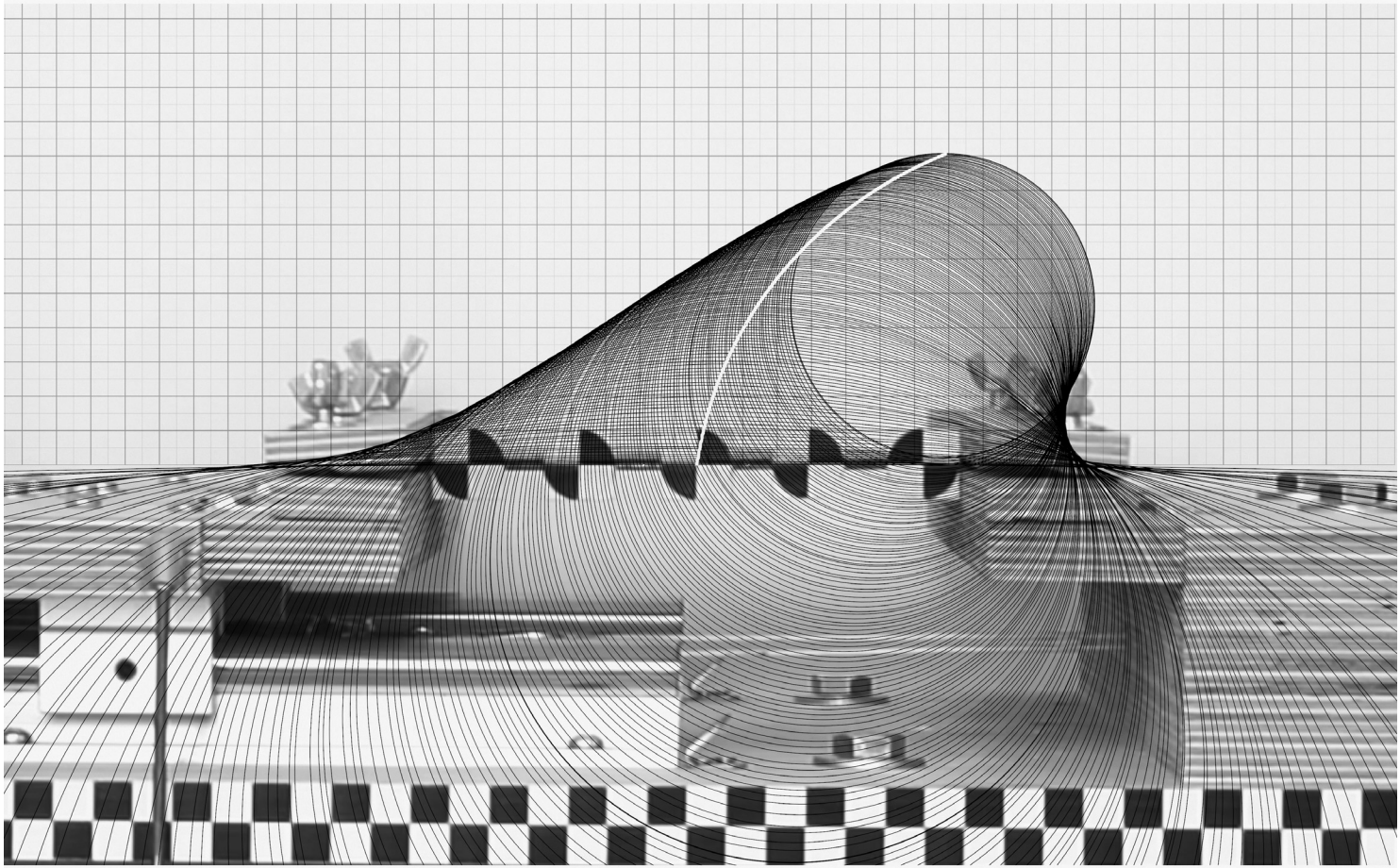

08

Grasshopper Definition

A hefty part of the definition sets up a video analysis report. Tracked values and results along with test sample information are visualised in order to output a video report for every selected test sample, in order to analyse and document the procedure and results and to compare various sample setups.

Also some key aspects of the tests like the speed of load application, the endurance of each sample etc can be observed in time only through these video reports, since the only sensor used is the diy force gauge.

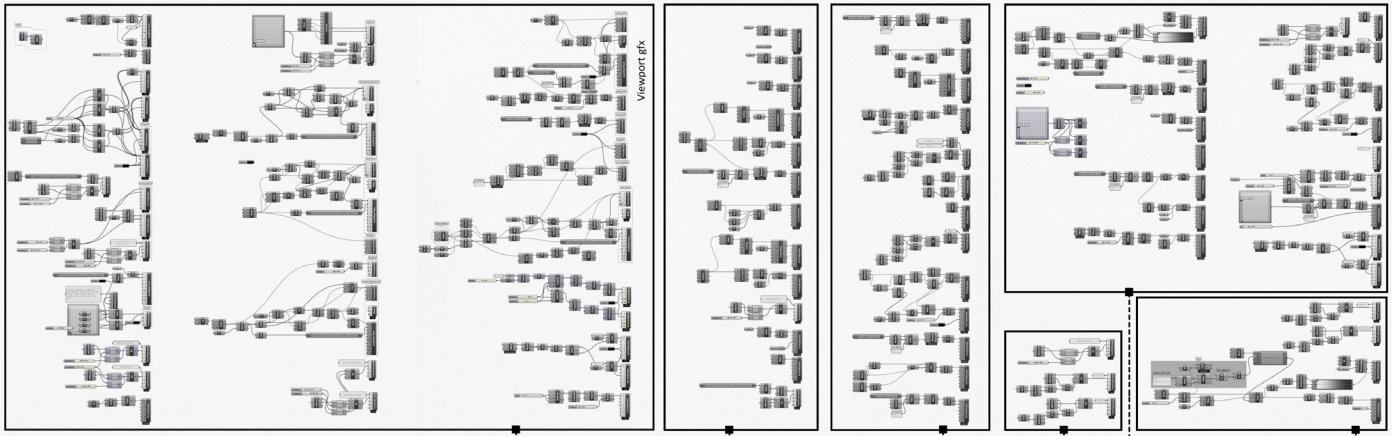

Video reports layout template

gauge view

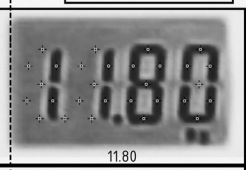

sample info view

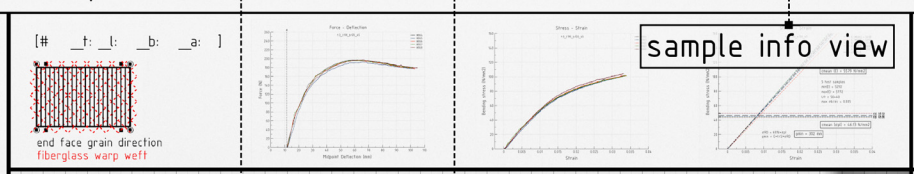

curves view

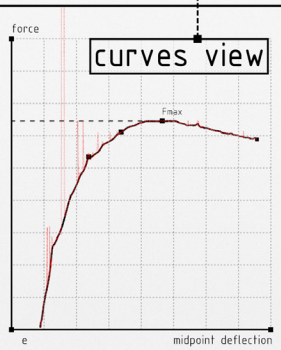

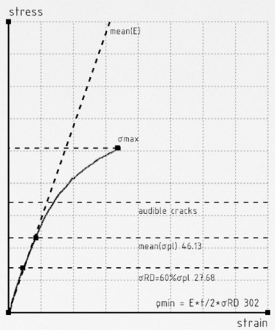

video view

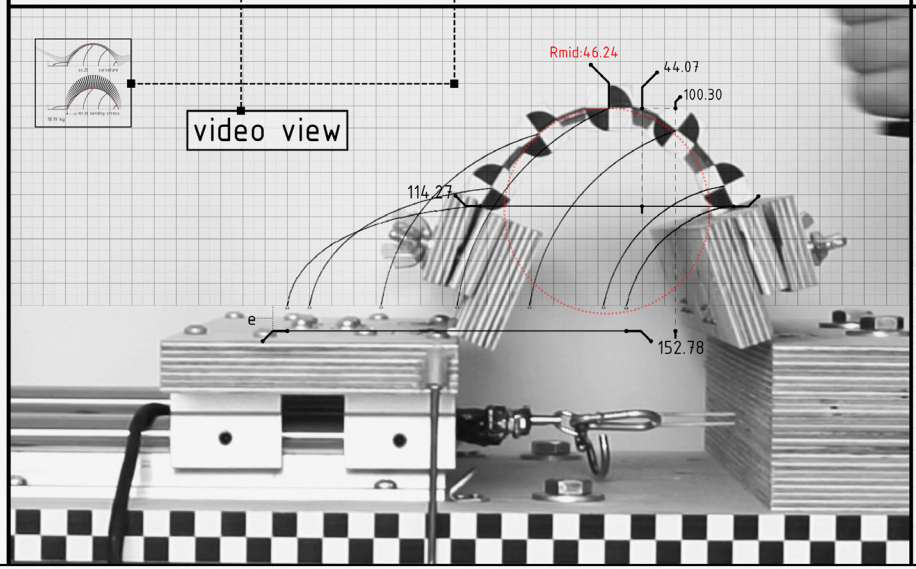

tracked geometry view

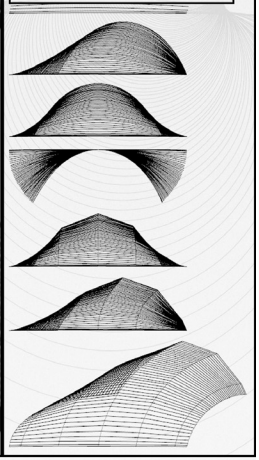

Video report frames

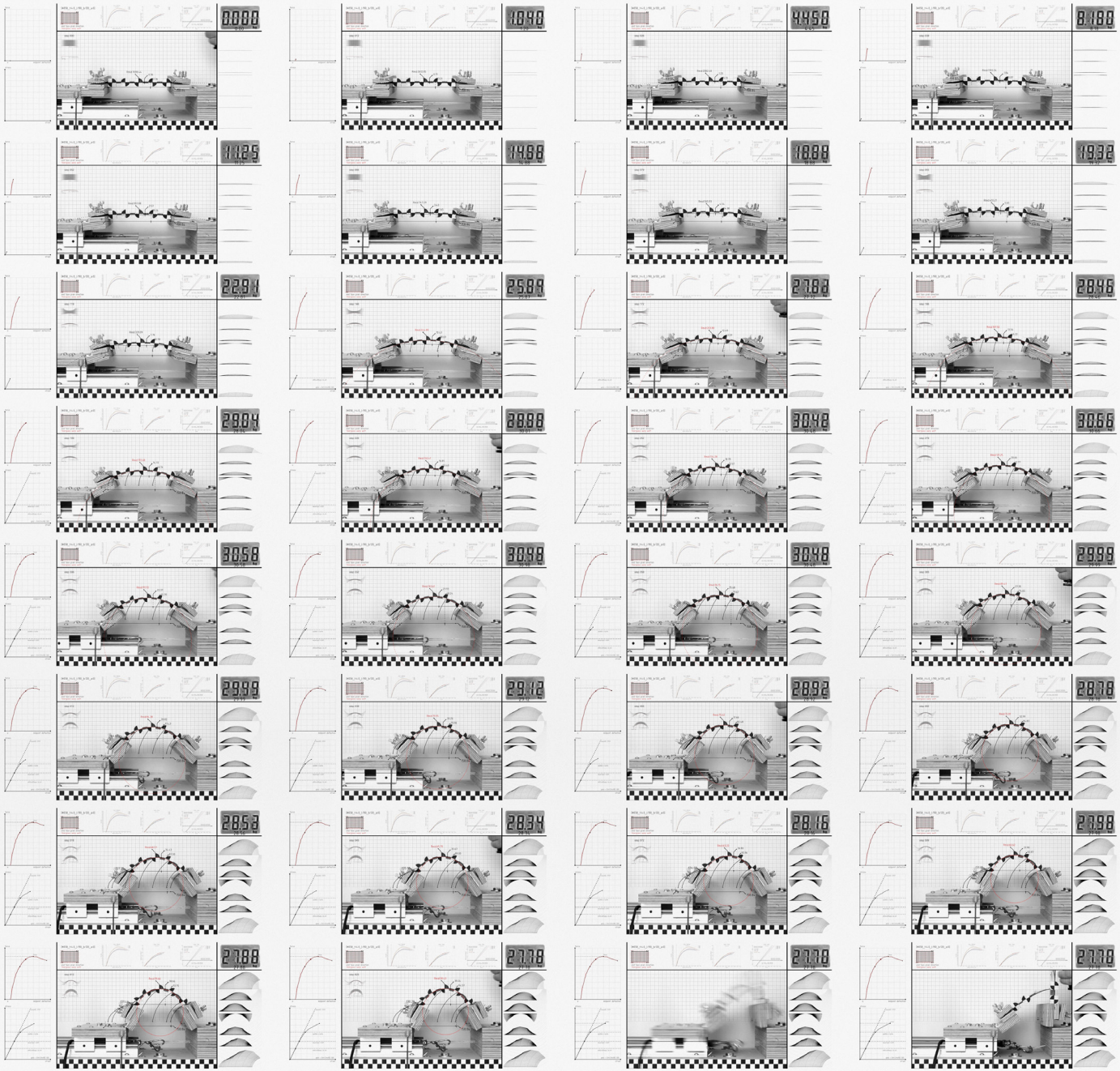

09

Grasshopper Definition

Calculations according to Fukuda H. and Lienhard J. published work.
Stress-Strain curves

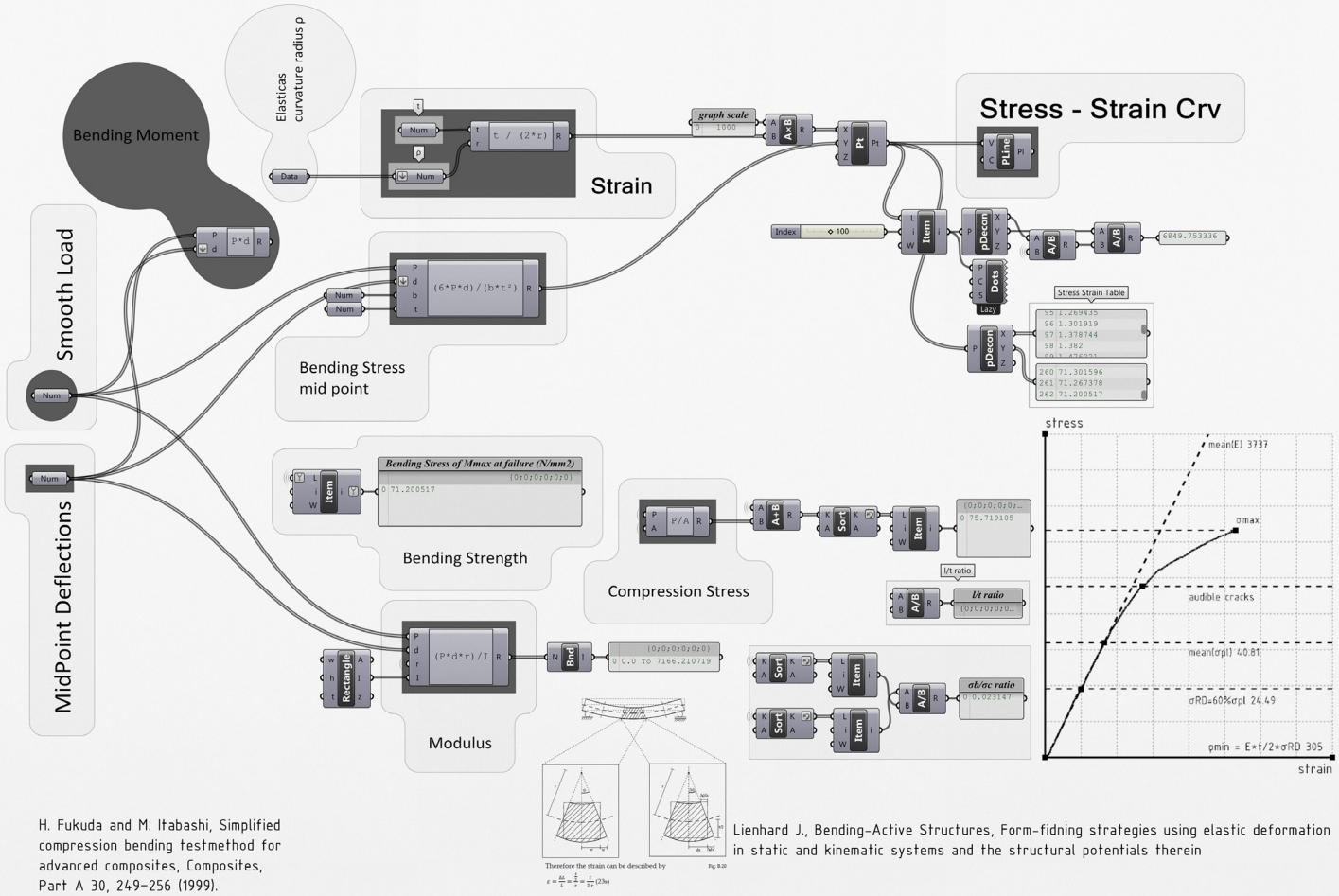

H. Fukuda and M. Itabashi, Simplified compression bending testmethod for advanced composites, Composites, Part A 30, 249–256 (1999).

Lienhard J., Bending-Active Structures, Form-fidning strategies using elastic deformation in static and kinematic systems and the structural potentials therein

2.2. Elastica-1

The elastica [7] is also applicable to calculate ρ_δ. Although the detail has already been reported in the previous papers [5, 6], a brief summary is again shown here for readers' convenience.

According to the elastica theory [7], the midspan deflection δ_δ and the radius of curvature ρ_δ of Fig. 1 can be expressed as functions of the angle of deflection at the loading point, α. They are

$$\delta_\delta/L = 2p/K(p) \tag{6}$$

$$\rho_\delta/L = 1/2pK(p) \tag{7}$$

where

$$p = \sin(\alpha/2) \tag{8}$$

$$K(p) = \int_0^{\pi/2} \frac{d\phi}{\sqrt{1 - p^2 \sin^2 \phi}} \tag{9}$$

The integral $K(p)$ is known as the perfect elliptical integral of the first kind. Therefore, ρ_δ can be calculated from δ_δ. Fig. 2 is the result. Thus, we can calculate Young's modulus from the midspan deflection even if we don't measure ρ_δ. Here, this is called the Elastica-1 method. In this method, however, the midspan deflection must be measured. One point to be noted is that the above equations were derived under the assumption of linear elasticity. As was already pointed out, the CFRPs exhibit material nonlinearity and therefore, the calculated Young's modulus includes more or less error. Further discussion will be made concerning this point at a later point.

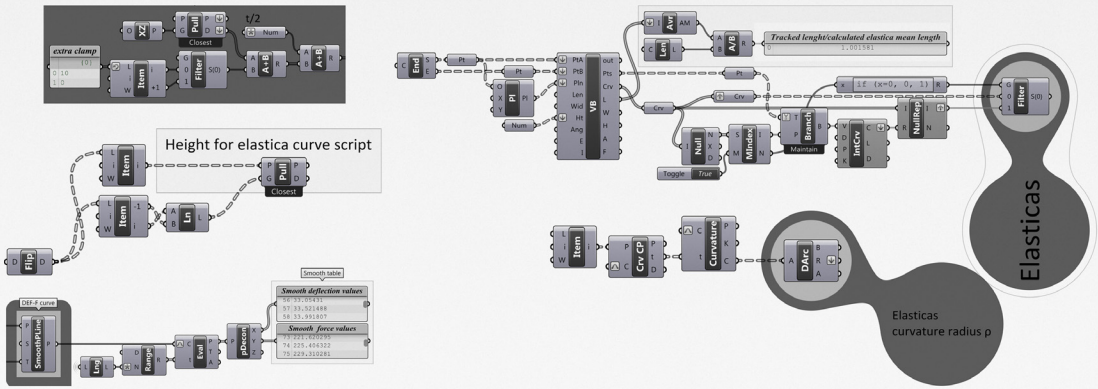

10

Results - Curves

Plywood 3mm, as base composite material
Single layer plywood-fiberglass composite at 4 warp-weft angles
Plywood 4mm and 6mm bending mechanism callibration tests

Force-Deflection curves
Stress-Strain curves
Bending modulus
active length/thickness ratio
bending/compression stress ratio
proportional limit stress
minimum bending radius

frame at proprtional limit stress-radius
frame at (just before) fracture stress-radius

Multiple layers composites at 4 warp-weft angles

Force-Deflection curves
Stress-Strain curves
Bending modulus
prorpotional limit stress
minimum bending radius
Linear approximation of fiberglass layers-bending modulus

Embedding results to Ashby Chart | Bending Active-ELastic kinetics material selection

Compression bending tests curves-results | Base layer 3mm plywood | Single layer fiberglass

Base layer composite material | Single layer plywood-fiberglass composite | @ four warp-weft angles | Test bench calibration tests | Reference results

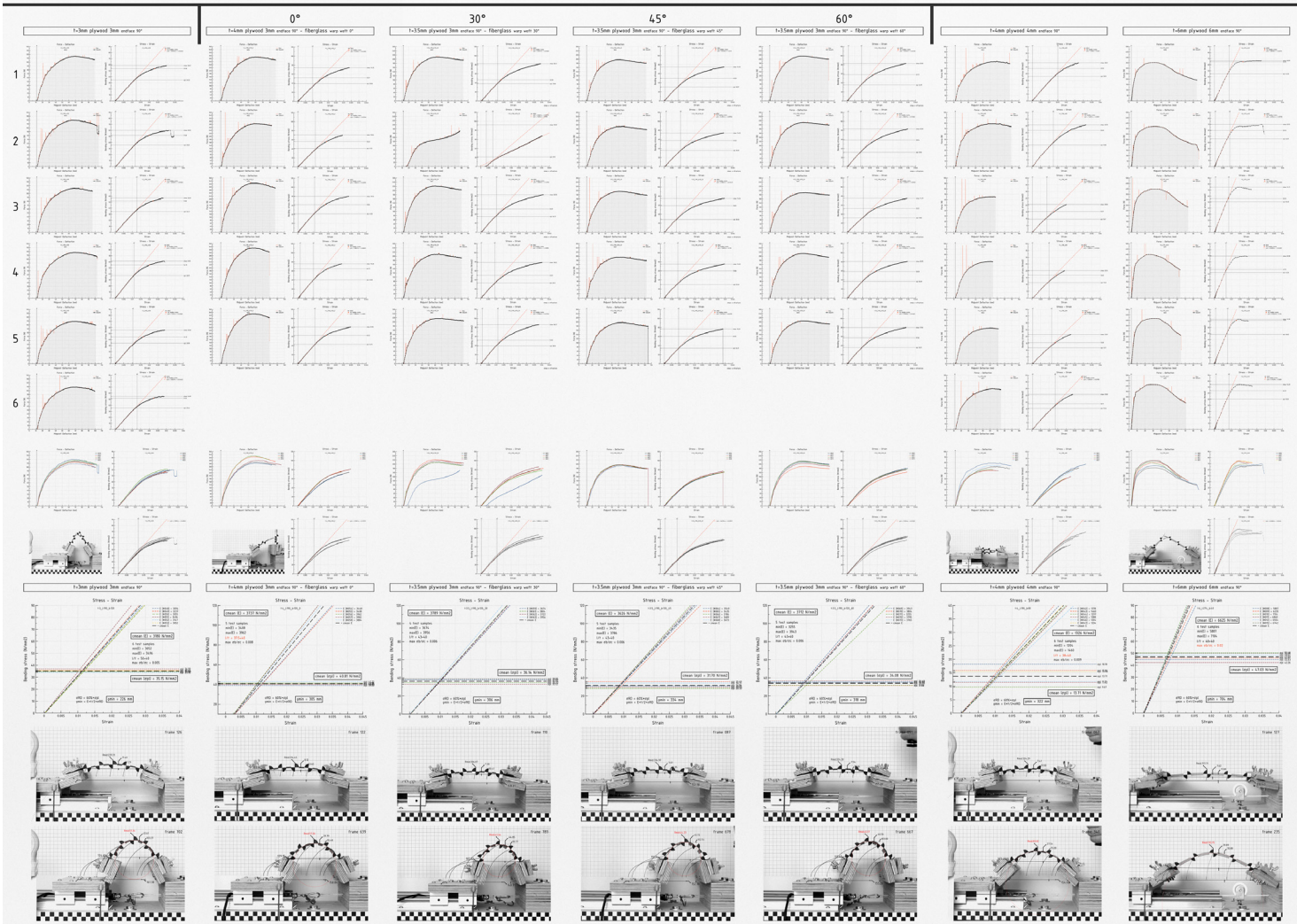

t:3mm plywood
l:190mm, b:120mm
active l:~150mm
6 tests
meanE=3180 N/mm2
meanσpl=35.15 N/mm2
φmin=226mm

t:4mm plywood-fiberglass
l:190mm, b:120mm
active l:~150mm
5 tests
meanE=3737 N/mm2
meanσpl=40.81 N/mm2
φmin=305mm

t:3.5mm plywood-fiberglass
l:190mm, b:120mm
active l:~150mm
5 tests
meanE=3789 N/mm2
meanσpl=36.14 N/mm2
φmin=306mm

t:3.5mm plywood-fiberglass
l:190mm, b:120mm
active l:~150mm
5 tests
meanE=3626 N/mm2
meanσpl=31.70 N/mm2
φmin=334mm

t:3.5mm plywood-fiberglass
l:190mm, b:120mm
active l:~150mm
5 tests
meanE=3712 N/mm2
meanσpl=34.08 N/mm2
φmin=318mm

t:4mm plywood
l:190mm, b:80mm
active l:~150mm
6 tests
meanE=1326 N/mm2
meanσpl=13.71 N/mm2
φmin=322mm

t:6mm plywood
l:274mm, b:40mm
active l:~234mm
6 tests
meanE=1326 N/mm2
meanσpl=13.71 N/mm2
φmin=322mm

Compression bending tests curves-results | Base layer 3mm plywood | Single layer fiberglass

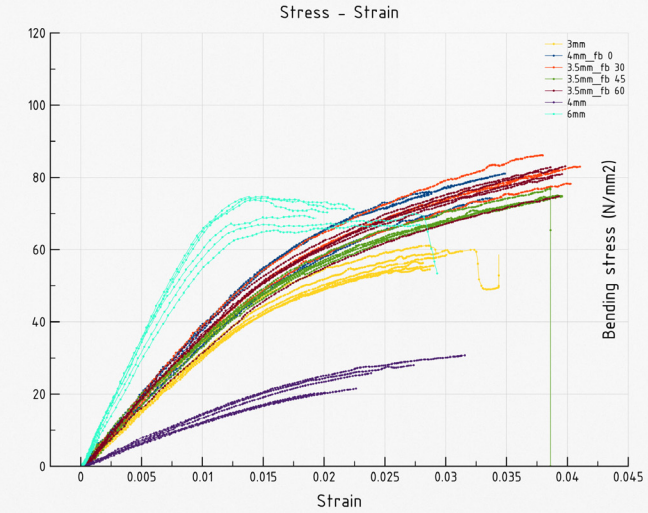

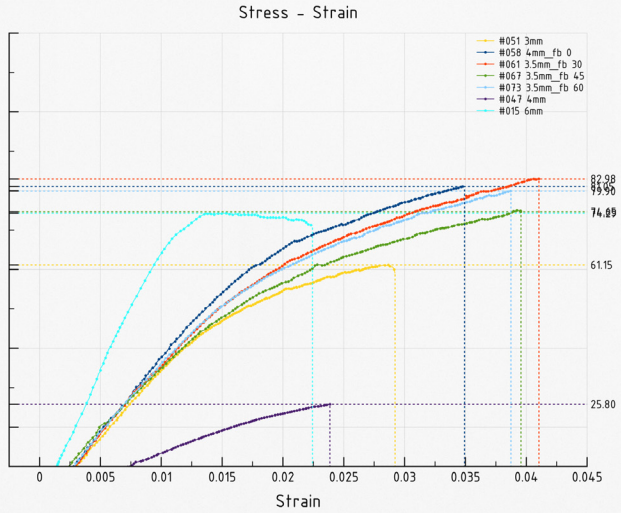

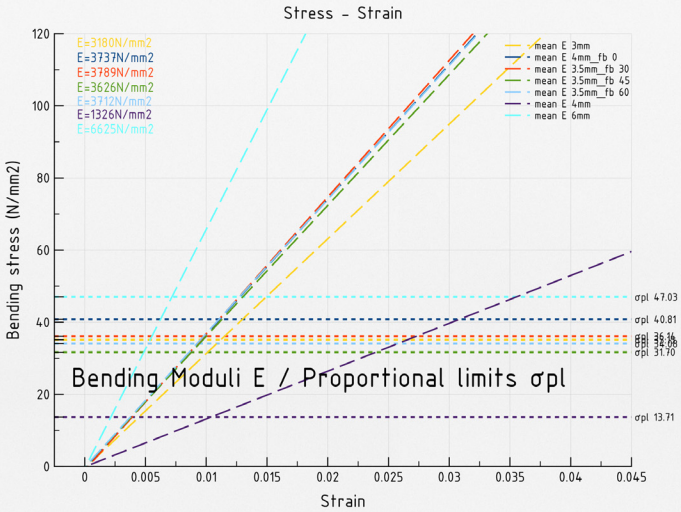

Bending Moduli E / Proportional limits σpl

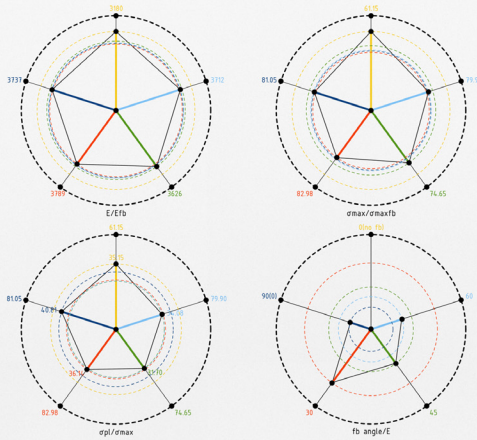

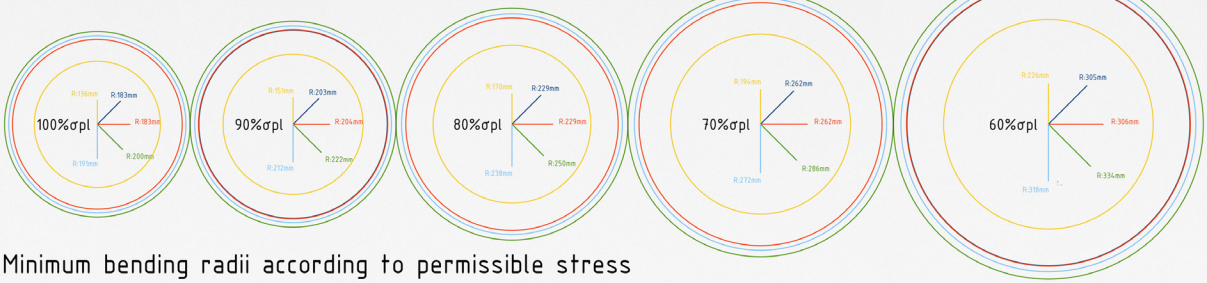

Minimum bending radii according to permissible stress

Compression bending tests curves-results | Base layer 3mm plywood | Multiple layers fiberglass

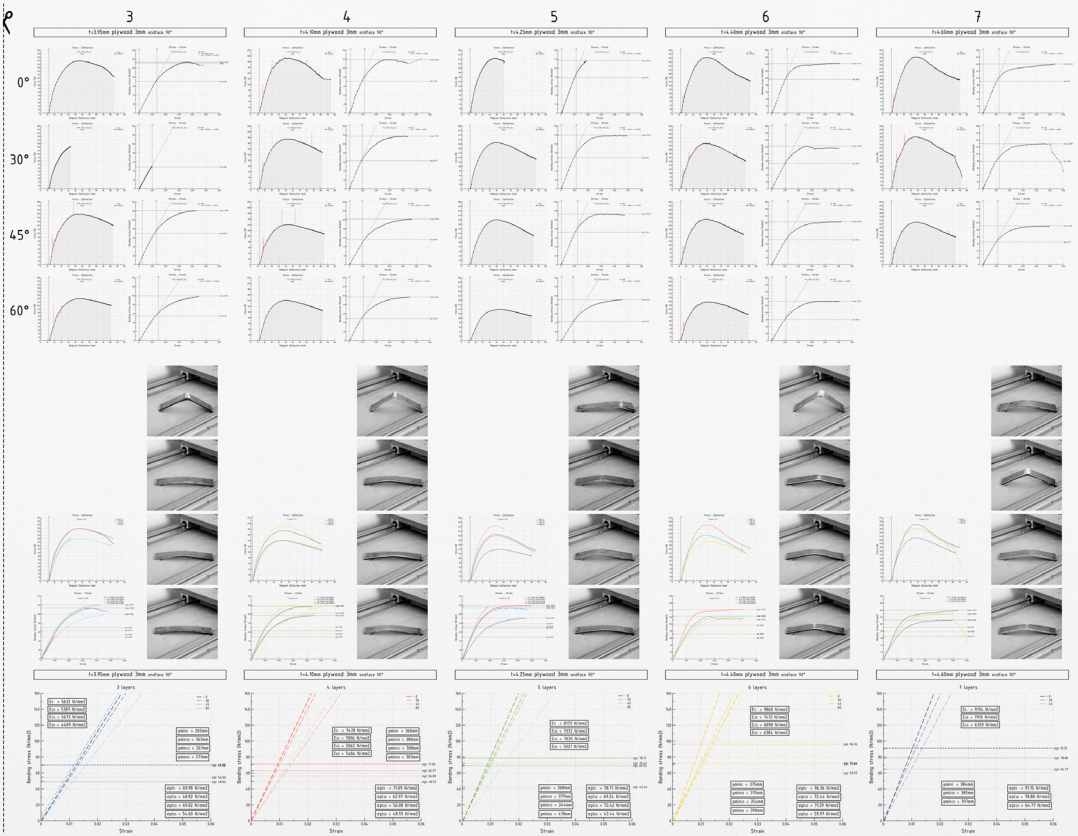

3 fiberglass layers
t:3.95mm plywood-fiberglass
l:190mm, b:40mm
active l:~150mm
1 test per angle setup

4 fiberglass layers
t:4.10mm plywood-fiberglass
l:190mm, b:40mm
active l:~150mm
1 test per angle setup

5 fiberglass layers
t:4,25mm plywood-fiberglass
l:190mm, b:40mm
active l:~150mm
1 test per angle setup

6 fiberglass layers
t:4.40mm plywood-fiberglass
l:190mm, b:40mm
active l:~150mm
1 test per angle setup

7 fiberglass layers
t:4.60mm plywood-fiberglass
l:190mm, b:40mm
active l:~150mm
1 sample per angle setup

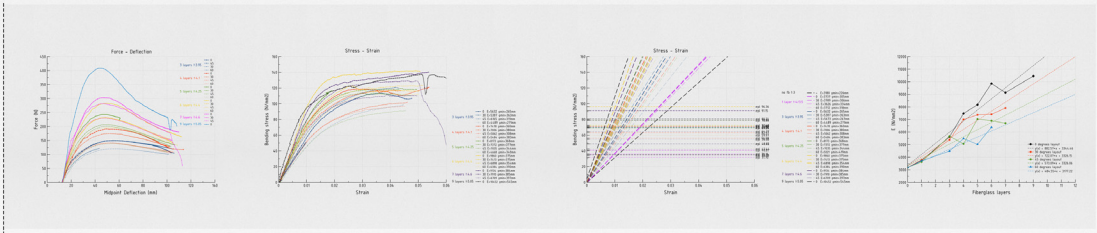

3mm plywood multiple layers fiberglass(0,30,45,60 angles) curves

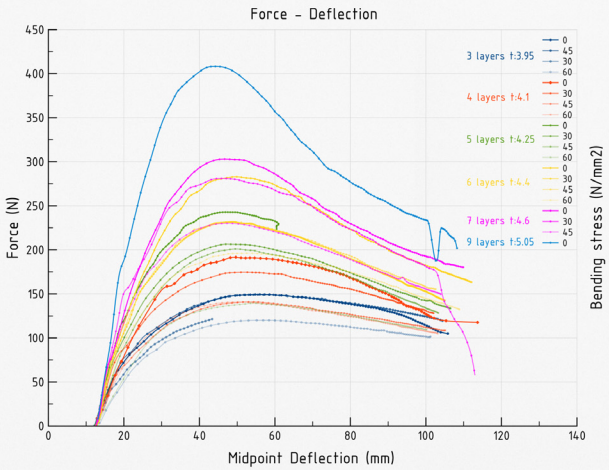

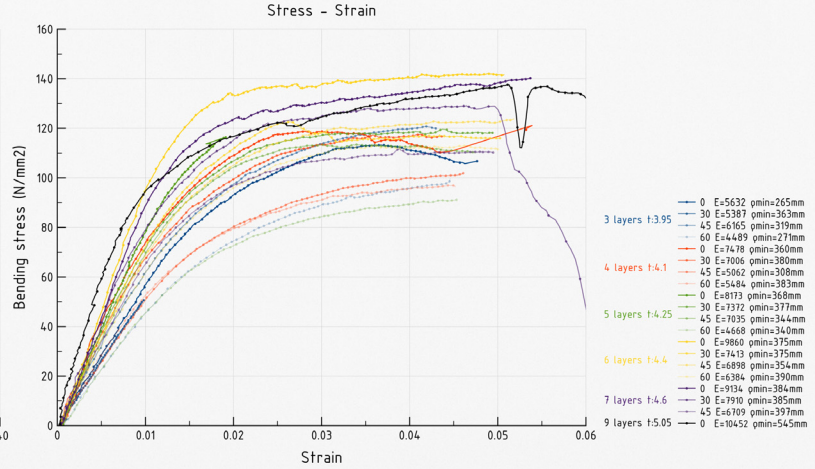

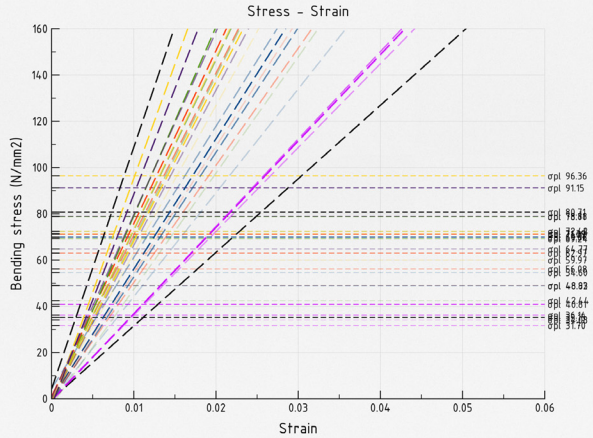

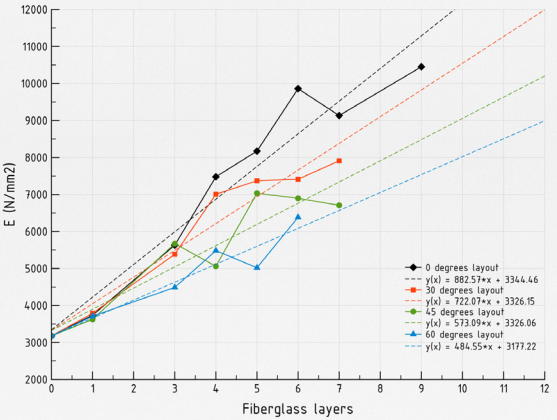

Bending Moduli E/Proportional limits σpl/Minimum Bending radii ρ

Linear approx. of fiberglass layers-Bending Modulus

Ashby Chart - Bending active / Elastic kinetics material selection

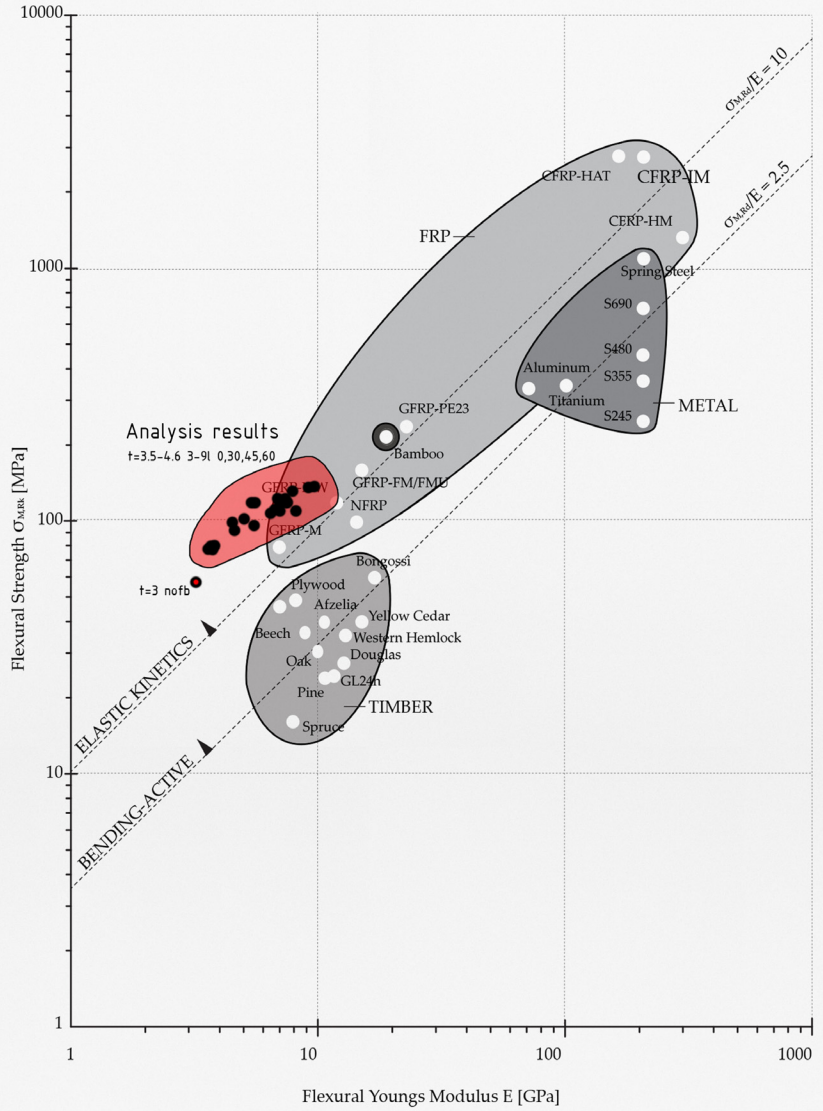

Fig. B.26 Common building materials with ratio of strength $\sigma_{M,Rk}$ [MPa] to stiffness E [GPa]

Ratio of flexural strength against stiffness on a logarithmic scale, based on the 'Ashby diagrams'.

Reproduced from

Bending-Active Structures

Form finding strategies using elastic deformation in static and kinematic systems and the structural potentials therein

Julian Lienhard 2014

11

Materially informed form-finding

Multiscalar materially informed form finding

Material composition according to general properties and local material distribution, in macro, meso and micro scale can output non symmetrical shapes of variable curvature, thus enabling the grading of the bending behavior of plywood-fiberglass composites and the encoding of 3d complex forms into 2d initially planar strips.

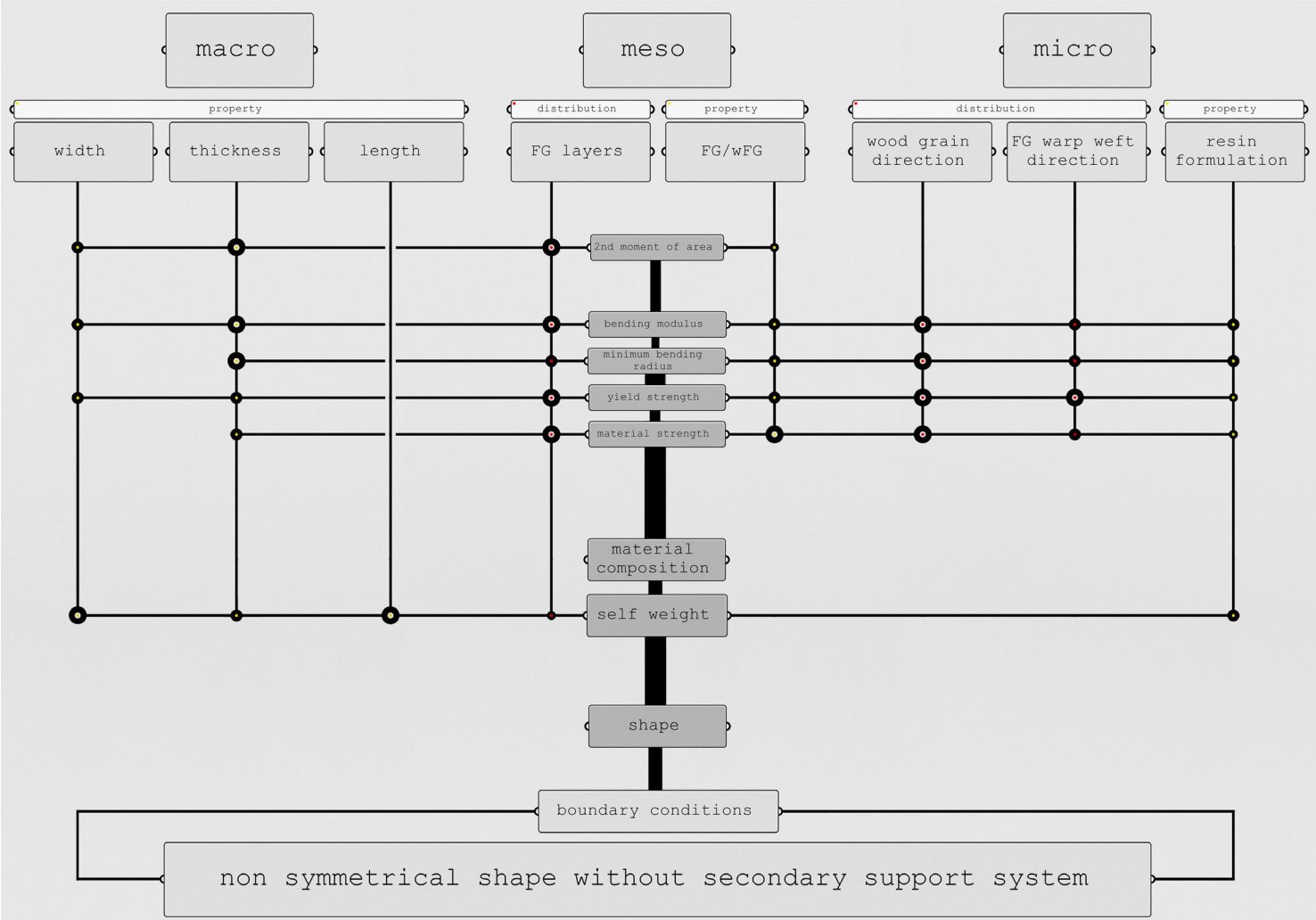

Multiscalar materially informed form finding

Finding shapes according to selected segmentation, fiberglass layout and layers count.

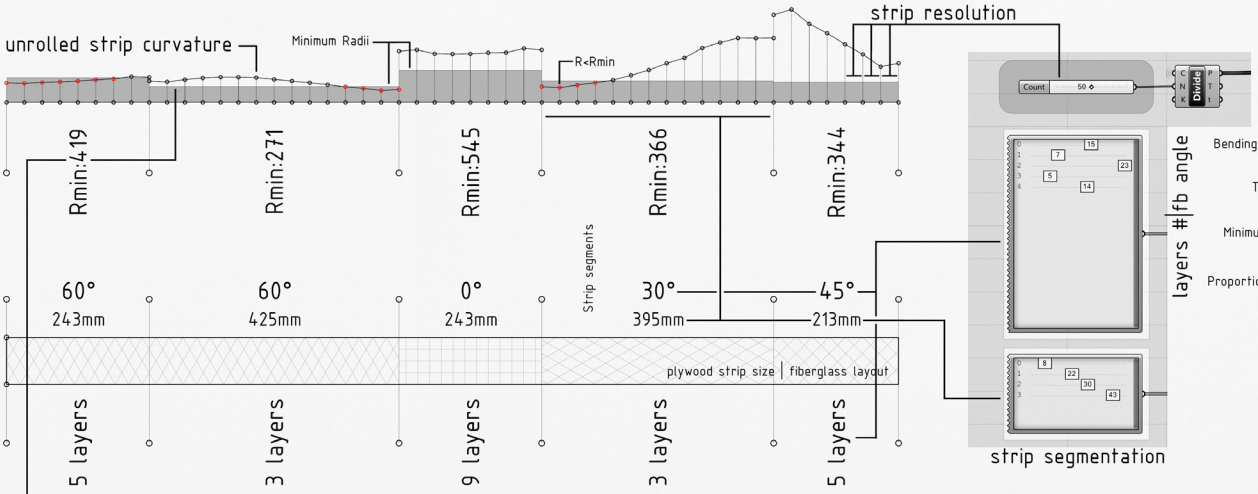

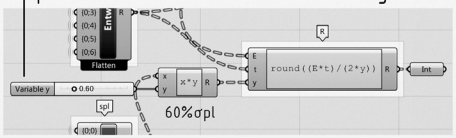

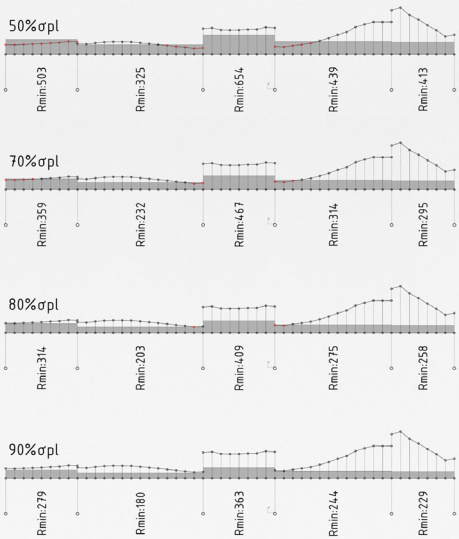

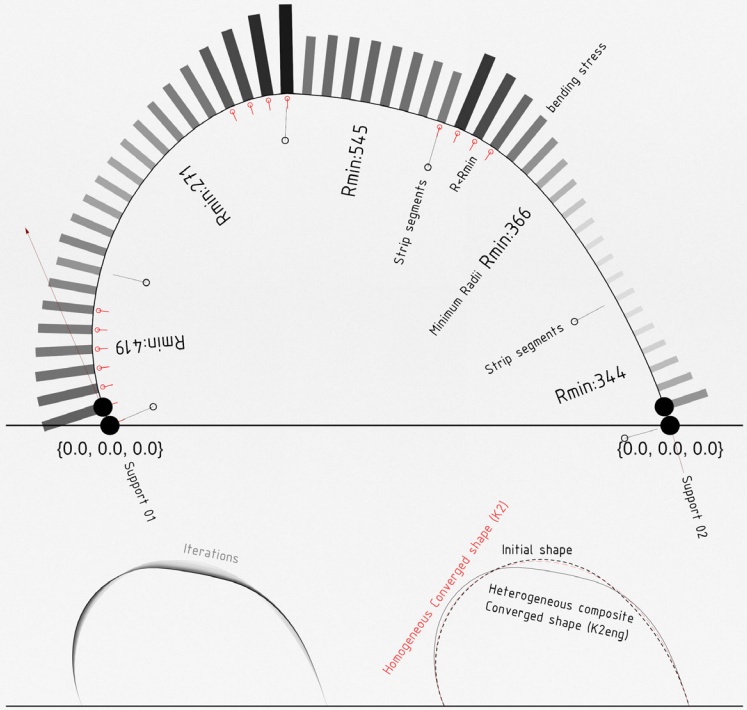

properties | fiberglass layers/angle distribution

Multiscalar materially informed form finding

Finding shapes according to selected segmentation, fiberglass layout and layers count.

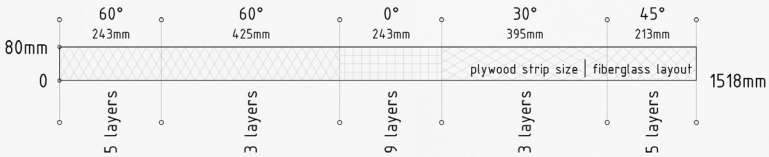

Initial state

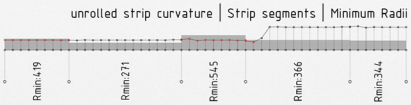

Iterations

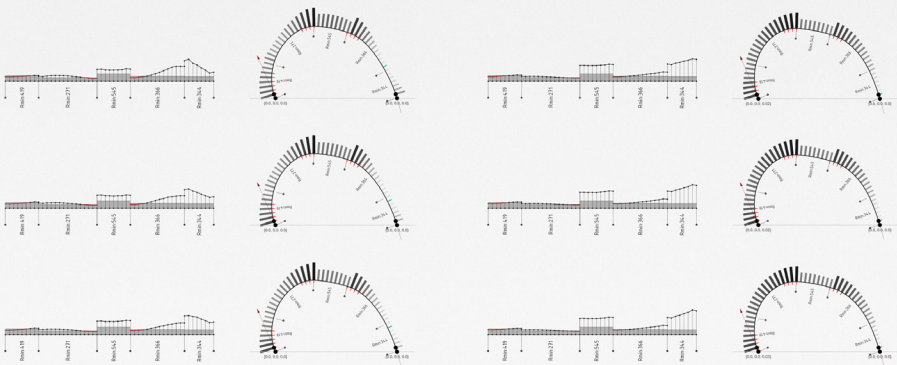

Converged state

Goals

1.Support		(K2eng)
2.Bar		(K2eng)
3.Rod		(K2eng)
4.Self	weight	(K2eng)
5.CoLinear		(K2)

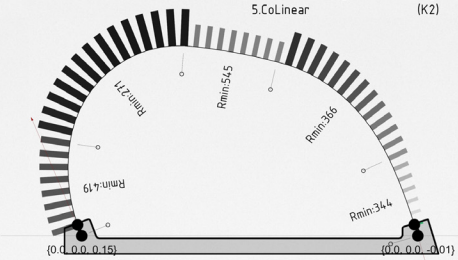

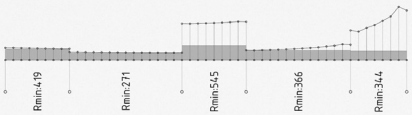

12

Appendix

Base layer plywood 3mm endface 90° (6 samples)

thickness:3mm, length:190mm, width: 120mm, active length~150mm

1

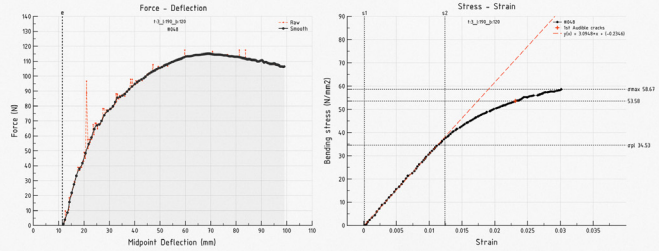

2

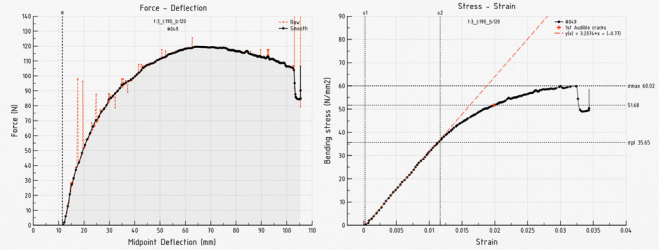

3

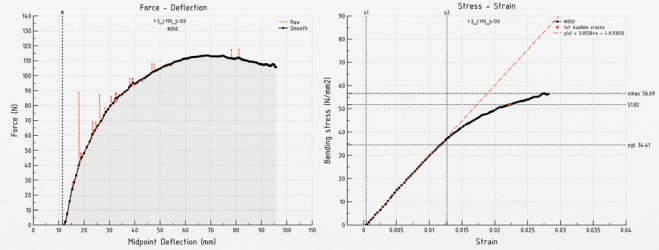

4

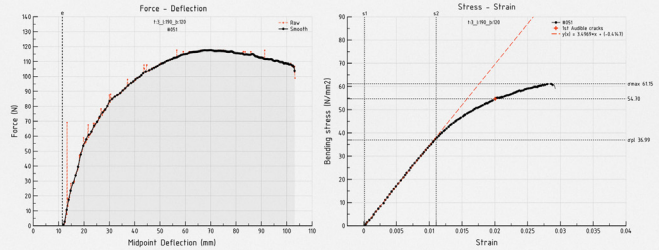

5

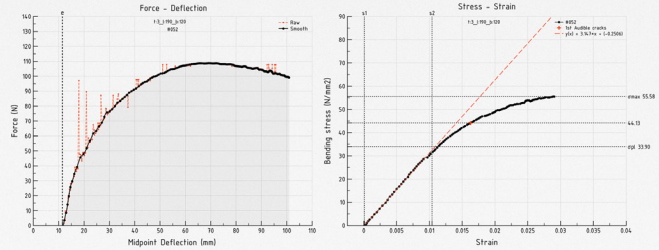

6

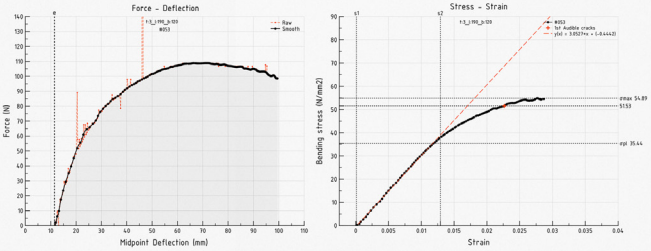

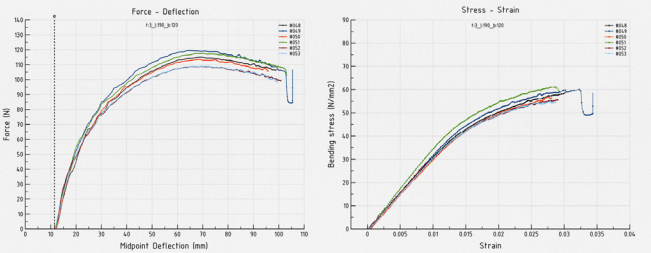

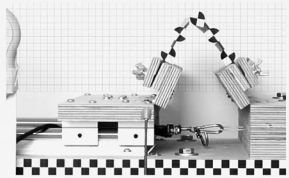

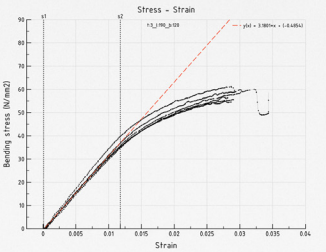

Base layer plywood 3mm endface 90° (6 samples)

Bending Modulus, Proportional limit stress, minimum bending radius | Proportional limit frame | Fracture frame

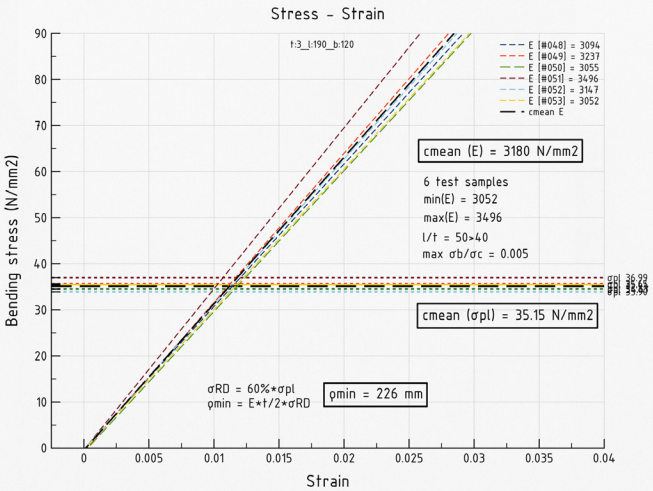

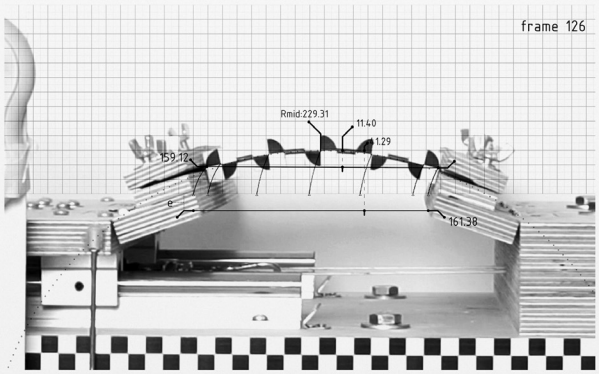

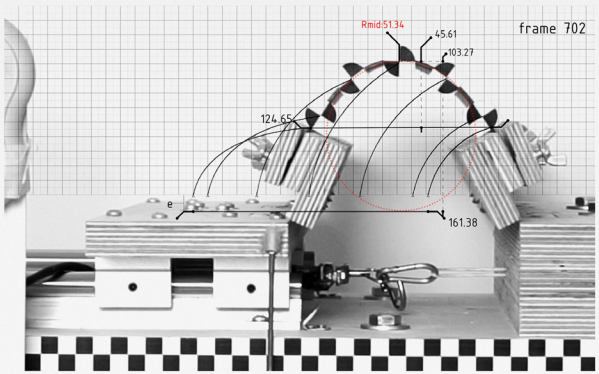

Composite plywood 3mm endface 90° | 1 layer fiberglass 0° (5 samples)

thickness:4mm, length:190mm, width: 120mm, active length~150mm

1

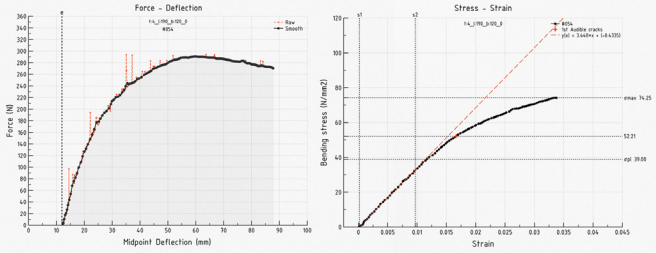

2

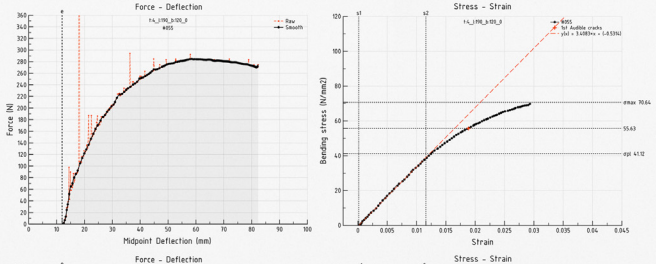

3

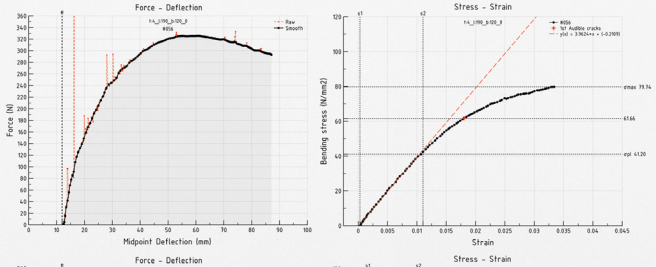

4

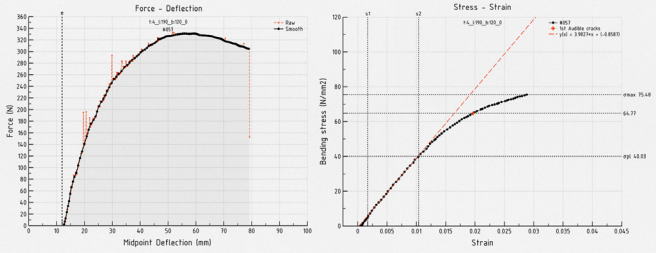

5

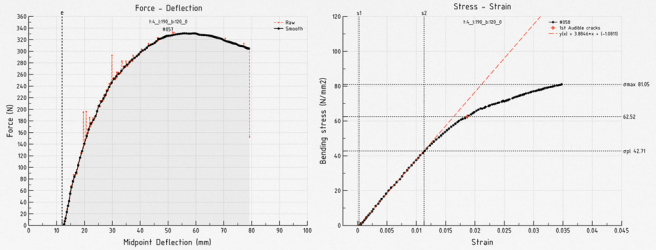

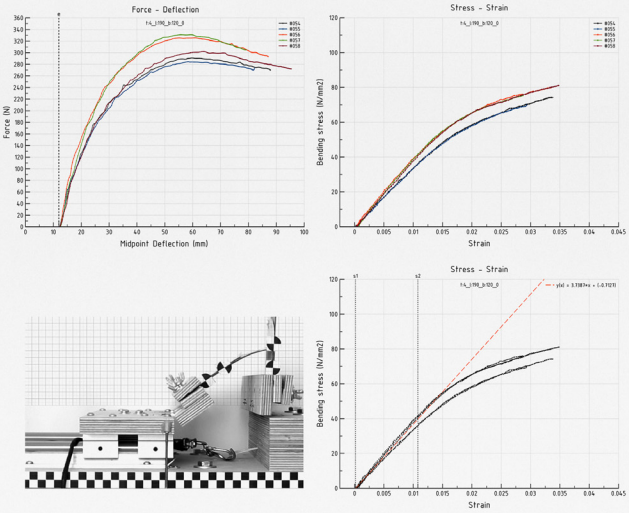

Composite plywood 3mm endface 90° | 1 layer fiberglass 0° (5 samples)

Bending Modulus, Proportional limit stress, minimum bending radius | Proportional limit frame | Fracture frame

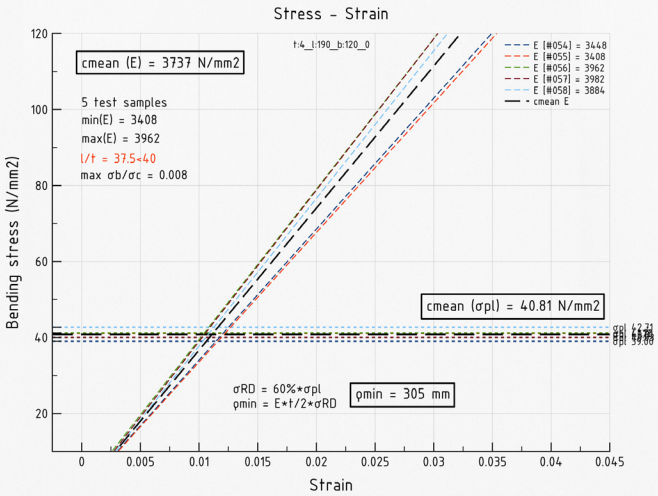

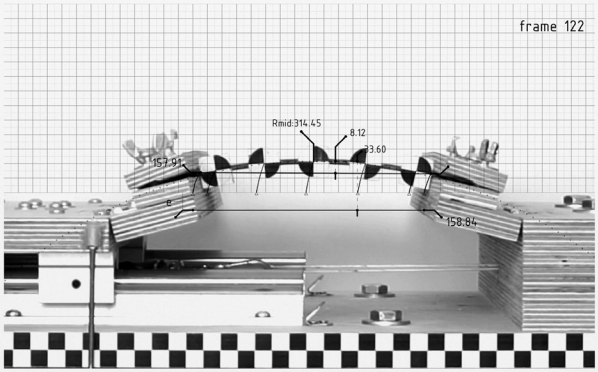

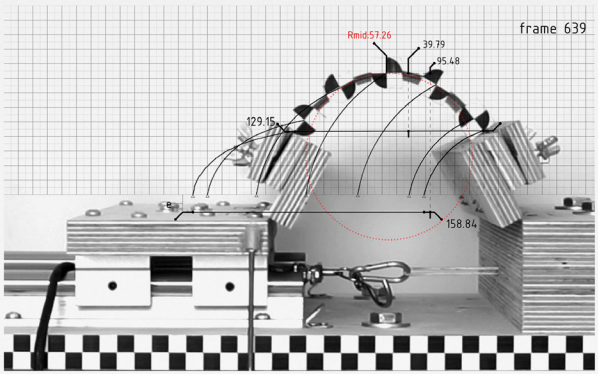

Composite plywood 3mm endface 90° | 1 layer fiberglass 30° (5 samples)

thickness:3.5mm, length:190mm, width: 120mm, active length~150mm

1

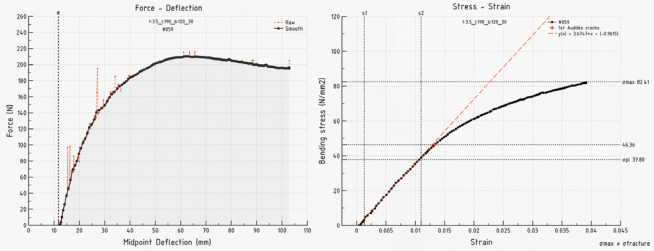

2

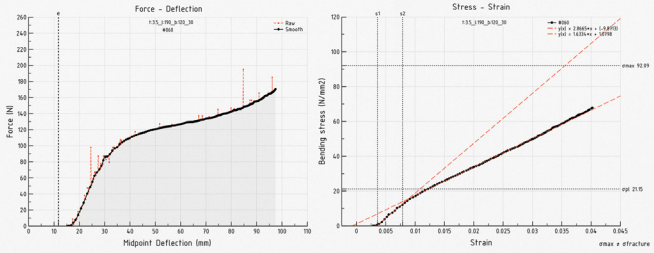

3

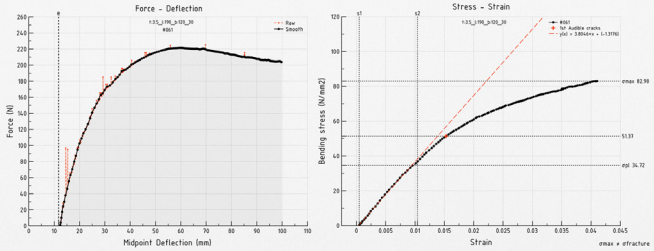

4

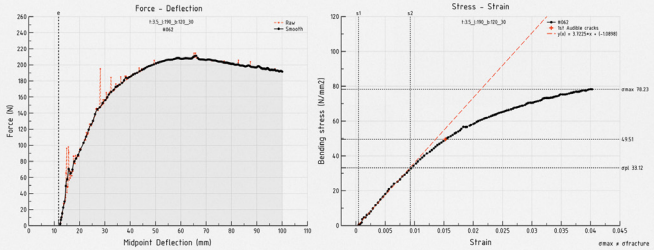

5

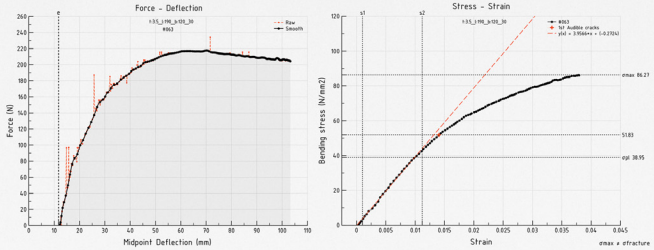

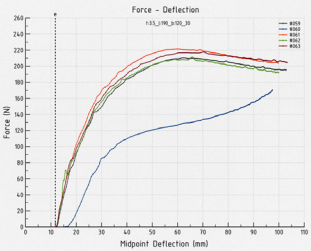

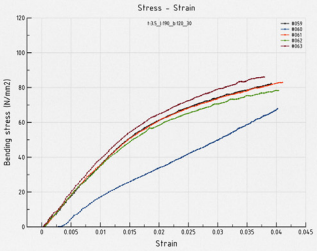

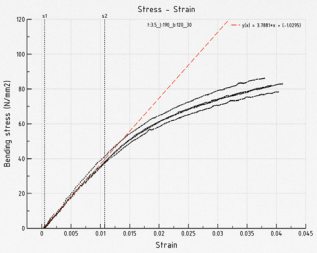

Composite plywood 3mm endface 90° | 1 layer fiberglass 30° (5 samples)

Bending Modulus, Proportional limit stress, minimum bending radius | Proportional limit frame | Fracture frame

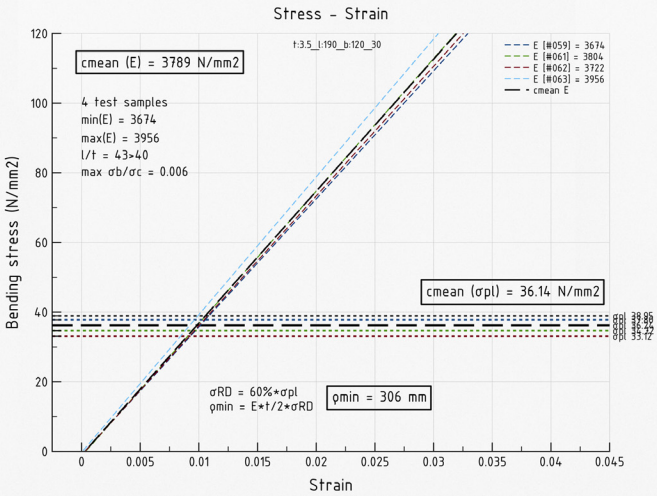

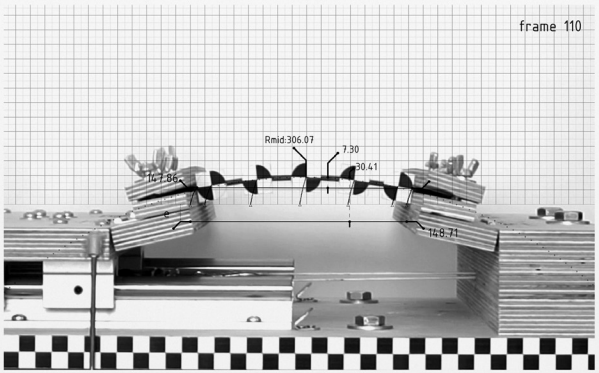

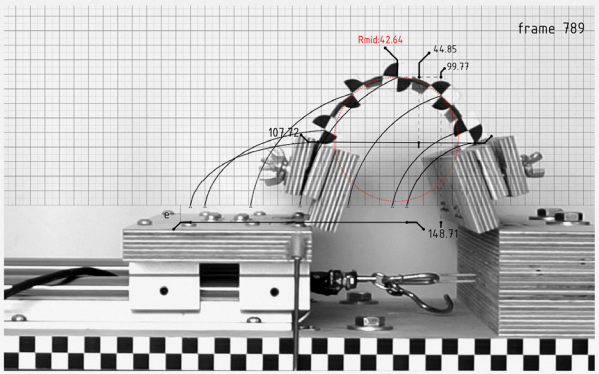

Composite plywood 3mm endface 90° | 1 layer fiberglass 45° (5 samples)

thickness:3.5mm, length:190mm, width: 120mm, active length~150mm

1

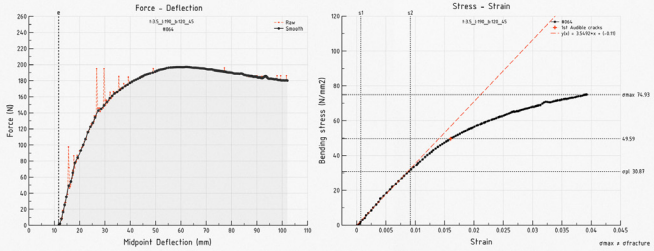

2

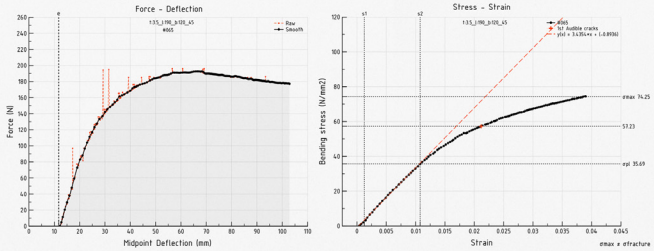

3

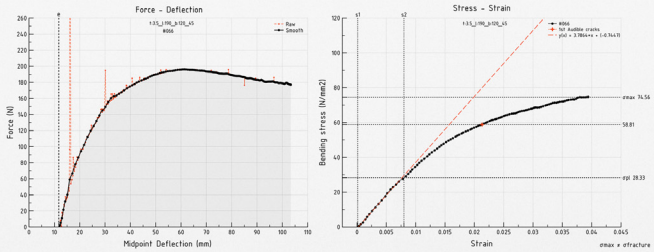

4

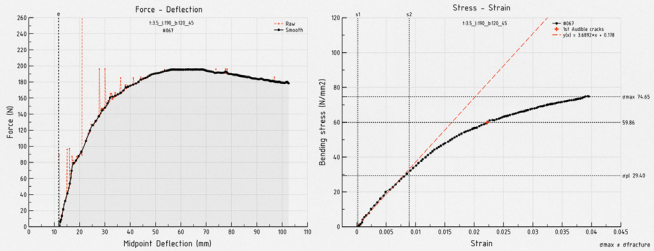

5

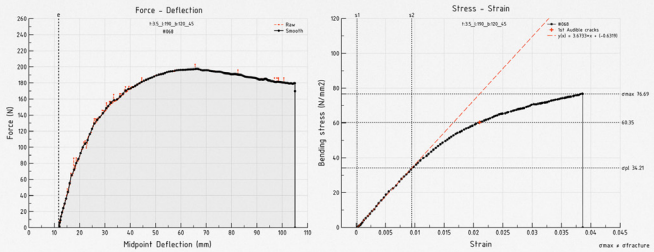

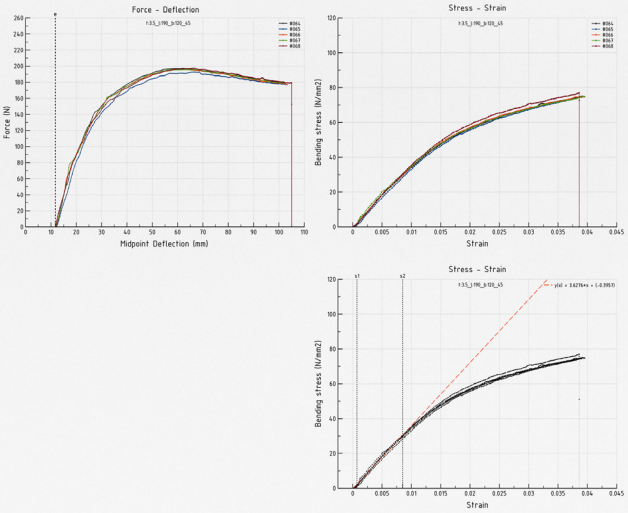

Composite plywood 3mm endface 90° | 1 layer fiberglass 45° (5 samples)

Bending Modulus, Proportional limit stress, minimum bending radius | Proportional limit frame | Fracture frame

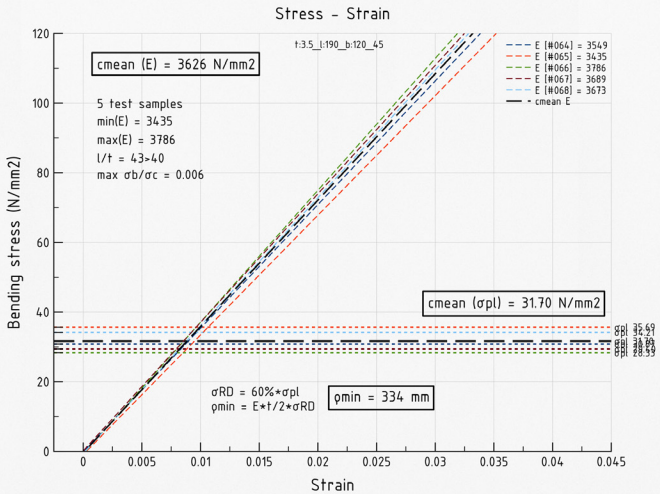

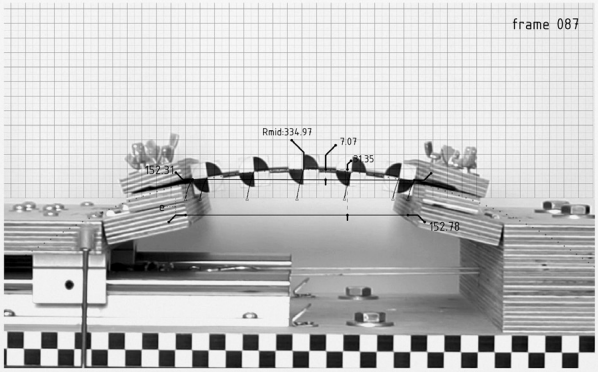

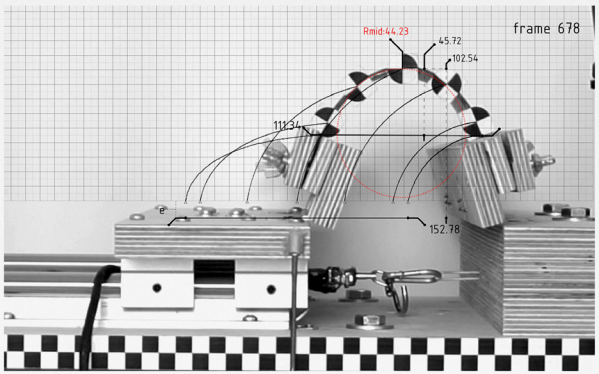

Composite plywood 3mm endface 90° | 1 layer fiberglass 60° (5 samples)

thickness:3.5mm, length:190mm, width: 120mm, active length~150mm

1

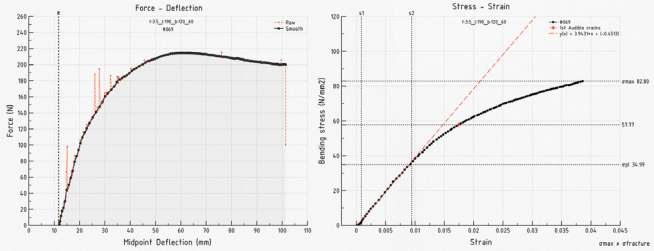

2

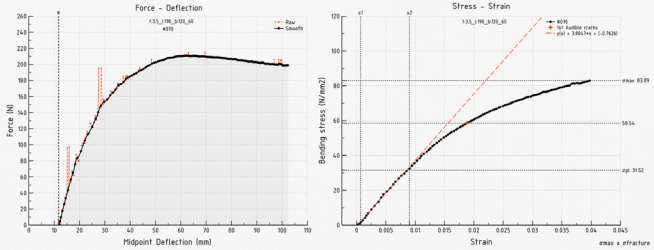

3

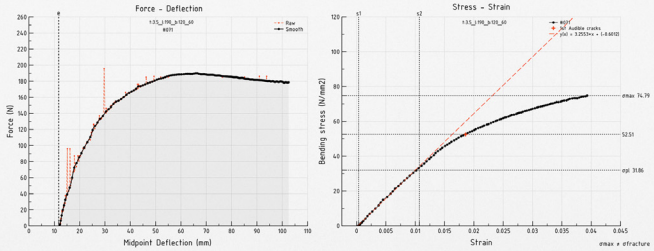

4

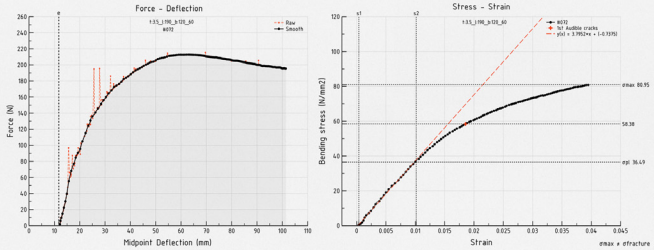

5

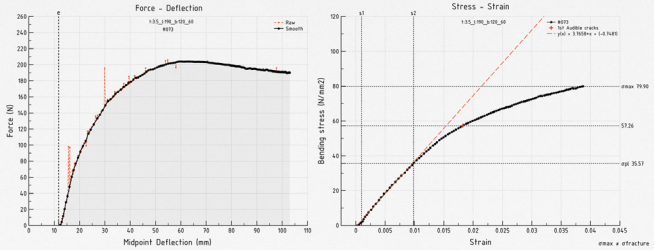

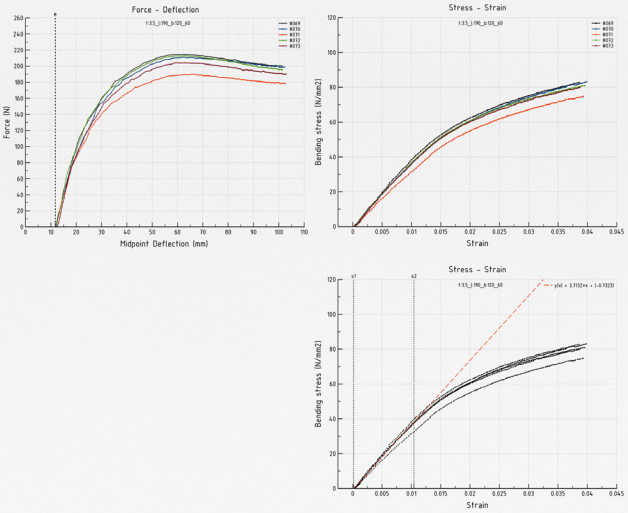

Composite plywood 3mm endface 90° | 1 layer fiberglass 60° (5 samples)

Bending Modulus, Proportional limit stress, minimum bending radius | Proportional limit frame | Fracture frame

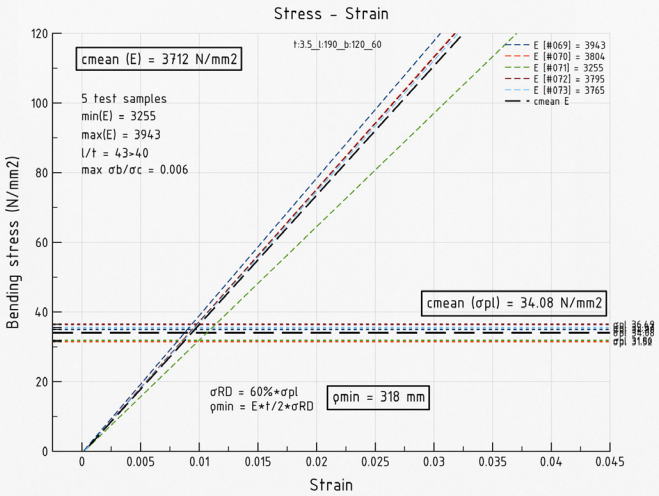

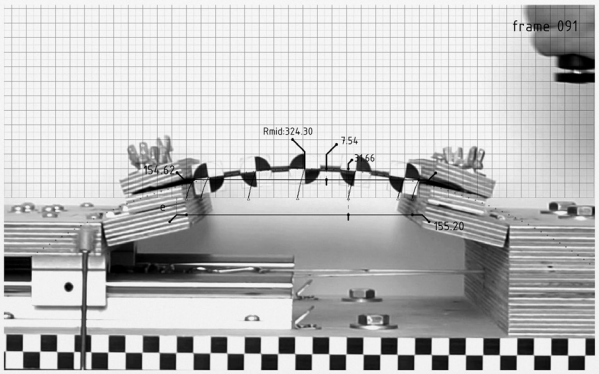

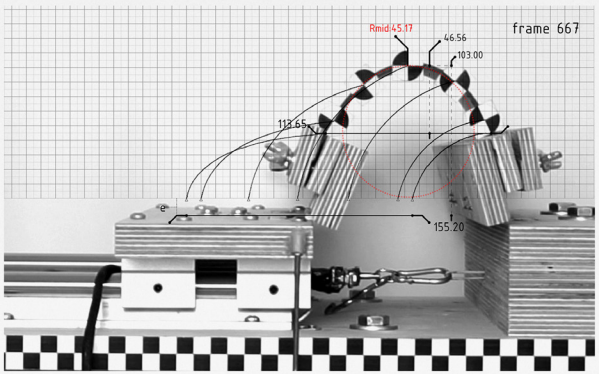

Calibration tests plywood 4mm endface 90° (6 samples)

thickness:4mm, length:190mm, width: 80mm, active length~150mm

1

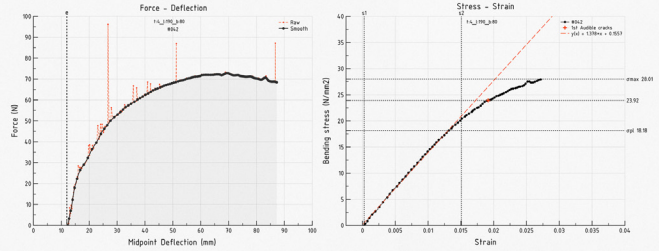

2

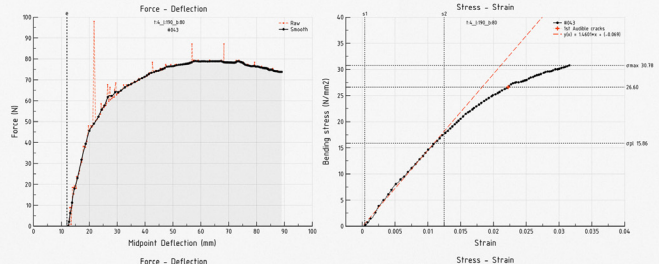

3

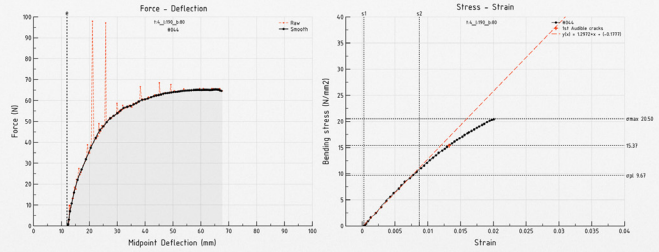

4

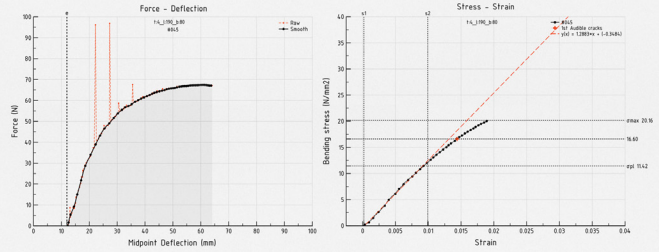

5

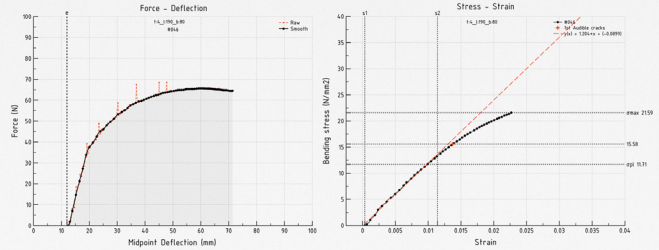

6

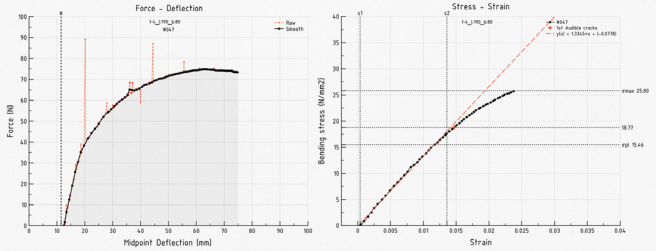

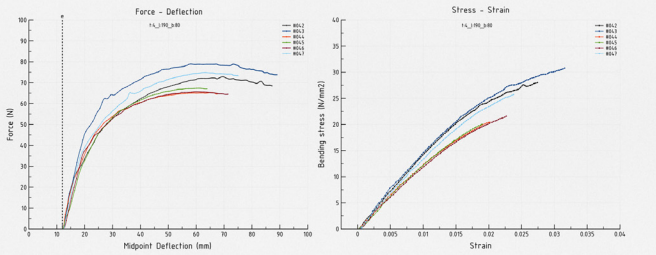

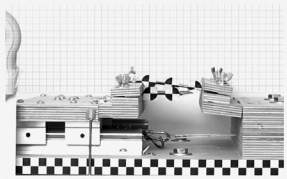

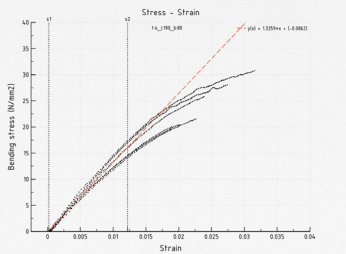

Calibration tests plywood 4mm endface 90° (6 samples)

Bending Modulus, Proportional limit stress, minimum bending radius | Proportional limit frame | Fracture frame

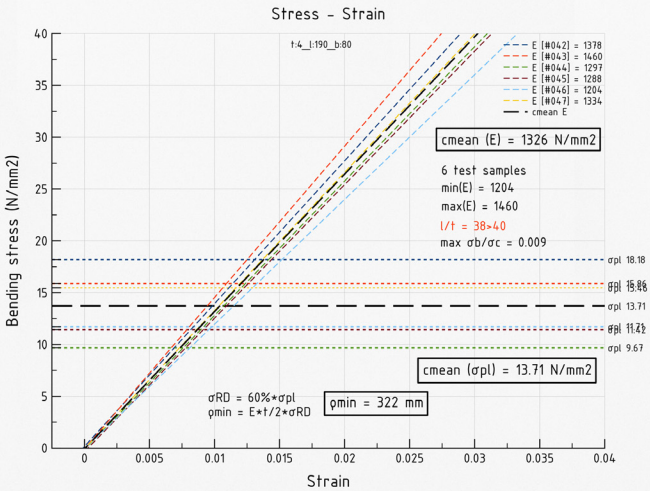

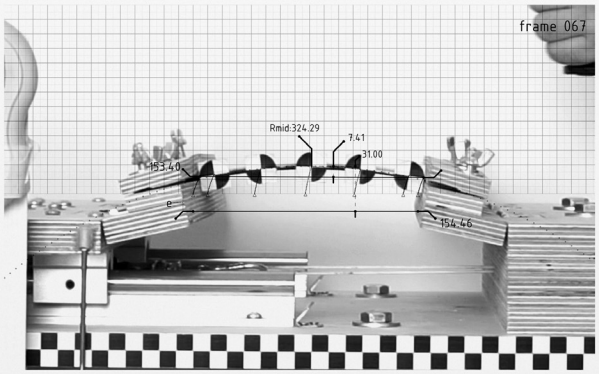

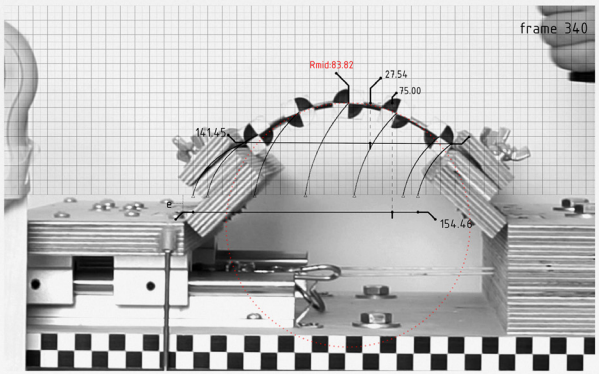

Calibration tests plywood 6mm endface 90° (6 samples)

thickness:6mm, length:274mm, width: 40mm, active length~234mm

1

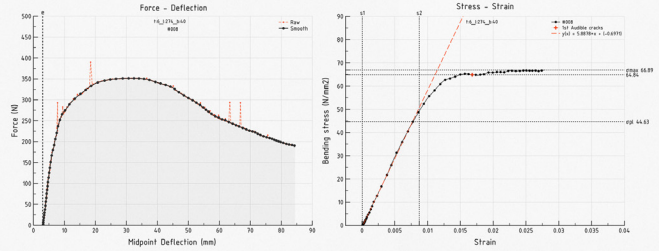

2

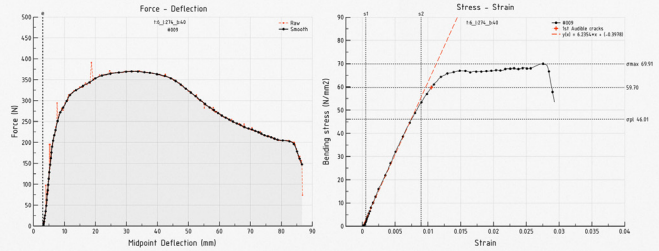

3

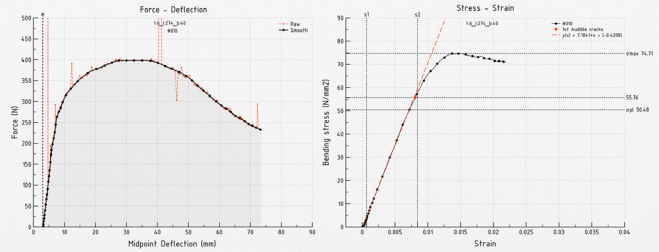

4

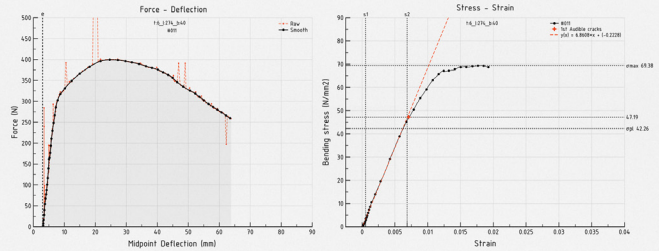

5

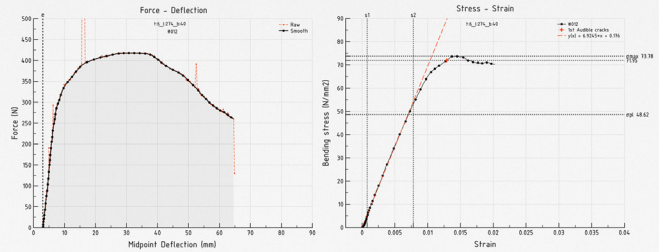

6

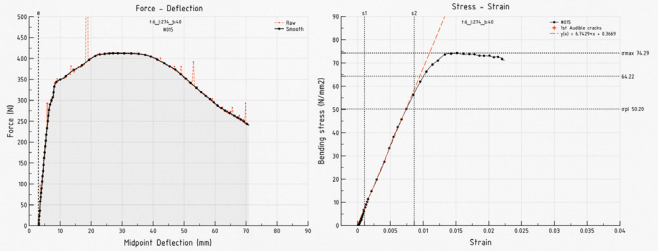

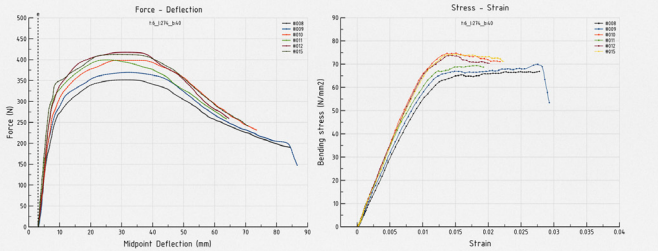

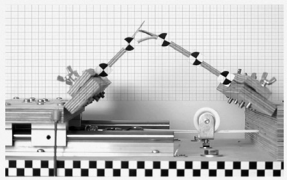

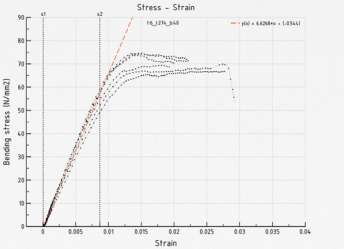

Calibration tests plywood 6mm endface 90° (6 samples)

Bending Modulus, Proportional limit stress, minimum bending radius | Proportional limit frame | Fracture frame

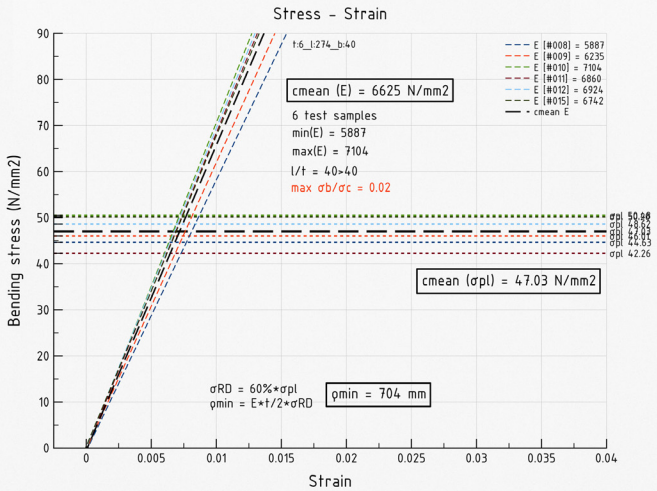

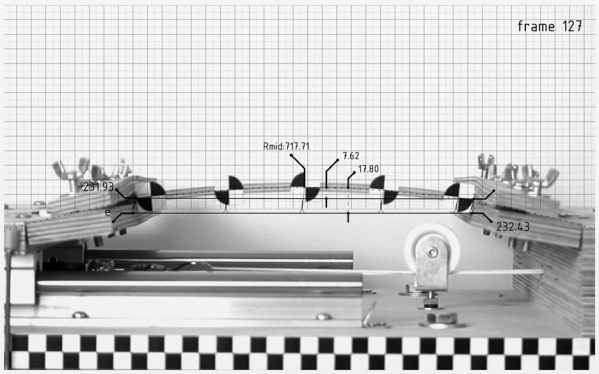

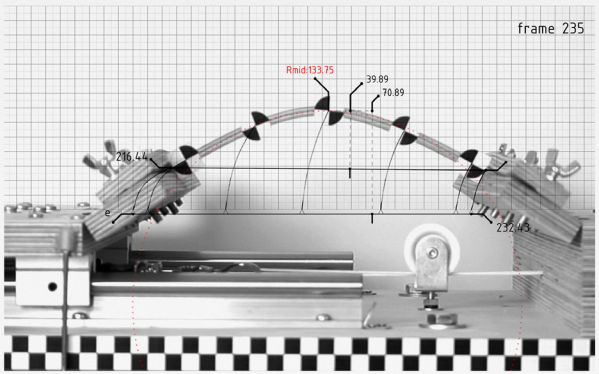

Composite plywood 3mm endface 90° | 3 layer fiberglass 0°, 30°, 45° and 60° (1 sample per angle layout)

thickness:3.95mm, length:190mm, width: 40mm, active length~150mm

0°

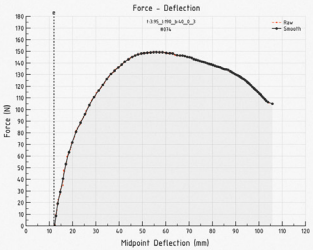

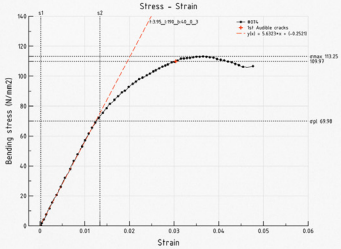

30°

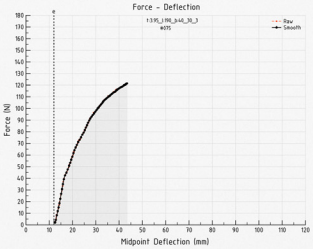

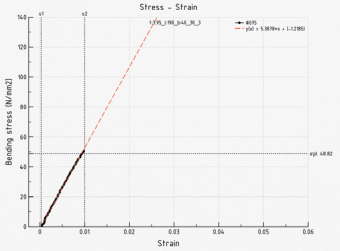

45°

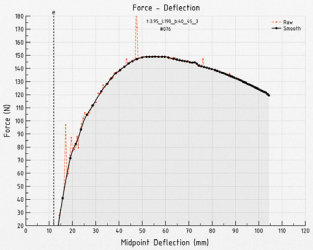

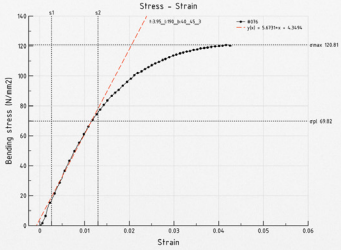

60°

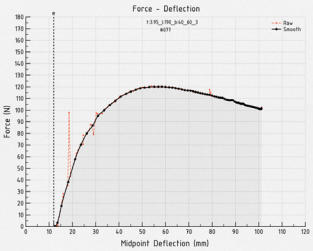

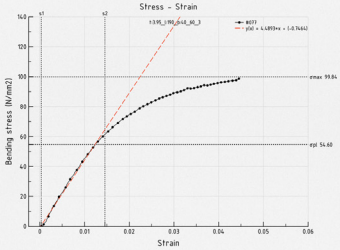

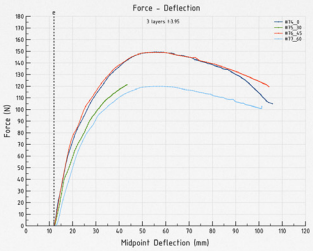

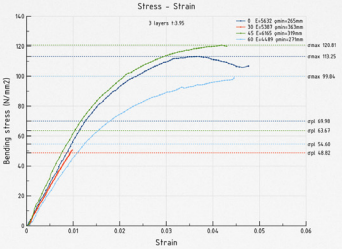

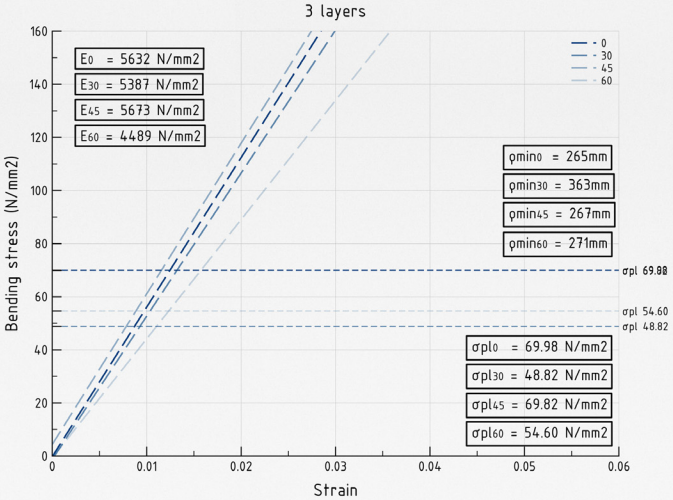

Composite plywood 3mm endface 90° | 4 layer fiberglass 0°, 30°, 45° and 60° (1 sample per angle layout)

thickness:4.10mm, length:190mm, width: 40mm, active length~150mm

0°

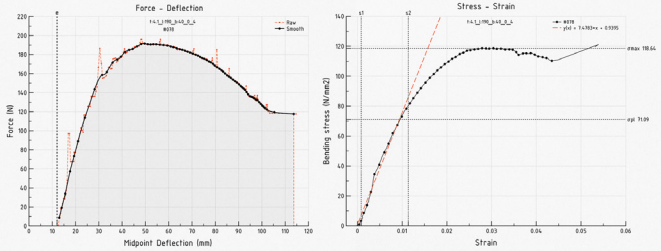

30°

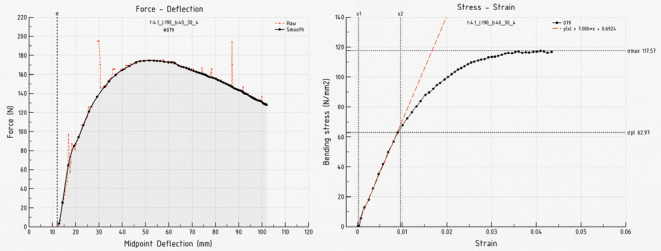

45°

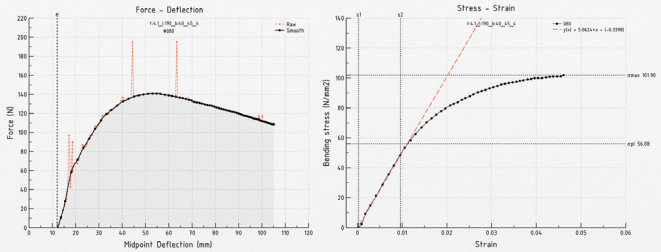

60°

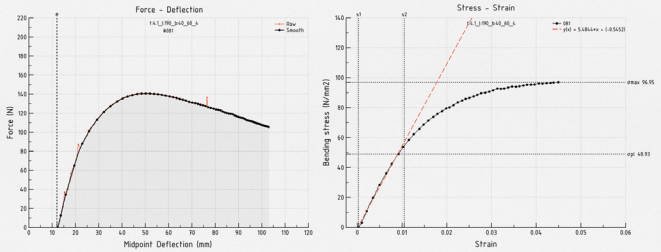

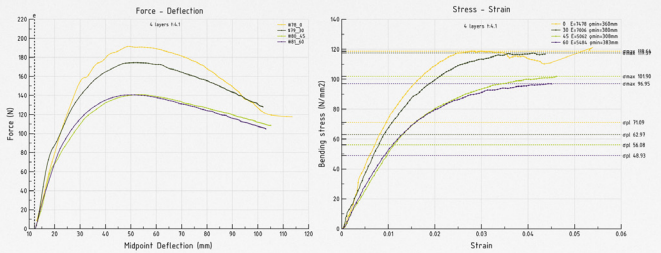

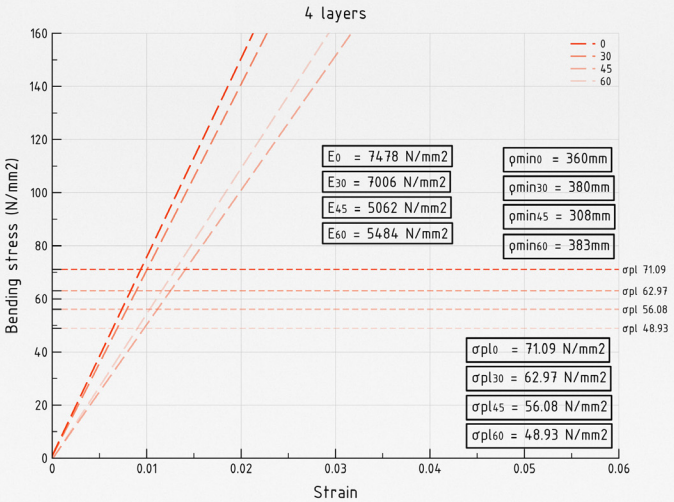

Composite plywood 3mm endface 90° | 5 layer fiberglass 0°, 30°, 45° and 60° (1 sample per angle layout)

thickness:4.25mm, length:190mm, width: 40mm, active length~150mm

0°

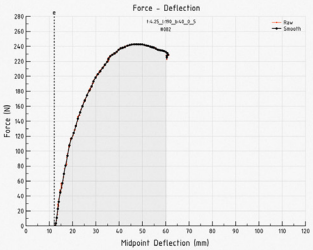

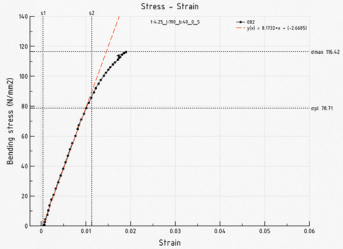

30°

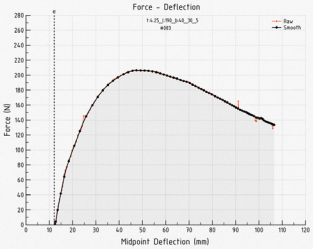

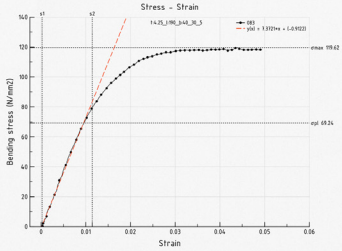

45°

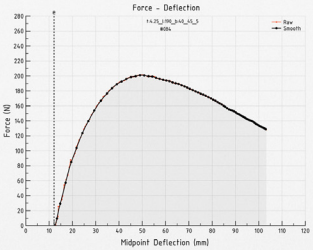

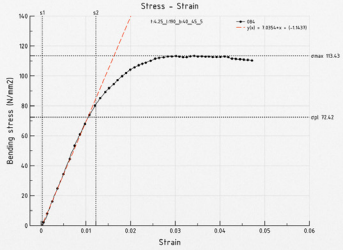

60°

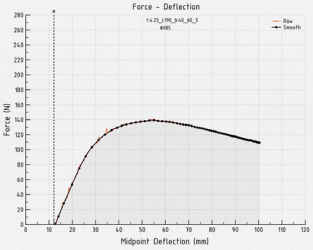

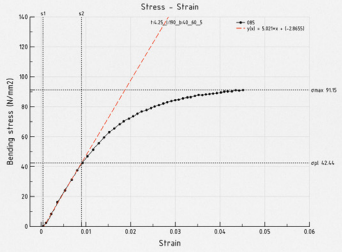

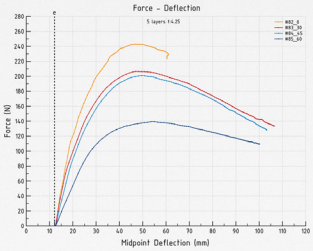

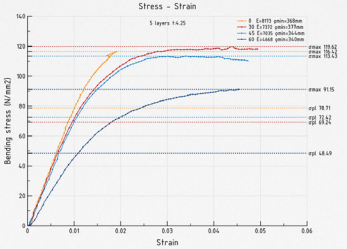

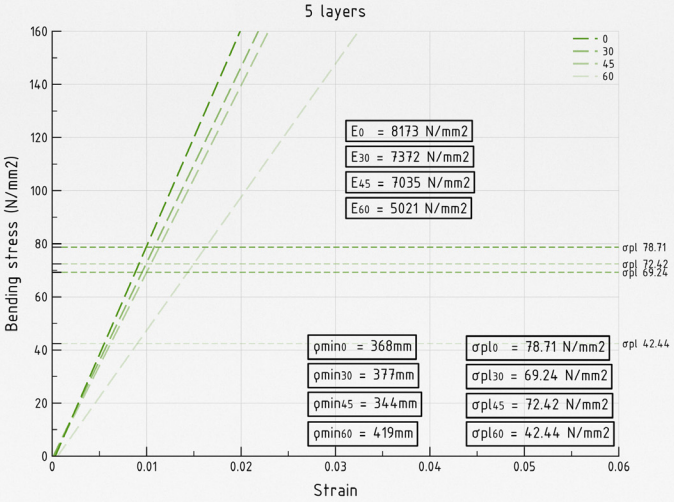

Composite plywood 3mm endface 90° | 6 layer fiberglass 0°, 30°, 45° and 60° (1 sample per angle layout)

thickness:4.40mm, length:190mm, width: 40mm, active length~150mm

0°

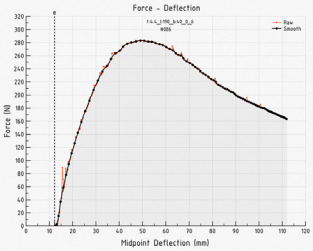

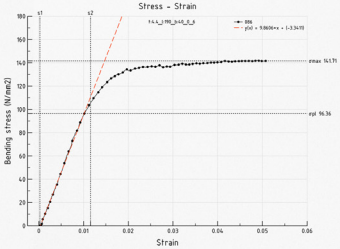

30°

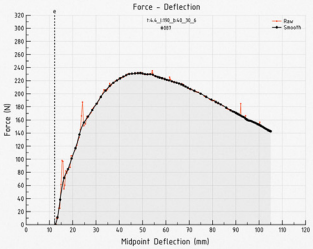

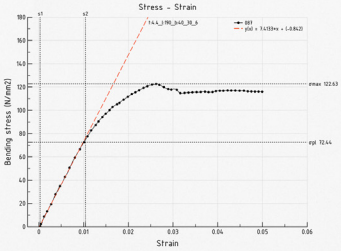

45°

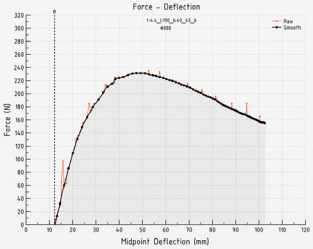

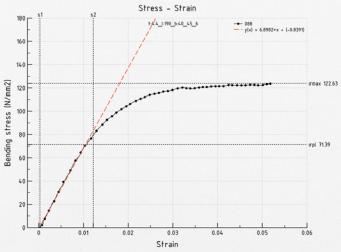

60°

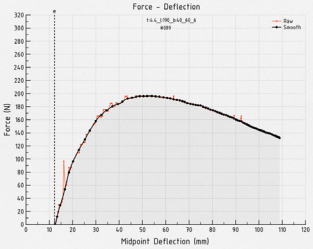

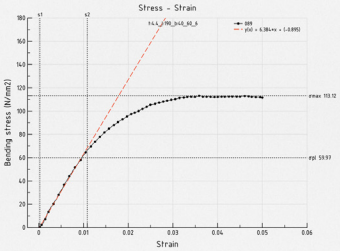

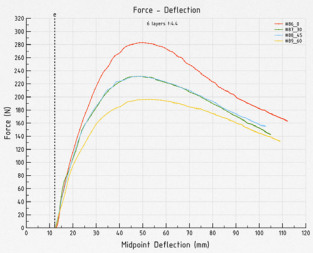

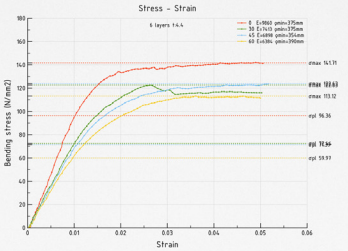

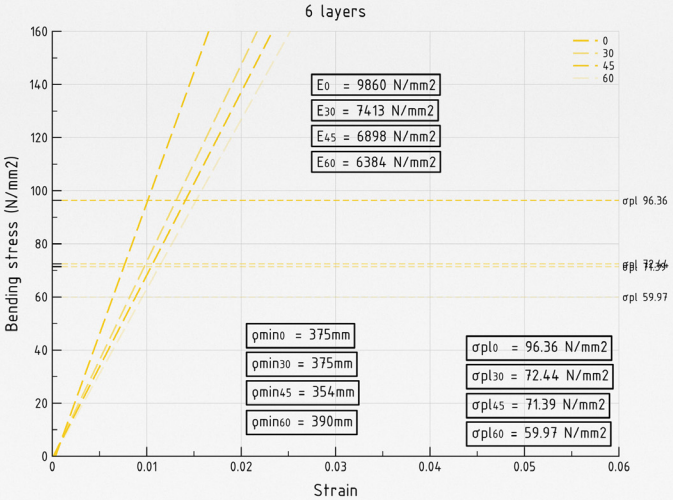

Composite plywood 3mm endface 90° | 7 layer fiberglass 0°, 30°, 45° and 60° (1 sample per angle layout)
thickness:4.60mm, length:190mm, width: 40mm, active length~150mm

0°

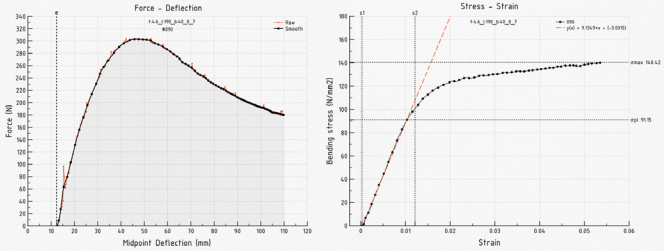

30°

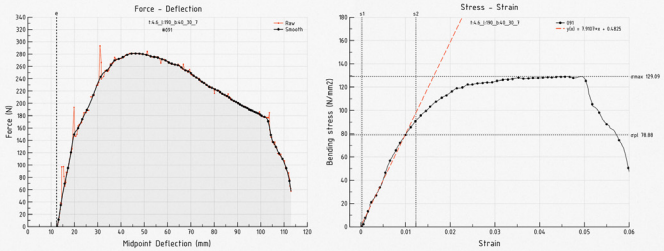

45°

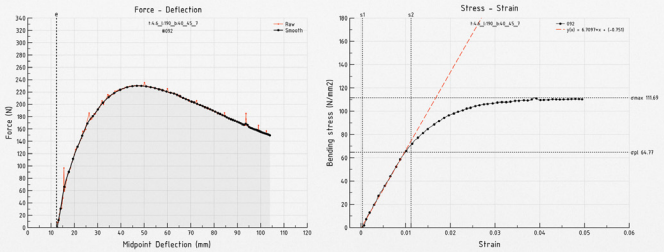

60°

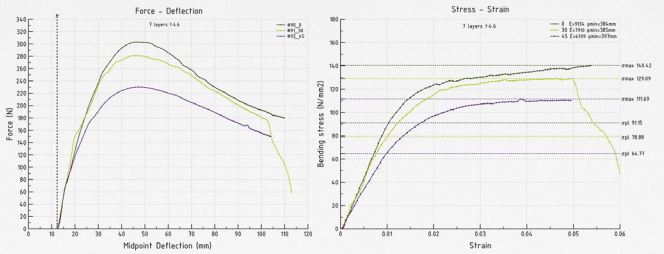

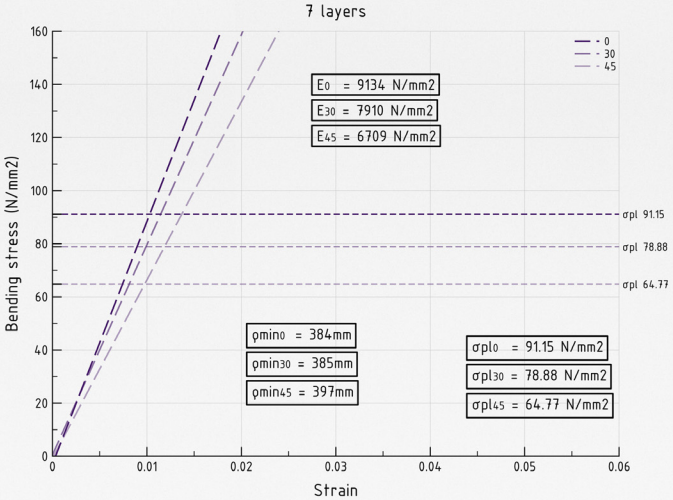

Bibliography – Articles – Papers – Online resources

Bechert, S., Knippers, J., Krieg, O.D., Menges, A., Schwinn, T. & Sonntag, D., 2016. Fabrication Techniques for Timber Shells: Elastic Bending of Custom Laminated Veneer for Segmented Shell Construction Systems. *Advances in Architectural Geometry 2016,* pp.159–164.

Biblis, E.J. & Chiu, Y.-M., 1970. Flexural Strength and Stiffness of Southern Pine Plywood. *Wood Science and Technology*, 4(1), pp.70–77.

Bigoni, D., 2014. *Nonlinear Solid Mechanics: Bifurcation Theory and Material Instability*, New York, NY: Cambridge Univ. Press.

Born, L. et al., 2017. Fiber-Reinforced Plastics with Locally Adapted Stiffness for Bio-Inspired Hingeless, Deployable Architectural Systems. *Key Engineering Materials*, 742, pp.689–696.

Brandt-Olsen, C., 2016. Calibrated Modelling of Form-active Structures. *MSc Dissertation, Technical University of Denmark.*

Elmendorf, A., 1920. *Data on the Design of Plywood for Aircraft*, Washington, D.C.: G.P.O.

Fiorelli, J. & Dias, A.A., 2003. Analysis of the strength and stiffness of timber beams reinforced with carbon fiber and glass fiber. *Materials Research*, 6(2), pp.193–202.

Fukuda, H., 1989. A New Bending Test Method of Advanced Composites. *Experimental Mechanics*, 29(3), pp.330–335.

Fukuda, H. & Itabashi, M., 1999. Simplified Compression Bending Test Method for Advanced Composites. *Composites Part A: Applied Science and Manufacturing*, 30(3), pp.249–256.

Fukuda, H., Itabashi, M. & Wada, A., 2004. Development of Compression Bending Test Method for Advanced Composites – A Review. *Science and Engineering of Composite Materials*, 11(2-3), pp.169-176.

Fukuda, H., Katoh, H. & Uesugi, H., 1995. A Modified Procedure to Measure Bending Strength and Modulus of Advanced Composites by Means of Compression Bending. *Journal of Composite Materials*, 29(2), pp.195–207.

Fukuda, H., Watanabe, O., Itabashi, M. & Wada, A., 2002. Eccentric Compression Bending Test for CFRP Pipe. *Advanced Composite Materials*, 11(2), pp.193–201.

Garti, F., 2015. Active-Bending Hybrid Structures: Parameter optimization of restraining membrane. *Msc Dissertation, INSA Strasbourg*.

Gere, J.M. & Goodno, B.J., 2010. *Mechanics of Materials*, Toronto: Cengage Learning.

Green, D.W., Winandy, J.E. & Kretschmann, D.E, 1999. Mechanical properties of wood. Wood handbook: Wood as an Engineering Material. Madison, WI: USDA Forest Service, Forest Products Laboratory, 1999. General technical report FPL; GTR-113: Pages 4.1-4.45

Goss, V.G.A., 2003. Snap Buckling, Writhing and Loop Formation in Twisted Rods. *PhD Dissertation, Center for Nonlinear Dynamics University College London*.

Kotelnikova-Weilera, N., Douthed, C., Lafuente Hernandezc, E., Baverel, O., Gengnagel, C. & Caron J-F., 2013. Materials for Actively-Bent Structures. *International Journal of Space Structures*, 28(3-4), pp.229–240.

Kuijvenhoven, M., 2009. A Design Method for Timber Grid Shells. *MSc Dissertation, TU Delft University of Technology*.

La Magna, R., Schleicher, S. & Knippers, J., 2016. Bending-Active Plates: Form and Structure. *Advances in Architectural Geometry 2016,* pp.170–186.

Levien, R., 2008. The Elastica: A Mathematical History. *PhD Dissertation report, University of California, Berkeley.*

Lienhard, J., 2014. Bending-Active Structures: Form-Finding Strategies Using Elastic Deformation in Static and Kinetic Systems and the Structural Potentials Therein. *PhD Dissertation, University of Stuttgart.*

Lienhard, J. Alpermann, H., Gengnagel, C. & Knippers, J., 2013. Active Bending, A Review on Structures Where Bending Is Used As A Self-Formation Process. *International Journal of Space Structures*, 28(3-4), pp.187–196.

Lienhard, J. & Knippers, J., 2013. Considerations on the Scaling of Bending-Active Structures. *International Journal of Space Structures*, 28(3-4), pp.137–148.

Lienhard, J. et al., 2013. Active Bending, a Review on Structures where Bending is used as a Self-Formation Process. *International Journal of Space Structures*, 28(3-4), pp.187–196.

Melville, S., Brandt-Olsen, C. & Harding, J., 2017. Calibrated modelling of form-active structures. *IABSE Symposium Report*, 108(1), pp.155–156.

Mesnil, R., 2013. Stability of Elastic Grid Shells. *MEng Dissertation, Massachusetts Institute of Technology.*

Mesnil, R., Ochsendorf, J. & Douthe, C., 2015. Stability of Pseudo-Funicular Elastic Grid Shells. *International Journal of Space Structures*, 30(1), pp.27–36.

Nabaei, S.S., Baverel, O. & Weinand, Y., 2013. Mechanical Form-Finding of the Timber Fabric Structures with Dynamic Relaxation Method. *International Journal of Space Structures*, 28(3-4), pp.197–214.

Nicholas, P. & Tamke, M., 2013. Computational Strategies for the Architectural Design of Bending Active Structures. *International Journal of Space Structures*, 28(3-4), pp.215–228.

Quinn, G., Holden Deleuran, A., Piker, D., Brandt-Olsen, C., Tamke, M., Ramsgaard Thomsen, M. & Gegnagel, C., 2016. Calibrated and Interactive Modelling of Form-Active Hybrid Structures. *Iaas Annual Symposium 2016 "Spatial Structures in in the 21st Century" Tokyo,* pp.1–9.

Otto, F., Schauer, E., Hennicke, J. & Hasegawa, T., 1974. *IL 10 Gitterschalen / Grid Shells. Stuttgart: Institut fur leichte Flachentragwerke.*

Oxman, N., 2010. *Material-based design computation*, *PhD Dissertation, Massachusetts Institute of Technology*

Peck, E.C., 1955. *Bending solid wood to form*, Madison, WI: United States Dept. of Agriculture, Forest Service, and Forest Products Laboratory.

Powell, P.C., 1994. *Engineering with fibre-polymer laminates*, London: Chapman and Hall.

Ramsgaard Thomsen, M., Tamke, M., Nicholas, P., Holden Deleuran, A., Ayres, P., La Magna, R. & Gegnagel, C., 2017. Simulation in Complex Modelling. *Symposium on Simulation for Architecture and Urban Design (SimAUD) proceedings, Toronto*, pp.

Ramsgaard Thomsen, M. & Tamke, M., 2015. Prototyping Practice: Merging Digital and Physical Enquiries. *Rethink! Prototyping*, pp.49–62.

Ramsgaard Thomsen, M. & Tamke, M., 2014. Digital Crafting: Performative Thinking for Material Design. *Inside Smartgeometry*, pp.242–253.

Rowell, R., 1984. *The chemistry of solid wood: based on a short course symposium sponsored by the Division of Cellulose, Paper and Textile Chemistry at the 185th Meeting of the American Chemical Society, Seattle, Washington, March 20–25, 1983*, Washington: American Chemical Society.

Schwinn, T., Krieg, O.D. & Menges, A., 2016. Robotic Sewing: A Textile Approach towards the Computational Design and Fabrication of Lightweight Timber Shells. *Posthuman Frontiers: Data, Designers and Cognitive Machines [Proceedings of 36th Annual Conference of ACADIA], Ann Harbor,* pp.224–233.

Taki, T., 2007. Application of MS-Excel "Solver" to Non-linear Beam Analysis. Available at: http://www.geocities.jp/toshimi_taki/structure/beam/beam.htm [Accessed November 3, 2017].

Takahashi, K., Korner, A., Koslowski, V. & Knippers, J., 2016. Scale Effect in Bending-Active Plates and a Novel Concept for Elastic Kinetic Roof Systems. *Iaas Annual Symposium 2016 "Spatial Structures in in the 21st Century" Tokyo,* pp.1–9.

Timoshenko, S.P. & Gere, J.M., 1961. *Theory of elastic stability*, New York: McGraw-Hill Book.

Toussaint, M.H., 2007. A Design Tool for Timber Gridshells: The Development of a Grid Generation Tool. *MSc Dissertation, TU Delft University of Technology.*

Valiente, A., 2004. An Experiment in Nonlinear Beam Theory. *American Journal of Physics*, 72(8), pp.1008–1012.

Wisnom, M.R., 1991. The Effect of Specimen Size on the Bending Strength of Unidirectional Carbon Fibre-Epoxy. *Composite Structures*, 18(1), pp.47–63.

Yoshihara, H., 2011. Bending Properties of Medium-Density Fiberboard and Plywood Obtained by Compression Bending Test. *Forest Products Journal*, 61(1), pp.56–63.

Yoshihara, H. & Oka, S., 2001. Measurement of Bending Properties of Wood by Compression Bending Tests. *Journal of Wood Science*, 47(4), pp.262–268.

Μαντάνης, Γ., 2003. *Δομή & Ιδιότητες Ξύλου – Μέρος 2. Ιδιότητες*. Τ.Ε.Ι. Λάρισας

Σοφιανόπουλος, Δ.Σ., 2015. *Μη Γραμμική Ευστάθεια Κατασκευών με Έμφαση στις Χαλύβδινες Κατασκευές*. Ελληνικά Ακαδημαϊκά Ηλεκτρονικά Συγγράμματα και Βοηθήματα / Κάλλιπος.

McElwain, W., 2014. A script for elastic bending (aka the elastica curve) in Discussion View Discussions et al., *Grasshopper*. Available at: http://www.grasshopper3d.com/forum/topics/a-script-for-elastic-bending-aka-the-elastica-curve [Accessed November 3, 2017].

Maurel, J., Teaching machine design & mechanics. *Teacher in Machine Design | FOAM BEAMS*. Available at: http://jacquesmaurel.com/foam-beams [Accessed November 3, 2017].

Recognizing digits with OpenCV and Python. *PyImageSearch*. Available at: https://www.pyimagesearch.com/2017/02/13/recognizing-digits-with-opencv-and-python/ [Accessed November 3, 2017].